Development of Methods for the Discovery of Small Molecule Biological Probes

Carrie Elizabeth Yozwiak

Submitted in partial fulfillment of the

requirements for the degree

of Doctor of Philosophy

in the Graduate School of Arts and Sciences

COLUMBIA UNIVERSITY

2017

ABSTRACT

Development of Methods for the Discovery of Small Molecule Biological Probes

Carrie Elizabeth Yozwiak

Advances in combinatorial chemistry have facilitated the production of large chemical libraries that can be used as tools to discover biological probes and therapeutics. High-throughput screening (HTS) strategies have emerged as the standard method to assess the biological activity of small molecules. These screens involve the individual analysis of each small molecule in multi-well plates, often requiring expensive automated methods and development of robust assays that may not translate to physiologically relevant contexts.

This problem of evaluating large numbers of reagents in physiologically relevant cell and animal models has been addressed for genetic reagents such as RNAi, CRISPR, and cDNA by creating barcoded retroviral libraries that can be used to infect target cells in culture or in animal models. Using these tools, effective reagents can be selected and decoded using a rapid and inexpensive procedure compared to testing of individual reagents one at a time in an arrayed fashion. In order to more efficiently analyze small molecules, a pooled approach would similarly be useful.

This dissertation describes the studies towards developing a pooled screening strategy for small molecules in cellular contexts. Through an initial screen, we set to phenotypically profile small molecule biological activity in a pooled fashion, while simultaneously gain insight about an individual, active molecule's mechanism of action. I first describe the design of the pooled screen and define the goals necessary for

successful application. Next, I outline the steps taken and challenges encountered during the invention of each component of the technology. Finally, I discuss a computational, target-based approach to design small molecules appropriate for future applications of the new screening technology.

Table of Contents

List of Figures

Tables

Schemes

Acknowledgements

The work presented in this thesis would not have been possible without the help and support of others, who I would like to thank and acknowledge. First, my academic advisor, Brent Stockwell, has been an inspiring mentor. He has guided my scientific development, encouraged my creativity, challenged my capabilities, and provided me with limitless opportunities to learn, collaborate, and grow. It has been a true privilege and pleasure to study and mature as a scientist under his guidance.

The laboratory environment cultivated by Brent is extremely special; I am very fortunate to have spent so much time alongside a diverse group of open-minded, curious, friendly, and helpful lab members. Thank you to the entire Stockwell Lab, as each person with whom I have had the opportunity to work has significantly shaped my perspectives, communication capabilities, and approaches to problem solving—and many lab members have become great friends. I have learned so much from how my colleagues approach challenges from unique standpoints, and am so happy to have worked with this dynamic team of individuals who make interdisciplinary science possible. Specifically, thank you to Scott Dixon for showing me what a human cancer cell looks like under the microscope and for endlessly questioning my chemistry-driven approach to biological problems, Gisun Park for teaching me everything about the biochemical aspect of the Mcl-1 project, and Tal Hirschhorn, for continuing to develop and apply the bead-based screening technology. I would like to acknowledge the undergraduate and high school students with whom I have worked: Hannah Bender, Luke Zhan, Christie Corn, John Hunt Jr., and Lauren Aldoloty, who are each extremely motivated students and researchers; their drive,

creative spirit, and awesome personalities made mentoring one of the best aspects of my educational experience.

I would also like to thank the members of my dissertation committee, Luis Campos, Laura Kaufman, Ann McDermott, and Daniel Heller, for their time and valuable input on this thesis. I am grateful to Jim Leighton and the Leighton Lab members for providing me with a strong basis in organic chemistry, which has significantly impacted my graduate career. I am also grateful for all of the administrative support received; through our lab manager Elise Jiang, and computer support- Anthony Gomez and James Shanley. Additionally Freddy Del Pilar, Jaya Santosh, Ellie Siddens, Al Rodriguez, Christopher Cecilio, Alison Doyle, and Dani Farrell have all greatly supported my research and education. I would also like to acknowledge the NCI Training Program in Cancer Biology (T32GG007284-13), for funding support.

Finally, I would like to thank my wonderful friends and family, especially my parents and my husband Nick who have showed me such love, encouragement, and support.

To my family:

My husband Nick Capps

My parents Bob and Stacy Yozwiak

My sister Nicole

My grandparents Ray and Betty Yozwiak, and Nick and Stella Naberezny

Chapter 1

Introduction

1.1   Screening Methods in Drug Discovery

The process to develop a new small molecule therapeutic from conceptualization to the clinic is extremely resource intensive and arduous (Hughes et al., 2011). Additionally, advances in combinatorial chemistry have facilitated the production of large numbers of novel chemical compounds to be tested for biological activity (Lee et al., 2012; Li et al., 2013). To efficiently assess the therapeutic potential of each of these drug-like small molecules, high-throughput screening (HTS) strategies have emerged as the industry and academia-wide standard method to accelerate drug discovery. These assays take advantage of automated screening methods to gain information about the activity of large libraries of chemical compounds for the disease of interest. The implementation of high-density multi-well plates for arrayed HTS assays makes it possible to test thousands of small molecules for biological activity per day (Szymanski et al., 2012).

High-throughput screens can be designed following two distinct philosophies: target-based drug design and phenotypic screening.

1.2   Target-based Drug Discovery

Target-based drug discovery is a hypothesis-driven approach that attempts to discover small molecules that very specifically modulate a particular gene, protein, or other defined biological 'target' with the goal of affecting the disease state by probing a distinct, understood pathway implemented in pathogenesis (Swinney, 2013). This rational and systematic approach to discovering small molecules that possess a defined mechanism of action was made possible through advances in genetics and molecular biology that allows for elucidation of particular protein targets and a more thorough picture of biological pathway components (Schenone et al., 2013).

Target-based discovery tactics rely on clearly understanding the biological basis of disease, allowing the scientist an opportunity to select a relevant biomarker to quantify the severity of the physiological disease state and predict which patient populations may respond to the particular drug (Dessi et al., 2013). A biomarker can be defined as a measurable biological indicator of (1) disease or (2) response to therapeutic intervention, and provides an objective means by which to quantify health state and determine therapeutic efficacy (Strimbu and Tavel, 2010). By understanding both the drug mechanism of action and the role the therapy assumes in the pathophysiology of the disease, co-development of a drug and a companion diagnostic for therapeutic efficacy is possible (Garcia et al., 2011). This strategy enables the selection of a suitable patient population for biomarker-driven clinical trials, thereby shortening the timeline needed to bring a drug to market (Dienstmann et al., 2013). Biomarker-driven clinical trials have been shown to be efficacious in oncology, where patient populations are selected based on molecular features of their tumors (Tan et al., 2009). This approach has been

successfully implemented in the development of the PARP (poly(ADP-ribose) polymerase) inhibitor olaparib for ovarian and breast cancer treatment. Clinical trial populations were enriched for carriers of *BRCA1 or BRCA2* mutations, which are the genetic aberrations that served as biomarkers indicative of therapy efficacy (Fong et al., 2009).

Once a protein target essential to disease biology is elucidated and a hypothesis of how it is implicated in disease is put forth, there are a variety of methods by which to embark on the search for a small molecule therapeutic candidate that preferentially engages with this target. The most commonly employed approaches of screening for small molecule lead compounds include 1) computer-aided drug design, 2) fragment-based screening and 3) high-throughput screening of lead-like compounds.

1.3   Computer-Aided Drug Design

Computer-aided drug design (CADD) involves the computational modeling of drug-receptor interactions to simulate the affinity for which a given small molecule has for its target protein (Sliwoski et al., 2014). In drug discovery efforts, computer-aided approaches can be used to predict which small molecules are the most promising candidates for experimental validation, thus reducing the time and cost associated with experimentally screening large libraries chemical compounds. Additionally, CADD also provides valuable insight into the specific pose a small molecule assumes when interacting with a receptor, which greatly assists the scientist in rationally elaborating upon and optimizing the structure of the lead small molecule to enhance pharmaceutical properties while maintaining target affinity (Baig et al., 2016).

Historically, successful applications of CADD have been achieved as early as the 1990s with the development of HIV protease inhibitors (Liao and Nicklaus, 2010), and continued to play an essential role to efficiently identify drug hits and leads (Becker et al., 2006; Boehm et al., 2000; Doman et al., 2002; Santos et al., 2015). The first HIV protease inhibitor, ritonavir, was discovered using structure-based approaches and was approved by the FDA in only 72 days. This drug required only eight years for development (Sliwoski et al., 2014), which is about half of the conventional timeline for a therapeutic to come to market. The efficient process was attributed to the successful implementation of CADD.

CADD can further be broken down into two broad categories of *in silico* techniques: 1) ligand-based drug design and 2) structure-based drug design. Structure-based methods are employed when there is an available three-dimensional structure of the target protein, whereas ligand-based methods are used when the protein structure of interest is unavailable (Baig et al., 2016).

1.4 Ligand-based drug design

If the structure of the protein target is unknown, but there are small molecules that have been identified to exhibit biological activity against the target of interest, indirect computational methods can be employed to find a better therapeutic candidate. In this ligand-centric approach, the structure of a small molecule can be broken down so that the characteristics of each atom in the molecule are recognized to represent a physical interaction (hydrogen bond donor, hydrogen bond acceptor, hydrophobicity, pi-interaction, etc.) with the protein that may be responsible for its observed biological

4

activity (Yang, 2010). Once the structure of the molecule is analyzed using the three-dimensional orientation of its steric and electronic features, a pharmacophore model is created and then superimposed with low-energy conformations of other small molecules. (Kapetanovic, 2008). In theory, if one physical phenomenon, like hydrogen bonding, is preserved in a similar region of superimposed chemical compounds, the interactions of small molecules with similar pharmacophores in the binding pocket of the biological target should remain. This strategy is especially useful when optimizing a lead compound for ADME properties or assessing whether drugs can have multiple biological targets (Lee et al., 2011).

1.5   Structure-based drug design

Structure-based drug design is a direct approach wherein small molecules are computationally fit into a three-dimensional protein structure. This protein structure can be elucidated by x-ray crystallography or NMR spectroscopy with good resolution (usually less than 2.5 angstroms), or virtually created using homology modeling of similar proteins of known structure (Anderson, 2003). With this structural data in hand, scientists can use the topography of the biological receptor to visualize the stereochemical and electronic interactions of small molecules with the target protein and tune the small molecule structure to optimize receptor binding affinity.

To virtually examine the binding affinity of a small molecule ligand for its target protein, molecular docking strategies are used. This technique most commonly involves the sampling of all possible three-dimensional orientations of a ligand into a fixed binding pocket on the receptor. Each of these docking poses is then ranked based on

binding affinity for the designated receptor (Gane and Dean, 2000). Molecular docking approaches are commonly applied in three ways that differ based on their computational complexity, and include (1) rigid docking (the least computationally complex), in which both the ligand and receptor geometries are held static in space, (2) flexible ligand docking, in which the conformation of the ligands is considered flexible, while the receptor is held rigid, and (3) the most complex simulation, flexible docking, in which both the ligands and target receptor geometries are considered flexible in space (Liao et al., 2011).

Once a docking strategy is selected, structure-based virtual screening can occur. This approach involves docking large, *in silico* libraries of small molecules into the target receptor to assess binding affinity. After docking each individual ligand, the most probable binding mode for each small molecule is predicted, and the quality of fit of this optimal binding mode for the designated target site is scored to predict binding affinity. This computational approach can be considered the virtual equivalent of high-throughput screening and is used to efficiently identify lead compounds to be synthesized and biologically evaluated (Lionta et al., 2014).

The ranking of goodness of fit for the ligand to the receptor, known as the docking score, of each ligand is taken into account to determine the subset of small molecules to further pursue and validate experimentally. The docking score is used to quickly and accurately evaluate the protein-ligand complex to differentiate accurate binding predictions from inaccurate modes. The aim is to achieve a good picture of which molecule will perform best empirically (Ferreira et al., 2015).

Scoring functions can be broken down into different categories based on what parameters each take into account. Force-field or molecular mechanics-based scoring functions use the sum of the electrostatic and van der Waals interactions to estimate the binding free energy of protein-ligand complexes. The physical atomic parameters included in this scoring function are derived from both *ab initio* quantum mechanical calculations and experimental data (Huang et al., 2010). Methods to account for the solvent effect on ligand binding present a major challenge to this method of scoring. To address this limitation, empirical scoring functions are commonly taken into consideration with force field functions.

Empirical scoring functions use weighted energy terms, like hydrophobicity, desolvation, electrostatics, entropy, etc. to approximate the binding affinity of the ligand for the target. The simple model of counting the number of favorable and unfavorable interactions between the small molecule and protein make this method most efficient in scoring assessment (Kitchen et al., 2004).

Knowledge-based scoring functions take into account experimentally determined parameters from known structure analysis. The interaction to be assessed is broken down atomistically, and the overall docking score is a sum of each individual atom-atom interaction. Because this approach relies on data collected from protein structural databases, molecular interactions that are not commonly accounted for in crystal structures, like cation-pi interactions or halogen bonding, are inadequately predicted. Consensus scoring functions take combinations of empirical, force-field, and knowledge based scoring functions in attempt to moderate the weaknesses of each individual method (Kitchen et al., 2004).

1.6 Fragment-based screening

Fragment-based screening involves the experimental analysis of low molecular weight (<300 Da) small molecules with the defined target protein by mass spectrometry, nuclear magnetic resonance (NMR) spectroscopy, x-ray crystallography, or *in vitro* biophysical assays (Rees et al., 2004). Although small fragment libraries have less functionality and therefore react more weakly with their target protein (a hit would be considered low mM to 30 μM range), the power in this method originates from the understanding that drug-like molecules can be dissected and simplified to contain a combination of distinct binding epitopes (or fragments). Screening for these binding epitopes, and then amalgamating the most promising fragments to build a larger, more potent active molecule, forms the essence of this tactic (Hajduk and Greer, 2007).

Compared to high-throughput screening approaches, fragment-based screening offers distinct advantages. Fragment-based screens can often comprise smaller libraries of chemical compounds than the libraries of larger, drug-like small molecules because smaller molecules more efficiently sample chemical space than larger molecular weight compounds (Hall et al., 2014). This leads to an efficient increase in information gained by the scientist over an initial screen; a larger representative set of chemical moieties is sampled to initially provide empirical data supporting which epitopes show affinity, leading to the discovery of molecular templates that conventional HTS may have overlooked. Additionally, the chemical simplicity of fragments allows the researcher to understand which moieties are reactive to a specific binding site while also demonstrating a higher hit rate since a smaller molecule exhibits less steric hindrance for the binding site, although at weaker affinity (Mortenson et al., 2014).

The binding information gained from fragment-based screens can also be extremely valuable when deciding on how to elaborate upon the fragment to better create the drug-like molecule--smaller fragments provide more freedom by which the medicinal chemist can embellish the structure to optimize affinity, selectivity for the target, and ADME properties for drug-success. A low-molecular weight, simple compound starting point expands the potential avenues a medicinal chemist can explore, generating a larger amount of novel chemical structures for diversity (Doak et al., 2016).

1.7   Challenges in target-based drug design

Conceptually, target-based drug discovery is a reductionist approach to therapeutic invention. The drug-organism interaction analysis is simplified to the study of the relationship of the drug for an individual target, which allows scientists to rationally design small molecules that address their hypothesized biological drivers of disease (Sams-Dodd, 2005). Although this route has triggered immense scientific advances into the understanding of disease progression and human biology, there are disadvantages to this tactic of drug discovery.

Validation of the target's role in human disease is critical to the drug development success, as even if a small molecule demonstrates potent and selective affinity for the defined protein, activation or inhibition of the target pathway may show no beneficial augmentation of disease state (Brown, 2007). One of the most powerful methods to demonstrate that a protein is instrumental in disease pathogenesis is to examine its implications in animal models of human disease, but often, development of an appropriate animal model is extremely challenging. Other methods of validation,

including proteomics, genomics, or computational modeling are efficacious to determine the functional role of a target protein *in vitro*, but each does not address the physiological complexity presented by a whole organism and does not present a comprehensive picture of whether the target is an essential driver of disease (Smith, 2003).

Approaching drug discovery from a target-based standpoint requires the detachment of physiology from drug design. Medicinal chemists prioritize the fit of the small molecule for the receptor, and adjusting the small molecule structure to optimize ADME properties are accounted for secondarily. Even if the small molecule demonstrates activity *in vitro*, it may be unable to access the appropriate location to functionally act, whether this involves low cell permeability or ineffective blood brain barrier penetration. Additionally, the molecule may fail plasma or metabolic stability testing, rendering the candidate futile for human consumption. Because small molecules are initially screened for their ability to probe a specific mechanistic pathway, the rate of 'hit' small molecules is inherently lower than in systematic phenotypic screens, while the physiological consequences of altering a well- defined portion of a whole organism's biology are not initially considered. Often, therapeutic candidates are not tested in animal models of disease until late in the production timeline, and molecules that have been thoroughly studied *in silico* and *in vitro* may be ineffective because the binding of the drug to the target may not sufficiently cause the relevant activity, or the engagement of a single target may not overcome the complexities of the disease state to elicit the desired physiological effect. Candidates may also be deemed unsafe because they cause off-target effects, and then rendered unfit to progress into the clinic.

1.8   Phenotypic Screening

Phenotypic screening is a systems-based, unbiased screening approach that involves testing a large number of small molecules in a biological system and observing how the compound alters the physiological state of the complex, disease-relevant model (Zheng et al., 2013). This approach does not require the elucidation of a defined biological target. Instead, lead compound determination relies on whether the molecule produces the desired biological effect, thus ensuring that the biology and chemistry are in sync from the initial stages of the discovery process (Mullard, 2015).

Phenotypic screens are essential to develop therapies for diseases in which specific biological targets have not been validated. In these cases, large numbers of randomly selected small molecules are screened for biological activity in functional assays. The major advantage of this method is that the 'hit' small molecules selected from these assays are more likely to possess therapeutically relevant molecular mechanisms of action, even if the specific way in which they function is unexpected or undetermined (Swinney, 2013). For example, the antibiotic linezolid was discovered through a phenotypic screen with live bacteria. This drug exhibits activity against multi-drug resistant gram-positive pathogens, and laid the foundation for elucidation of oxazolidinones, an entirely new class of antibiotics (Swaney et al., 1998; Wilson et al., 2008).

Phenotypic assays have been used to both elucidate clinically relevant therapies and provide great insight into the biological mechanisms of disease, which can lay the groundwork for target-based discovery approaches. When the disease biology is unknown, careful consideration should be made to select an assay system that is most

11

physiologically representative of the disease under examination (*i.e.,* through the use of primary or patient derived cells instead of immortalized human cancer cell lines) (Vincent et al., 2015). Indeed, phenotypic assays have successfully demonstrated translational value. Patient-derived airway epithelial cells were used as an excellent *in vitro* model of cystic fibrosis, and a phenotypic screen led to the discovery of the first therapies that improve lung function in patients who possess G551D and F508del mutations (Ashlock and Olson, 2011).

Despite examples of successes, phenotypic screens have limitations towards drug discovery. Often, it is difficult to create assays that appropriately portray biological conditions of disease. When applied to oncology, cell based assays are often designed using immortalized human cancer cell lines, which are widely considered to be a poor representation of malignancy. Furthermore, assays developed to screen for cytotoxic agents by investigating cell viability often reveal drug-like candidates that bind to established and extensively drugged targets; small molecules screened hit the 'low hanging fruit' of proteins and rarely expand upon the disease mechanism of action, making discovery of novel classes of drugs challenging through this method. Because phenotypic screens do not elucidate the biological target upon which the candidate compound acts, it is often difficult to discover a biomarker to assess future phase trial efficacy en route to market. The hunt for the mechanism of action of hits derived from phenotypic screens can often lead researchers on a time-intensive 'wild goose chase' that may not deliver answers.

1.9   Combinatorial library synthesis

Efficient screening strategies are dependent on the accessibility of large small molecule libraries. Merrifield's revolutionary development of solid –phase peptide synthesis set the stage for technologies that generate large libraries of diverse peptides and small molecules (Merrifield, 1963). Split-pool synthesis methods rely on chemical conjugation of peptides or small molecules to a resin in a one-bead-one-compound (OBOC) format. After the initial coupling reaction is performed on different aliquots of beads, the beads are pooled and re-split, and a new moiety is added to each group of beads. This cycle of split-pool synthesis is repeated to efficiently generate large libraries of structurally diverse compounds for screening (Furka et al., 1991; Lam et al., 1991; Tan et al., 1998).

Once the small molecules are cleaved from the beads after the completion of library synthesis, phenotypic, arrayed screens using the small molecule libraries have shown success in the discovery of biologically relevant compounds with novel properties (Lokey, 2003). Using biomimetic reactions on beads to generate a small molecule library of 2,527 compounds, Pelish *et.al.* discovered a structurally unique galanthamine-like small molecule that perturbs the secretory pathway in mammalian cells; a pathway distinct from the acetylcholinesterase inhibitory biological activity of the native galanthamine natural product (Pelish et al., 2001). In order to identify the small molecule that exhibits biological activity from this diversity oriented approach, each molecule in the library must be tested individually in multi-well plates to avoid complex deconvolution.

Screening of these compound-bead libraries has been demonstrated in isolated

13

protein systems, but not in intact cells without release of the small molecule from the bead, because cells generally do not internalize the synthesis beads used for split-pool synthesis (Chen et al., 1993; You et al., 1997).

Additionally, evaluating the effects of compounds in vivo in animal models requires great time, expense and numbers of animals, since these compounds must be tested in a one molecule per one animal basis.

1.10 Pooled approaches to screening

To improve the efficiency of testing large libraries of reagents for biological activity, pooling methods provide an alternative to arrayed high-throughput screening strategies. In a pooled screen, mixes, or 'pools' of candidate compounds or RNA are tested simultaneously in one well, as opposed to individually testing each component of the collection (Kainkaryam and Woolf, 2009).

Pooling has emerged as a powerful approach to efficiently perform genetic screens. Specifically, pooled RNAi barcode screens provide a convenient method to evaluate large shRNA libraries. In this method, shRNA vectors are tagged with a unique oligonucleotide sequence before incorporation into cells, and then identified via PCR amplification and barcode sequencing. The understanding of gene function acquired by large-scale RNAi screens has greatly contributed to signaling pathway elucidation and drug target discovery in cancer and infectious diseases (Agaisse et al., 2005; Diehl et al., 2014; Moffat and Sabatini, 2006). In addition, such pooled barcode shRNA screens have been performed both in culture and in animals (Blakely et al., 2011; Gargiulo et al., 2014).

There is no pooled small molecule screening method for cell-based assays analogous to the pooled, RNAi screening technology. A major limiting factor is that multiple small molecules can easily penetrate one cell. The current paradigm is a one compound in one well approach, which provides a straightforward analysis, at the cost of being inefficient and prohibitively expensive to screen small molecule libraries without substantial automation (Kainkaryam and Woolf, 2009).

Available approaches for small molecule pooling include adaptive strategies, where small pools of compounds (n = 5) are tested in one well. If the pooled collection induces the desired biological phenotype, each compound must next be tested individually to discover which compound to pursue. Without individual testing, deconvolution strategies can become complex because multiple compounds are acting on each cell in the well; the biological response may be a result of synergistic or additive effects of the combination of small molecules, leading to false positive hits (Kainkaryam and Woolf, 2009). Additionally, multiple compounds in a well can interact with each other or aggregate to antagonize an otherwise favorable biological interaction between target and individual lead compound. These factors lead to unavoidable false negative screening results.

1.11 DNA-encoded libraries

DNA-encoded small molecule libraries have emerged as a method to screen pools of compounds against isolated protein targets (Brenner and Lerner, 1992). These libraries contain drug-like molecules tagged with DNA barcodes (Gartner et al., 2004). The covalently bound genetic component functions as a unique identifier of the small molecule. Extremely large libraries are most commonly built in a combinatorial fashion;

construction begins with one small chemical building block tagged with a small

nucleotide sequence. As the second chemical building block is added, the DNA tag is

also lengthened with an oligonucleotide sequence that encodes the new building block.

These components are pooled, and subsequent building blocks with corresponding tags

are added to quickly assemble large libraries. Pharmaceutical companies have

implemented this strategy to build libraries that contain as many as 1 trillion unique

molecules, each with DNA identifiers (Mullard, 2016).

Libraries can be interrogated using affinity-based techniques, where the entire

library is incubated with a protein target equipped with a purification tag. After

incubation in one well as a single mixture, the proteins are purified from the system; any

small molecules bound to the protein will accompany the target throughout the

purification. Because each small molecule isolated is linked to a DNA identifier, the

barcodes from the purified system can be amplified and sequenced to reveal the 'hit'

small molecules from the pool (Goodnow et al., 2017).

This technique has been implemented to discover small molecules that potently

interact with defined targets of interest (Franzini et al., 2015). An 800-million- member

DNA-encoded library was assembled and screened to discover inhibitors of both p38

MAP kinase and Aurora A kinase (Clark et al., 2009). Moreover, screening a DNA-

encoded macrocyclic library resulted in the discovery of a selective insulin-degrading

enzyme inhibitor that can be developed as a strategy to treat type-2 diabetes and used to

elucidate the role of the enzyme in glucose and hormone regulation (Maianti et al., 2014).

DNA-encoded libraries have become a valuable screening strategy, with the

potential to elucidate novel lead candidates for historically challenging targets (Buller et

al., 2009). By eliminating the need to distribute the protein target to millions of wells, as in arrayed HTS strategies, pooled screening of DNA-encoded libraries can yield results using unstable protein targets produced in minute quantities (Decurtins et al., 2016).

DNA-encoded small molecule screening has distinct limitations when applied to drug discovery. Because the small molecule cannot cross the cellular membrane when conjugated to the DNA tag, this screening technique is restricted to biochemical, protein-based methods or cell-based screens for proteins present on the cell surface. Additionally, the DNA barcode remains attached to the small molecule, which can alter the interaction of the small molecule with the protein target; false negative hits may arise because the small molecule's activity cannot be assessed independent of the oligonucleotide modification (Franzini et al., 2014). The affinity-based purification step introduces additional challenges when interpreting screening results. Small molecules and their tag may bind to the purification column individually, without interacting with a protein, thereby introducing false positive 'hits'. Finally, as with any affinity-based purification screening strategy, the purification tag added to the protein may interfere with the native protein structure, abrogating appropriate binding mode of the small molecule (Mullard, 2016).

1.12 Screening strategies in oncology

The ultimate objective for oncology therapeutic discovery is to create medicines that exclusively eradicate or reprogram malignant cells without adversely effecting normal cell populations. In order to achieve this differential drug activity, researchers often base therapeutic development on molecular aberrations that drive cancerous cells (Yap and Workman, 2012). The breakthrough development and success of the tyrosine

17

kinase inhibitor imatinib to treat *BCR-ABL* driven chronic myeloid leukemia confirmed the idea that small molecule therapies can effectively be designed to exploit specific genetic abnormalities known to drive malignant transformation in particular patient populations (Iqbal and Iqbal, 2014). Based on this prototype, target-based screening strategies have widely been implemented to create clinically successful therapies: *e.g.,* sorafenib, a multi-kinase inhibitor discovered by a high-throughput small molecule screen for inhibitory activity against Raf1 kinase (Wilhelm et al., 2006); erlotinib, a non small cell lung cancer (NSCLC) treatment that inhibits the epidermal growth factor receptor (EGFR) (Dowell et al., 2005); and vemurafenib, for metastatic melanoma patients who possess the BRAF V600E mutation (Chapman et al., 2011).

The significant challenge in designing therapies that address key molecular mechanisms responsible for tumorigenesis, however, is that cancer is an extremely heterogeneous disease; often there are unique physiologic profiles that occur within one patient, one tumor, or even in one cancer type (Welch, 2016). Because there is rarely one biological target that solely drives the phenotype of a specific cancer, there are very few efficacious 'magic bullet' type therapies, where a molecule designed to target one molecular abnormality observed in the cancer entirely cures the disease.

Phenotypic profiling can be implemented as an alternate, or concurrent, approach to drug candidate selection. In this case, assay design is based on the biological characteristics of cancerous cells (unrestrained proliferation, resistance to cell death, evasion of growth suppressors, etc.) (Moffat et al., 2014). Therapeutic candidates screened using these assays are selected for further study based on their ability to elicit a specific biological response. Historically, the most common high-throughput phenotypic

screens for oncology therapeutics are based on cytotoxicity assays using human-derived

cancer cell lines that demonstrate unconstrained, rapid growth. Lenalidomide, a structural

derivative of thalidomide, was discovered to possess anticancer properties using

cytotoxicity assays in the 1990s. Although efficacious to treat multiple myeloma, only

recently was its mechanism of action related to antitumor activity understood (Lu et al.,

2014). Two histone deacetylase (HDAC) inhibitors, vorinostat (Grant et al., 2007) and

romidepsin (Ganesan, 2016), were also both discovered purely using phenotypic

screening methods, demonstrating the value of incorporating physiologically relevant

parameters in the discovery of clinically efficacious oncology therapeutics.

1.13 Evasion of apoptosis

Apoptosis, a form of programmed cell death, is an essential biological process for

both embryonic development and the maintenance of cellular homeostasis (Elmore,

2007). The dysregualtion and evasion of cellular apoptosis is a main cause of

tumorigenesis and chemotherapy resistance, and is consequently characterized as one of

the six hallmarks of cancer (Hanahan and Weinberg, 2000). A popularized strategy by

which to develop oncology therapeutics is to encourage this highly regulated process to

promote cell death; either through the phenotypic discovery of apoptosis inducing

compounds, or by directly designing a molecule to inhibit pro-survival biological

machinery.

Apoptosis is characterized by distinct morphological and biochemical changes

including cell shrinkage, nuclear condensation and fragmentation, and plasma membrane

blebbing (Ouyang et al., 2012). An evolutionarily conserved family of cysteine proteases,

19

known as caspases, are the central components of the apoptotic response and are largely responsible for these morphological changes (Hengartner, 2000). In most cells, caspases are widely expressed as inactive proenzymes. Upon apoptotic pathway stimulation, caspases are proteolytically activated to generate a cascade of biochemical events that irreversibly commit the cell to death (Riedl and Shi, 2004; Thornberry and Lazebnik, 1998). The highly controlled death process cumulates with fragmentation of the cell into independent vacuoles known as 'apoptotic bodies', which are rapidly recognized and removed by phagocytes to prohibit an inflammatory cellular response (Taylor et al., 2008).

Apoptosis can be subdivided into two main mechanistic categories that both converge on caspase activation: (1) the extrinsic or death receptor pathway, and (2) the intrinsic or mitochondrial pathway. The extrinsic pathway begins when transmembrane receptors belonging to the tumor necrosis factor (TNF) superfamily (*e.g.,* Fas, also known as APO1 or CD95, TNF receptor I (TNFR1), or TNF-related apoptosis-inducing ligand receptor 1 (TRAILR1, also known as DR4)) engage with their extracellular ligand counterpart (Ichim and Tait, 2016). Ligand binding induces a dimerization event that provokes recruitment of adaptor proteins such as FAS-associated death domain protein (FADD), creating a death-inducing signaling complex (DISC). DISC formation mediates the activation of initiator caspases 8 and 10, which proteolytically cleave and activate effector caspases 3 and 7, committing the cell to apoptosis (Nair et al., 2014).

Multiple signal transduction pathways in normal and malignant cells converge on the B-cell lymphoma-2 (Bcl-2) family of proteins to police the intrinsic, or mitochondrial pathway, of apoptosis (Adams and Cory, 2007). In healthy cells, the pro-survival

proteins, (Bcl-2, Mcl-1, Bcl-X$_L$, Bcl-w, and A1) bind to the effector proteins Bax and Bak, sequestering their pro-apoptotic function. Upon receipt of an intracellular damage signal, pro-apoptotic BH3-only proteins (Bad, Puma, Noxa, etc.) selectively insert their alpha helical BH3 domain into the hydrophobic groove of the pro-survival proteins, initiating their displacement from Bax and Bak. This release of Bax and Bak activates them for homo-oligmerization, which triggers mitochondrial outer membrane permeabilization to release pro-apoptotic factors, like cytochrome *c*, into the cytosol. Cytochrome *c* associates with apoptotic protease-activating factor 1 (APAF-1) and pro-caspase 9 to assemble an apoptosome, which activates caspase 9 (Elmore, 2007). Activation of caspase 9, in turn, enables the cleavage and activation of the caspases 3 and 7, which irreversibly commit the cell to death.

Another model of Bax and Bak activation establishes a set of "activator" BH3-only proteins that can directly bind to Bax and Bak. These BH3-only proteins are sequestered by pro-survival Bcl-2 proteins, and can be released from pro-survival proteins upon competitive displacement by the set of BH3-only "sensitizer" proteins (Westphal et al., 2014). In either model, cell death is the result of BH3-only proteins binding to pro-survival proteins to activate Bax and Bak.

1.14 Caspases as a biomarker for apoptosis

Caspases, or cysteine-dependent aspartate-specific proteases, can be thought of as the central executioners that drive apoptosis, as the activation of these inert zymogens is an essential contributor to the cell death pathway (Li et al., 2014). The role of caspases in cell death was first studied in the nematode *Caenorhabditis elegans,* where the cysteine protease *ced-3* was discovered through genetic analysis of cell-death defective (CED)

21

mutants to be required for cell death process related to development (Ola et al., 2011). The first mammalian homologs of *ced-3*, caspase-1 and caspase-2, were subsequently discovered to play important roles in apoptosis and inflammation, and since, over a dozen caspases have since been elucidated in humans, mammals, insects, worms, and hydra (Hengartner, 2000).

All known caspases possess an active site cysteine, and specifically cleave peptide substrates on the carboxy-terminal side of aspartic residues. This aspartate preference is a unique phenomenon among proteases (Poreba et al., 2013), yet caspases do show overlapping substrate specificity within the family.

Caspase 3 is the most highly expressed activated member of the family during apoptosis, and the most readily active caspase -3/-7 cleavage motif is Asp-Glu-Val-Asp (DEVD) (McStay et al., 2008). Assays using fluorogenic substrates that include the DEVD sequence have been developed and broadly implemented as a reliable and convenient method to detect apoptosis in mammalian cell extracts or animal models of disease (Ding et al., 2015; Thornberry and Lazebnik, 1998; Timmer and Salvesen, 2007). This target specificity, combined with the rapid, reliable, and robust means of measurement, make caspases an attractive biomarker for apoptotic cell death.

Caspases are most commonly present as inactive 'pro-caspases' that transform to the active, cleaved protease during apoptosis, and obligate the cell to death. This extremely apparent change in activity provides a detectable measure by which to assess drug intervention. Detection and quantification of cleaved caspase 3 is currently used as a proof of concept biomarker for oncology therapy by immunohistochemistry, ELISA, or fluorescent based flow cytometry assays (Ward et al., 2008). Careful consideration

should be taken to determine an appropriate time for analysis, as the kinetics of apoptosis differ based on cell type and the drug MOA and PKPD properties (Ward et al., 2008).

1.15 FRET- based fluorescent probes

A FRET (Fluorescence Resonance Energy Transfer) sensor can act as a reporter of protease activity, to allow for selection of compounds that induce specific protease activity (Edgington et al., 2011). The integrity of the FRET pair should be maintained in live cells and disrupted upon activation of a protease to yield a detectable change in fluorescence.

For effective fluorescence quenching, FRET relies on three principles: (1) overlap between the emission spectrum of the donor fluorophore and the excitation spectra of the acceptor fluorophore, (2) a donor-acceptor pair distance of 1-10 nm, and (3) suitable orientation of the FRET pair for effective non-radiative, resonance transfer of energy (Nagy et al., 2006). The acceptor identity is not limited to small molecule organic, fluorescent quenchers; quantum dots, larger gold nanoparticles, and carbon allotropes also add to the library of effective quenching agents.

Applications of FRET-based probing of cellular physiology are wide ranging. Because of the highly sensitive, distance dependent quenching effect, FRET pairs have been employed as a powerful technique to study real-time protein conformational changes and localization in living cells or biochemical assays (Sekar and Periasamy, 2003). Proteins can be site-specifically labeled with minimally perturbing FRET pairs to dynamically examine protein folding or stability (Haney et al., 2015), protein-protein

23

interactions (VanEngelenburg and Palmer, 2008), or interactions of target molecules with proteins (Rowland et al., 2015).

1.16 Targeted approach to apoptosis-inducing molecule discovery

Observations associated with protein involvement in the intrinsic apoptosis pathway spawned the concept of the 'BH3 mimetic': a small molecule that acts as a BH3-only protein, binding to the hydrophobic groove in the prosurvival proteins to obstruct their functional activity, thereby activating apoptosis (Becker et al., 2014). Each of the BH3-only proteins bind to the pro-survival proteins with varying specificity, defined by the electrostatic interactions between the BH3-region of the pro-apoptotic protein and the lipophilic binding groove created by the BH1, BH2, and BH3 regions of the pro-survival proteins (Chen et al., 2005). These observations suggest that apoptosis is regulated by the interactions between particular subsets of these proteins, and cell death can be initiated by inhibiting members of the prosurvival family.

This approach was first successfully demonstrated in 2005 by Oltersdorf and coworkers at Abbot (now AbbVie) with the development of small molecule ABT-737 (Oltersdorf et al., 2005) and later, its orally bioavailable analog, ABT-263 (navatioclax) (Tse et al., 2008), which are considered "Bad-like" BH3 mimetics because they selectively bind to pro-survival proteins Bcl-2, Bcl-X$_L$, and Bcl-w (van Delft et al., 2006). These compounds show clinical utility, but are often ineffective as a single agent for cancer treatment. Several studies have shown that Mcl-1 overexpression is a common

mechanism of chemoresistance to these small molecules, as well as frequently used anti-cancer therapies vincristine (Wertz et al., 2011), paclitaxel (Wertz et al., 2011), and gemcitabine (Wei et al., 2008). Additionally, Mcl-1 has been identified as one of the most common genetic aberrations observed in human cancer (Beroukhim et al., 2010), including lung (Song et al., 2005), prostate (Krajewska et al., 1996), breast (Ding et al., 2007), pancreatic (Miyamoto et al., 1999), ovarian and cervical cancers (Brotin et al., 2010), as well as melanoma (Boisvert-Adamo et al., 2009) and leukemia (Derenne et al., 2002). Thus, there is an intense interest in developing a potent and selective inhibitor of Mcl-1.

Inspired by the discovery of ABT-737, strategies taken to elucidate small molecule BH3 mimetics that target Mcl-1 have been based on high-throughput screening or NMR-derived fragment library screens. In each case, the small molecules discovered suffer from one (or more) of three main issues 1) low to moderate potency for Mcl-1 (Bernardo et al., 2010; Richard et al., 2013), 2) low to no efficacy demonstrated *in vivo* cellular studies, or a lack of cellular effectiveness completely (Petros et al., 2014; Varadarajan et al., 2013), or 3) insignificant selectivity for Mcl-1 over other pro-survival Bcl-2 family members (Friberg et al., 2013; Song et al., 2013; Tanaka et al., 2013).

1.17 Overview of dissertation

The current state of drug discovery often relies on a combination of phenotypic screening and target directed discovery approaches to produce a first-in-class therapy. Appropriately, these philosophically disparate screening paradigms should not be taken as completely independent paths on the way to discovering an optimized therapeutic

small molecule; instead, they can work synergistically so that phenotypic assays can be mechanistically informed, and the optimization of the small molecule can benefit from target-based approaches. Additionally, understanding the molecular mechanism of action of drugs is beneficial not only for drug efficacy and specificity, but also so that the appropriate patients receive effective treatment based on the molecular understanding of their disease.

This dissertation describes the studies towards developing a pooled screening strategy for small molecules in cellular contexts. Through an initial screen, we set to phenotypically profile small molecule biological activity in a pooled fashion, while simultaneously gain insight about an individual, active molecule's mechanism of action. I first describe the design of the pooled screen and define the goals necessary for successful application. Next, I outline the steps taken and challenges encountered during the invention of each component of the technology. Finally, I discuss a computational, target-based approach to design small molecules appropriate for future applications of the new screening technology.

CHAPTER 2

Design of a Pooled Small Molecule Screening Technology

2.1   Introduction

Therapeutic candidates often fail upon exposure to the complex physiology found in animal models and human patients, which are not captured in simple high-throughput tissue culture screening systems. In addition, the time and expense needed to assess the effects of large numbers of small molecules limits the number of compounds that can be tested, and adds to the time and cost required for discovery of drugs and probes.

This problem of evaluating large numbers of reagents in physiologically relevant cell and animal models has been addressed for genetic reagents such as RNAi (Boutros and Ahringer, 2008), CRISPR (Zhou et al., 2014) and cDNA (Wan et al., 2006), by creating barcoded retroviral libraries that can be used to infect target cells in culture or in animal models. Using these tools, effective reagents can be selected and decoded using a rapid and inexpensive procedure compared to testing of individual reagents one at a time in an arrayed fashion. In order to more efficiently analyze small molecules, a pooled

approach would similarly be useful. Large scale pooling of small molecules is not possible, because all cells are exposed to each compound, creating uninterpretable effects of large mixtures of compounds. This problem was solved for genetic reagents by physically packaging each test reagent into separate viral particles, which can deliver one genetic reagent to each infected cell, when the multiplicity of infection (MOI) is suitably calibrated.

Using fluorescent silica microparticle beads coated with carboxylate groups, we covalently attached three components to the bead surface—(1) small molecules to be assayed via a cleavable linker, (2) a fluorescent reporter and (3) a photocleavable barcode encoding the identity of each test small molecule. This chapter will focus on outlining the design of the system, as well as the rationale for selecting an appropriate bead system and fluorescent sensor of small molecule activity.

2.2   Results

2.2.1 Initial design of pooled small molecule screening technology

We designed a microparticle-bead-based system that could deliver small molecules into cells and report on the identity of the small molecule tested and its cellular activity (**Figure 2.1**). Once taken up into cells, the beads were designed to release the small molecule either by disulfide bond cleavage or cleavage of a linker peptide by cellular proteases. We envisioned that a fluorescent reporter could indicate if the small molecule delivered to a particular cell was exerting a desired biological activity. For example, if a small molecule initiates apoptosis, executioner caspase 3 should be

activated; caspase 3 is known to cleave the DEVD amino acid sequence (Poreba et al., 2013); other fluorescent peptide reporters could similarly report on the activity of other proteases in cells. A fluorescent reporter attached to beads was thus designed to detect caspase 3 activation; we would separate the bead from a fluorophore with the DEVD caspase substrate. Upon apoptotic pathway activation, the DEVD sequence would cleave to disconnect the fluorophore from the bead. Apoptotic activity would be designated by a loss of fluorescent signal from the bead. Those beads without the fluorescent signal could be harvested from the original, fluorescent population by fluorescence-activated cell sorting (FACS). Finally, an oligonucleotide, indicative of small molecule identity, is the third component attached to the bead. Upon bead collection, the identification tag would be PCR amplified and sequenced to reveal the lethal small molecule.
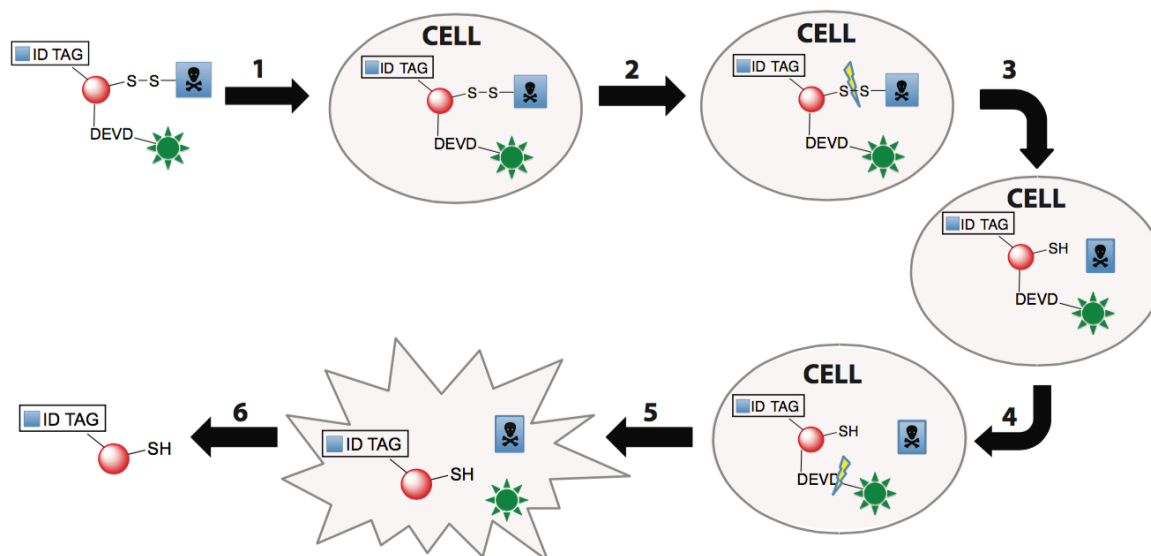
Figure 2.1 | Design of bead-based system for pooled screening of small molecules. (1) The technology, containing the covalently bound small molecule, identification tag, and activity reporter, is internalized by the cell. (2) Once inside the cell, the small molecule is released through the reduction of the disulfide bond linker. (3) The small molecule exists inside the cell without chemical modification. (4) If the small molecule causes apoptosis, activated caspases will cleave the DEVD peptide sequence connecting the fluorophore to the bead. (5) Loss of fluorophore results in absence of signal. (6) The activated system will be sorted based on this change in fluorescence, and the barcode sequenced to identify the small molecule that caused cell lethality. Red bead, silica microparticle; S-S, disulfide linker; blue square, lethal small molecule; green star, fluorescent dye.

2.2.2 *Selection of the bead component for technology delivery*

We reasoned that during the course of a pooled small molecule screen, the beads must be harvested in order to sequence barcodes that encode the identity of the test compounds attached to each bead. The beads must thus be made of a material that does not affect cell viability, and that does not decompose upon cellular internalization or cell lysis. Additionally, the beads must be small enough to be adequately internalized by the cell, yet large enough to carry a suitable amount of each component (reporter, small molecule, identification tag) for detection. Our goal was to find a bead type that demonstrates sufficient cellular uptake with a maximum of functional handles for chemical synthesis.

Moreover, the surface of the beads must contain synthetic handles amenable to bioconjugation of DNA, peptides, and small molecules. Initial studies of carboxylate-coated, polystyrene beads show that smaller beads (with 0.1 and 0.2 µm diameter) were taken up by virtually all HT-1080 fibrosarcoma cells after 6 hour incubation (**Figure 2.2)**, but the surface area available and fluorescence intensity were less favorable for small molecule delivery and cellular tracking, respectively. Beads with a diameter of 1 µm exhibited a balance of size for conjugation and cellular uptake, so this size of beads were used for technology development.

Different Diameter Beads incubated with HT-1080 Cells, 6 h

585 Fluorescence Emission Intensity

- HT-1080 cells
- 0.1 μm Beads + HT-1080 cells
- 0.2 μm Beads + HT-1080 cells
- 1 μm Beads + HT-1080 cells
- 2 μm Beads + HT-1080 cells
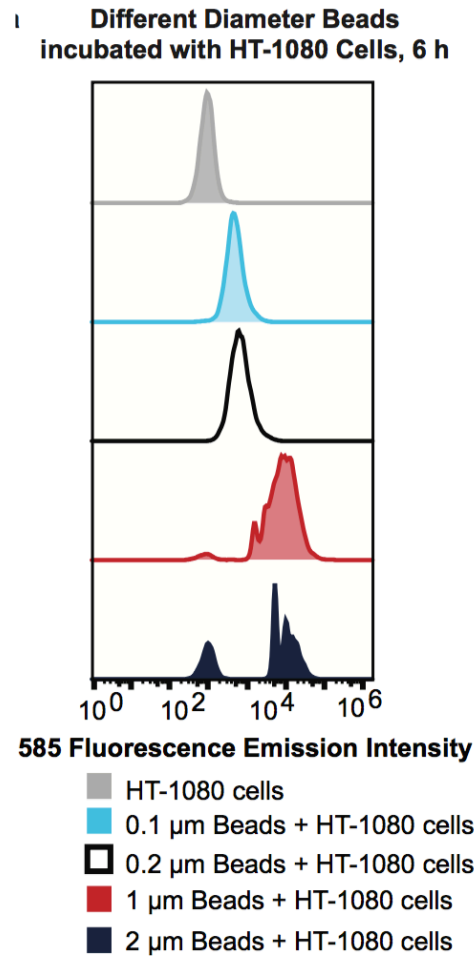
Figure 2.2 | Cellular uptake of polystyrene beads. HT-1080 cells show uptake of polystyrene beads with differing diameter after 6 h incubation at 37 $^{\circ}$C. Beads 1 μm in diameter were selected for technology development because they demonstrate sufficient cellular uptake and maximize surface area for optimal chemical conjugation.

Bead material considerations

Although polystyrene is a biologically inert material compatible with cellular assays, Life Technologies's FluoroSpheres include a fluorescent component that we

discovered to not be chemically conjugated to the polystyrene polymer. Bead incubation with organic solvents (dimethylformamide, DMF, or dimethylsulfoxide, DMSO) resulted in the polystyrene matrix swelling to release the trapped fluorescent components.

We turned our attention to silica microspheres, 1 μm in diameter, with hope that they would maintain their structure and fluorescence upon incubation with solvents necessary for chemical modification.
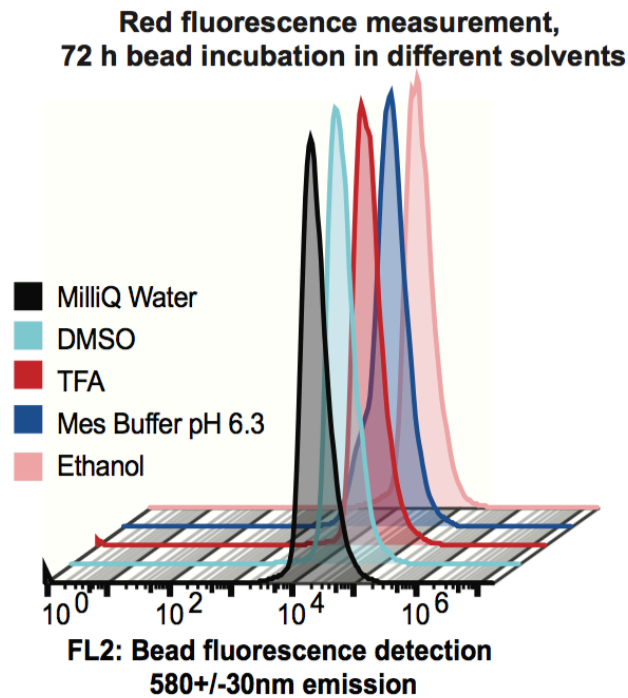
Figure 2.3 | Fluorescence analysis of 1 μm silica beads. Flow cytometry data of beads (540 nm excitation/ 625 nm emission) show diverse solvents do not alter bead fluorescence detected on the 585±40 nm bead emission detection (FL2) channel.

Microparticle fluorescence and structure were both preserved after incubation in dimethylsulfoxide (DMSO), dimethylformamide (DMF), ethanol, water, and 2-(*N*-morpholino)ethanesulfonic acid (MES) buffers, suggesting that silica beads are compatible with a variety of organic synthesis conditions, in contrast to the polystyrene microparticle material. Regardless of the solvent environment, the fluorescence intensity of the beads on the appropriate emission detection channel of a flow cytometer remained constant (**Figure 2.3**).

Dynamic light scattering (DLS) was used to analyze the microparticle size distribution profile of beads (**Figure 2.4**). DLS measurements assess the scattering of a monochromatic light source by particles in a solution; the similar size distribution of each group of beads demonstrated bead stability across diverse solvents. Additionally, we found that the carboxylate functionality on these beads is compatible with bioconjugation reactions with oligonucleotides and peptides.
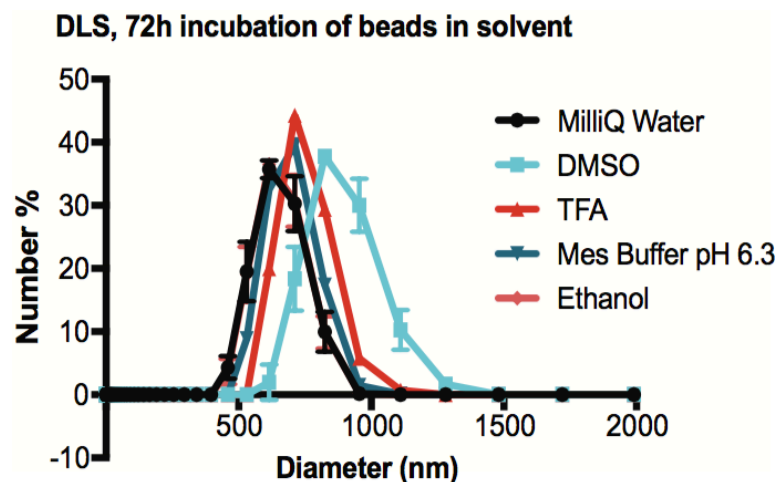
Figure 2.4 | Silica bead diameter measurement. Dynamic Light Scattering (DLS) analysis of beads after 72 h incubation with diverse solvents shows no bead degradation.

Silica Bead biocompatibility

We envisioned that these silica particles would act as the delivery vehicle for the system. Given the robust solvent stability of silica microparticles and their compatibility with diverse synthetic organic chemistry reaction conditions, we next examined the biocompability of this material. Cell viability experiments with varying concentrations of 1 μm silica microparticles showed no lethality after incubation for 72 h (**Figure 2.5**).
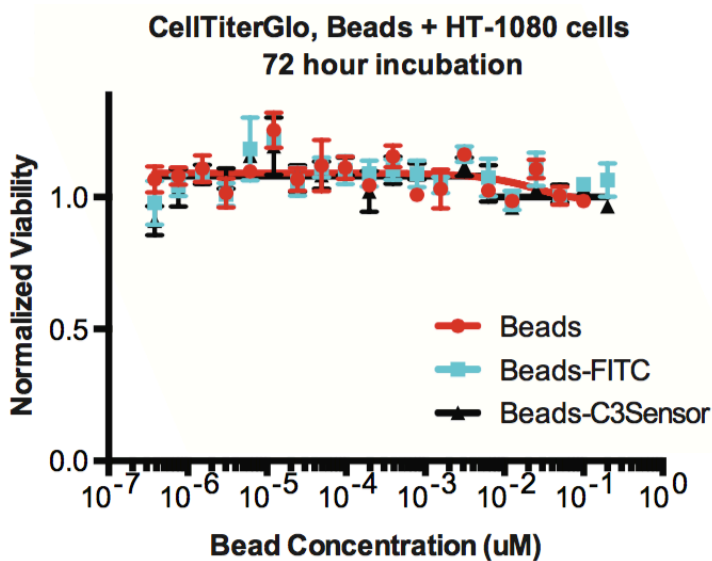
Figure 2.5 | Biocompatibility of silica beads. Cell viability, measured by CellTiter-Glo- based luminescence assay of HT-1080 fibrosarcoma cells incubated for 72 h with red fluorescent silica beads. ATP presence, indicative of live cell population, was unaffected, regardless of bead concentration.

To evaluate the appropriate balance of these factors, we studied cellular uptake of fluorescent microparticles that were 1 μm in diameter in HT-1080 fibrosarcoma cells. Because the beads possess a fluorescence emission maximum at 625 nm, cells that internalized the beads showed an increase in fluorescence on the FL2 channel of the flow cytometer, which detects fluorescence emission of 585/40 nm (**Figure 2.6**). The fluorescence of 10,000 live HT-1080 cells without beads (n = 4) was examined as a control to develop a suitable gate on the bead emission detection channel of the flow cytometer versus the fluorescence emission of the reporter component (FITC, excitation 488 nm, emission recorded on 535 nm channel) such that the gate encompassed 99.8 +/- 0.2% of the population. The gate was applied to each sample, and was used to discriminate between cells without beads versus cells associated with fluorescent beads. Of the live cell population analyzed, 8.2 +/- 0.4% of cells did not take up a 1 μm bead after six-hour incubation (n = 3); this population did not show an increase in fluorescence intensity on the 585 nm channel, the bead emission fluorescence channel.

d Population of cells incubated with beads distinguished from cells alone by 585nm emission fluorescence
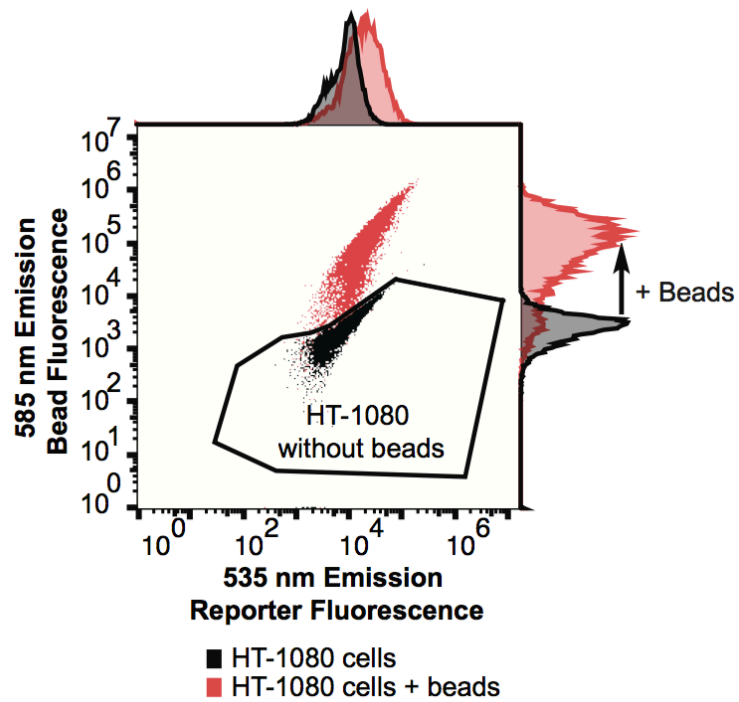
Figure 2.6 | HT-1080 cells that internalize beads show increased fluorescence.
Scatter plot of flow cytometry data. A gate of the live cell population before bead incubation was applied, and 10,000 events for each trial were recorded inside the gate. 92 +/- 0.40% of HT-1080 cells incubated with 1 μm diameter bead showed a 99-fold average increase in 585/40 nm filter (FL2 detectable fluorescence), bead emission channel, over control population after 6 hours.

Uptake studies of bead with diverse human derived cell lines were completed to assess the applicability of silica bead delivery system (**Figure 2.7**). In addition to HT-1080 fibrosarcoma cells, 293T human embryonic kidney and RKN ovarian cancer cell lines also internalized the 1 μm diameter beads.

1 μm Silica beads incubated with different cell lines, 14 h

585 Fluorescence Emission Intensity

- □ 1 μm Beads + HT-1080
- □ HT-1080 Cells
- ■ 1 μm Beads + 293-T Ce
- ■ 293-T Cells
- ■ 1 μm Beads + RKN Cell
- ■ RKN Cells
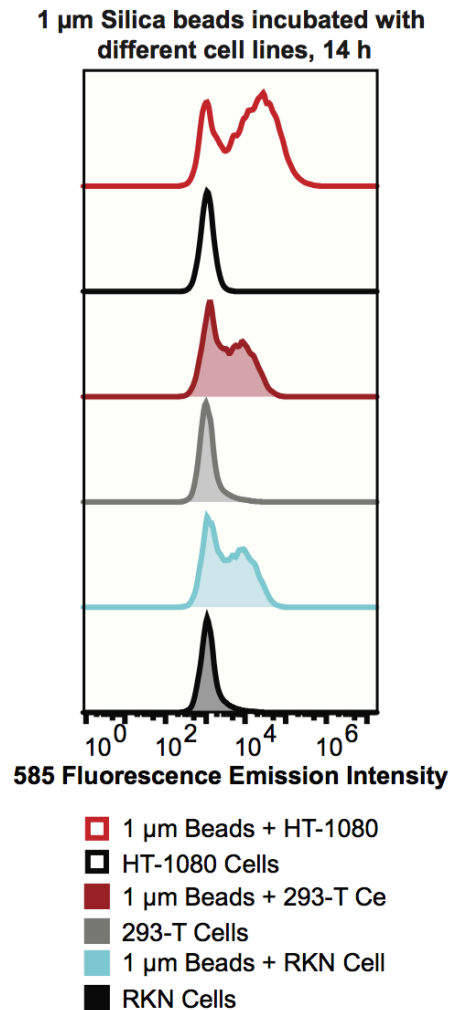
Figure 2.7 | Diverse cell lines show sufficient bead uptake. 1 μm diameter silica beads can be internalized by human cell lines derived from different tissues. HT-1080 cells demonstrated the largest change in fluorescence, motivating our choice to use this cell line for assay development throughout technology assembly.

Successful implementation of the technology relies on the delivery of one type of small molecule per cell. Each bead would have only one type of small molecule conjugated to its surface; if only one bead is incorporated into one cell, we ensure that only type of one molecule is incorporated, even in the presence of a pool of small molecules. By adapting the multiplicity of infection concept from viral screening, a single bead could be delivered into individual cells (**Figure 2.8**), demonstrating the feasibility of the one compound/cell approach.
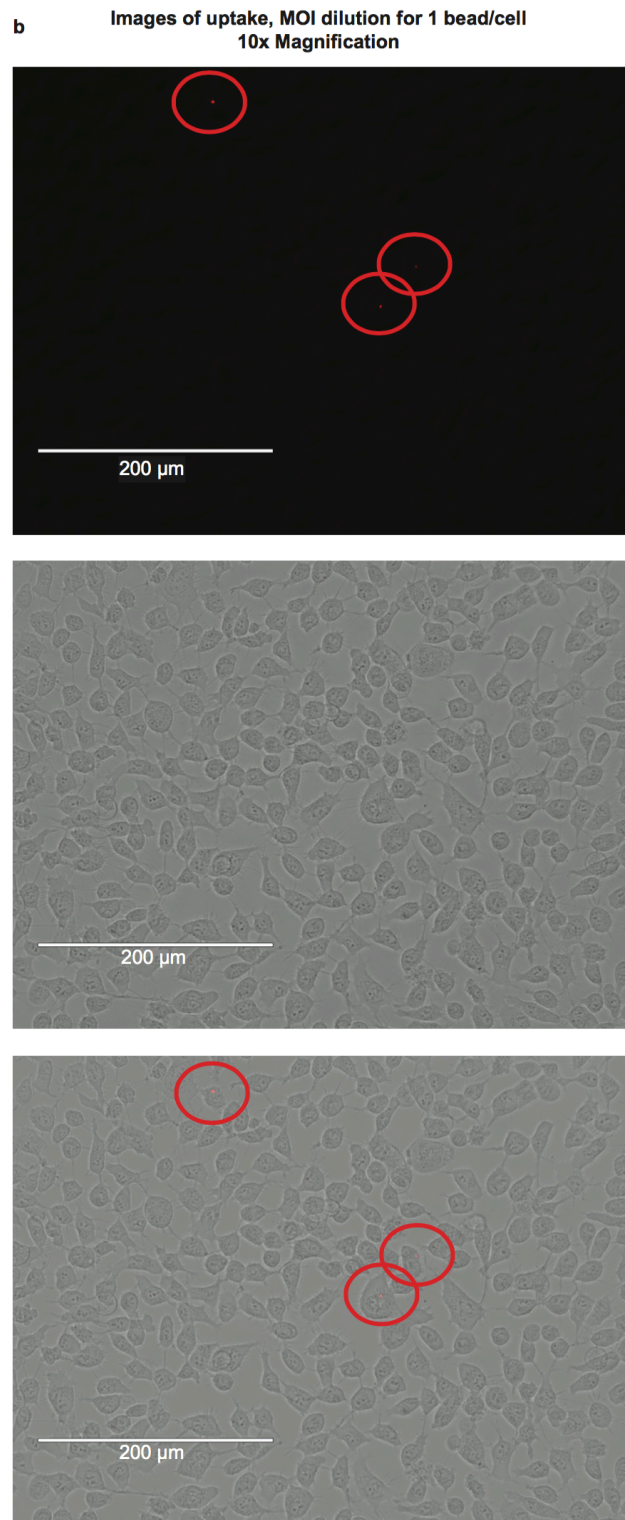
Figure 2.8 | Adjusting MOI allows for one bead per cell uptake rate. 10x Microscope image of 1 μm beads incubated for 6 h in HT-1080 cells. After dilution, 9,000 beads / 200,000 HT-1080 showed uptake at a rate of one bead per one cell.

Confocal microscopy confirmed cellular internalization of these 1 μm diameter beads (**Figure 2.9**); thus, we determined that this size would be ideal for maximizing available microparticle surface, while still being amenable to cell uptake.
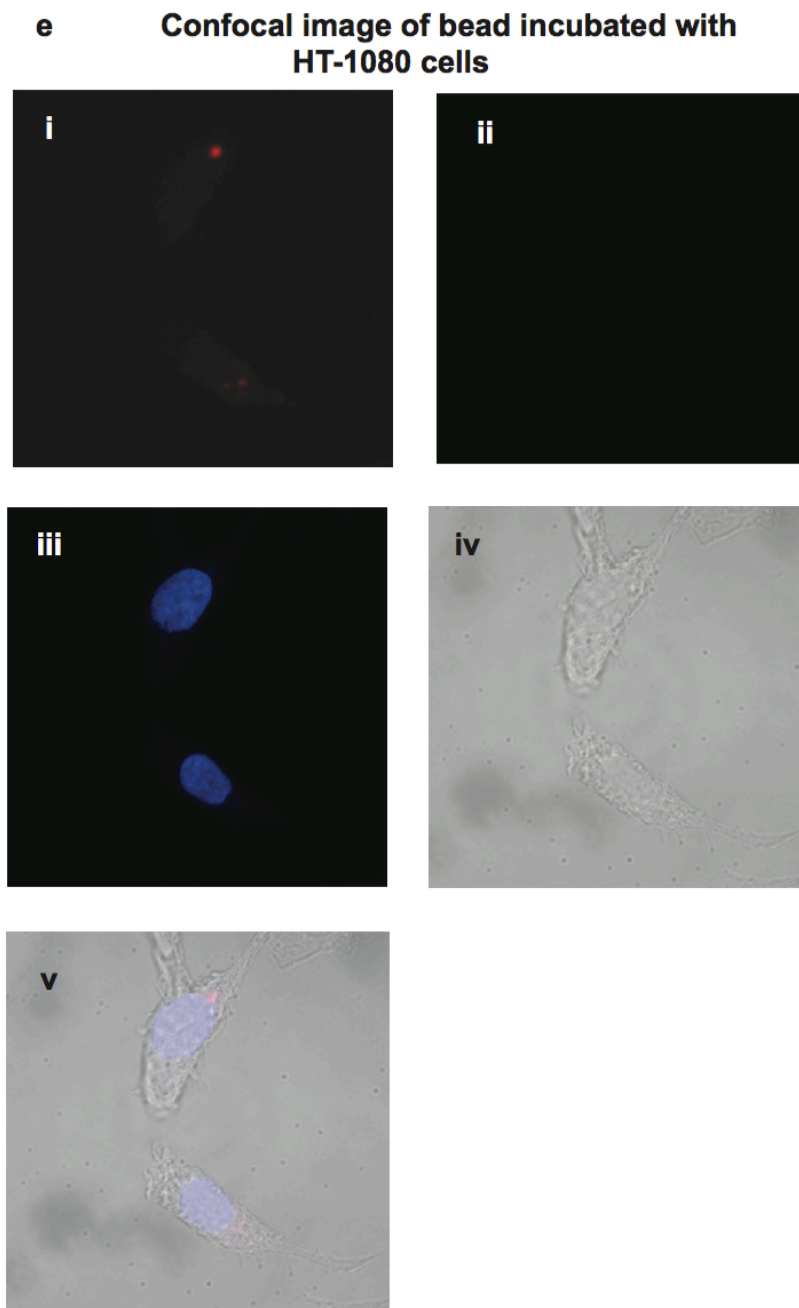
Figure 2.9 | Internalization of bead incubated with HT-1080 cells. Confocal Z-stack image of HT-1080 cells incubated for 6 hours with 1 μm diameter silica beads show microparticle uptake. (i) Red bandpass filter shows fluorescent bead. (ii) Green bandpass filter shows no bead fluorescence bleedthrough. (iii) Transmitted light. (iv) DAPI. (v) Overlay.

2.2.3 Design and analysis of the fluorescent, loss-of-function reporter

The goal of the fluorescent sensor is to report on the biological activity of the small molecule under investigation. The sensor for this system was designed to enable the selection of compounds that induce protease activity. Specifically, we set out to detect small molecules that cause cell death by activation of apoptosis, because this highly regulated form of cell death has well established biomarkers available for reliable detection. One well-evaluated biomarker of apoptosis is caspase 3 transformation from the pro-enzyme to active protease. This main executioner enzyme for apoptosis is known to cleave the DEVD peptide sequence. As such, we decided to separate the bead from the fluorophore with this DEVD peptide substrate (**Figure 2.10)**.
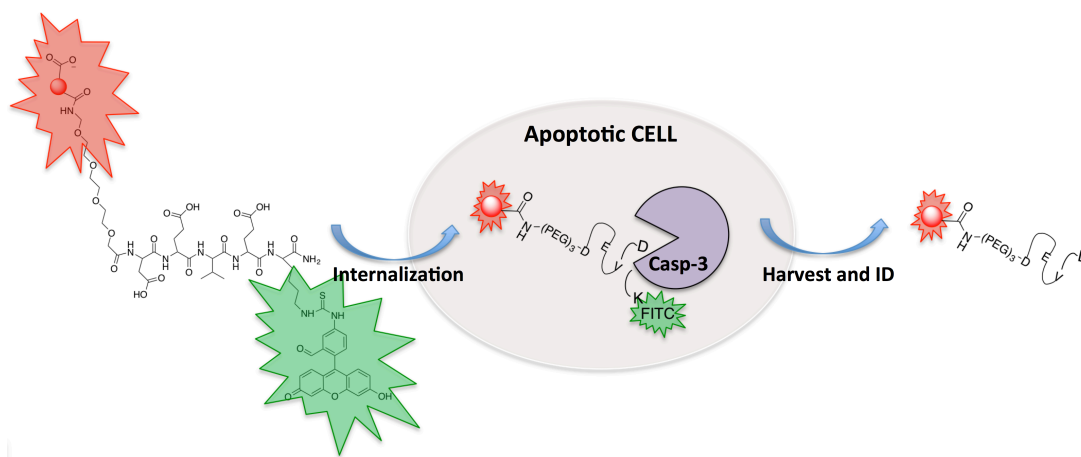
Figure 2.10 | Design of bead-fluorescent reporter. FITC dye was separated from the bead by a DEVD peptide chain. A rigid polyethylene glycol chain was included at the N-terminus of the peptide, to distance the cleavage site from the bead, allowing for protease accessibility. The PEG linker included a primary amine terminus, utilized for EDC coupling to carboxylate reactive sites on the bead surface.

Upon apoptosis induction with a lethal small molecule, we hypothesized active caspase 3 would detach the fluorophore from the bead though DEVD cleavage. A loss of fluorescent signal would distinguish the bead conjugated to a small molecule that caused apoptotic cell death from beads carrying inactive drug-like compounds; we hoped this loss of fluorescence would be distinguishable for sorting by fluorescence-activated cell sorting (FACS) so to allow for harvesting of the population for eventual barcode amplification and sequencing. Fluorescein isothiocyanate (FITC) was used as the fluorescent reporter of activity because it is a small molecule that would not greatly affect the size of the bead upon conjugation (unlike large fluorescent proteins, like GFP or RFP). Additionally, FITC has an excitation maximum of 490 nm, which corresponds with the 488 nm laser on our flow cytometer. Moreover, FITC has an emission wavelength of 535 nm, which is distinct from the bead fluorescence by microscopy and detectable by a unique emission channel on the flow cytometer. FITC is also a well-studied dye, amenable to facile peptide conjugation and functions appropriately for our flow cytometry studies at a much lower price tag than fluorophores with similar excitation and emission spectra (*i.e.,* Alexa dyes).

The fluorescent sensor was designed to have a primary amine terminus, by which we used a robust *N*-(3-Dimethylaminopropyl)-*N'*-ethylcarbodiimide (EDC) coupling for conjugation to the carboxylate handles coating the bead. The goal was to determine the lowest amount of peptide to the bead to maximize carboxylate 'parking area' for the barcode and small molecule components, yet a sufficient amount for clear detection of FITC fluorescence by flow cytometry for convenient distinction from unconjugated beads. In order to satisfy this requirement, it was necessary to include 0.001 equivalents

of fluorophore to 1 equivalent of carboxylate handle. Through the use of Beer's Law, the reaction efficiency of conjugation was calculated to be consistently 80%, regardless of scale (**Figure 2.11**)
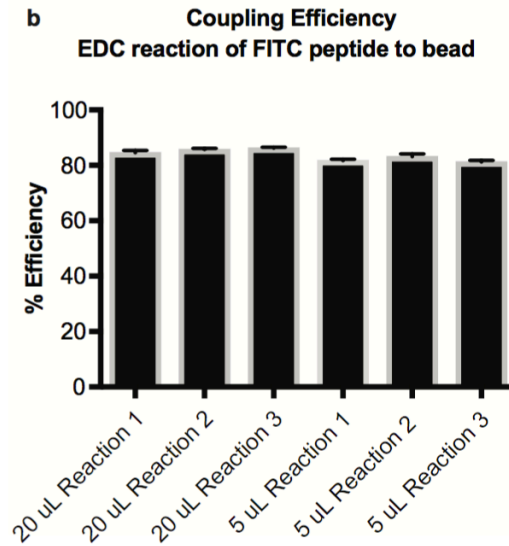
Figure 2.11 | Reaction efficiency of EDC conjugation reaction to create Bead-FITC. Supernatant taken after completion of the EDC coupling reaction was fit to a Beer's law curve. FITC concentration remaining in the supernatant was calculated using the molar absorptivity coefficient of the dye. Reaction efficiency was determined by subtracting the FITC concentration from the reaction without EDC (the whole amount of peptide included) from the remainder calculated after coupling.
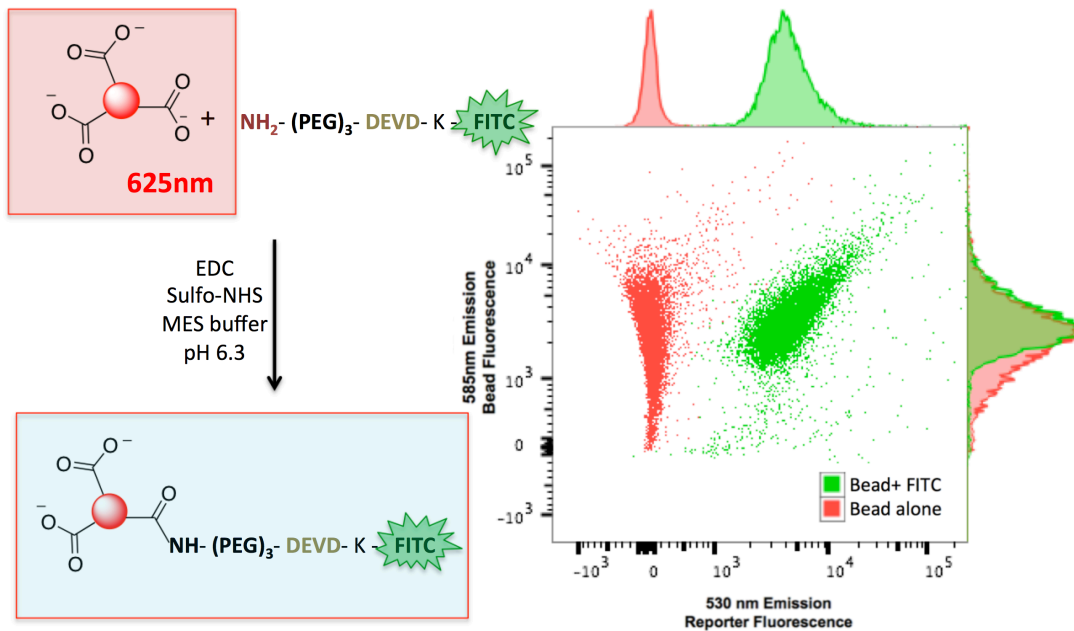
Figure 2.12 | FITC conjugation with silica bead. The primary amine terminus of the fluorescent reporter was covalently conjugated to the carboxylate coating on the bead by EDC coupling. Formation of the amide bond, and corresponding increase in 530 nm fluorescence intensity, was detected by flow cytometry. The FITC had no observable impact on the bead fluorescence, denoted by the overlay in histograms of Bead and Bead-FITC intensity on the 585 nm emission axis.

Incubation of the Bead-FITC system did not induce cell death, as viability experiments were conducted using CellTiter Glo luminescence assays (**Figure 2.5)**. This reagent was required for all bead-based cellular viability experiments, as it detects ATP presence. Alamar Blue or Presto Blue assays, where cellular viability is assessed by reagent reduction, gave false positive results in the presence of the carboxylate-coated

silica beads. Additionally, the Bead-FITC pair demonstrated association with HT-1080 cells after incubation at 37 °C for 6 hours.

Subsequent attempts to cleave the fluorophore from the bead by caspase 3 activation did not result in a detectable loss of signal, as there was no observable, distinct population after incubation with a purified, cleaved caspase 3 protein to enable its isolation (**Figure 2.13)**
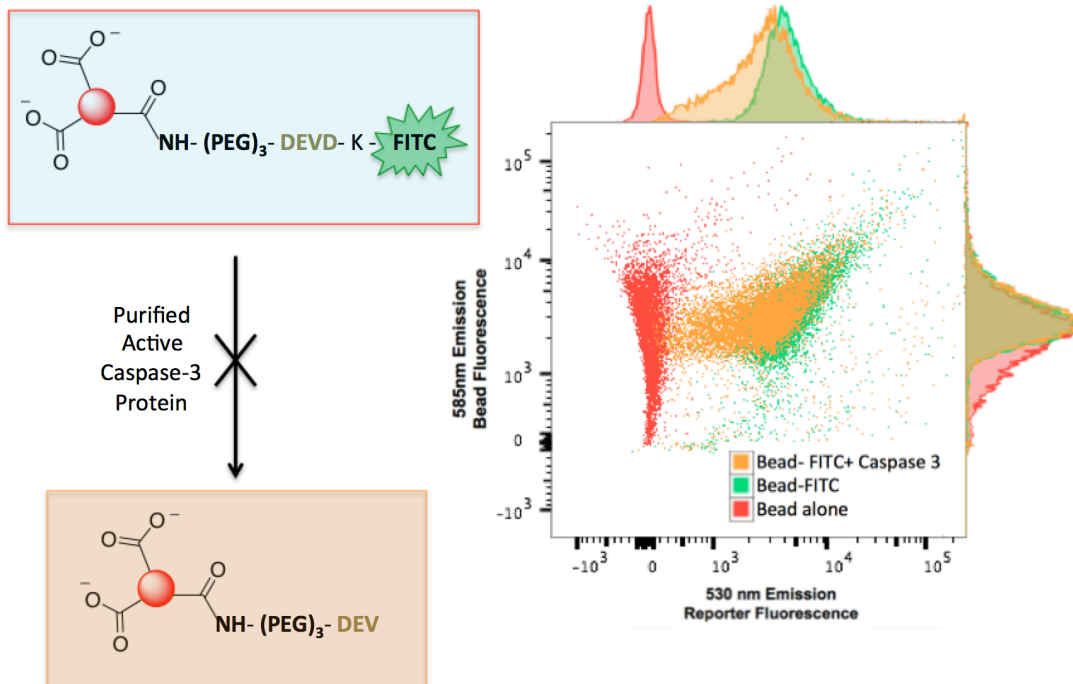
Figure 2.13 | Caspase 3 incubation with Bead-FITC. The Bead-FITC system was incubated with purified cleaved caspase 3 protein. Expected activity would be shown by a decrease in reporter emission intensity (x axis). After 2 h at 37 °C, there was no distinct loss of reporter fluorescence.

Fluorescent techniques have become a widely used and powerful tool to probe biological systems because of the sensitivity of their detection; a single fluorophore can generate many thousands of detectable photons. Moreover, the cycle of dye excitation and emission can be repeated many times for the same molecule. We attribute these fundamental characteristics of fluorescence to our inability to detect a loss of fluorescent signal; we hypothesize that the protease inefficiently cleaved the DEVD peptide, such that the residual, uncleaved dye had a fluorescence intensity comparable to the original, untouched Bead-FITC system (**Figure 2.14)**.

Starting material and product
fluorescence 'equivalent' intensity
in flow cytometry

Product shows increase in
fluorescence detectable
by flow cytometry
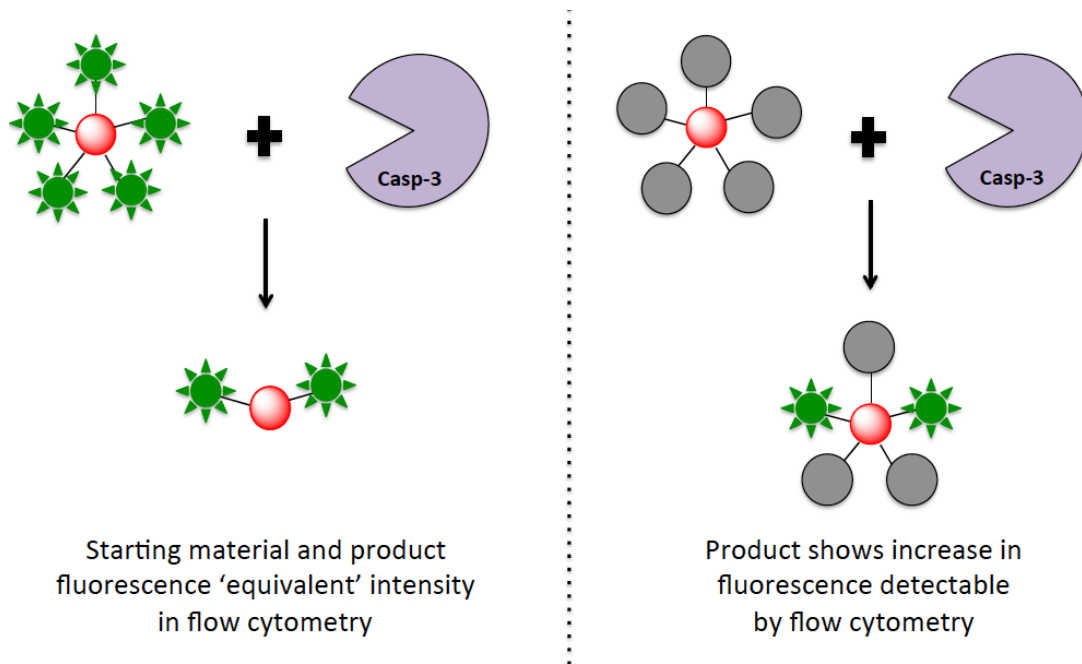
Figure 2.14| Design of new reporter system. Cartoon schematic representing our gain-of-sensor approach to use the sensitivity of fluorescence measurements to our advantage.

This observation motivated a new approach to the reporter design. Instead of scanning for a loss-of-fluorescence event to gauge biological activity, a gain-of-function event may be more sensitive for convenient measurement. To achieve this, the new reporter would include a small molecule quencher of fluorescent signal that would separate upon exposure to active proteases, yielding an increase in fluorescence detectable at assay completion (**Figure 2.15).**
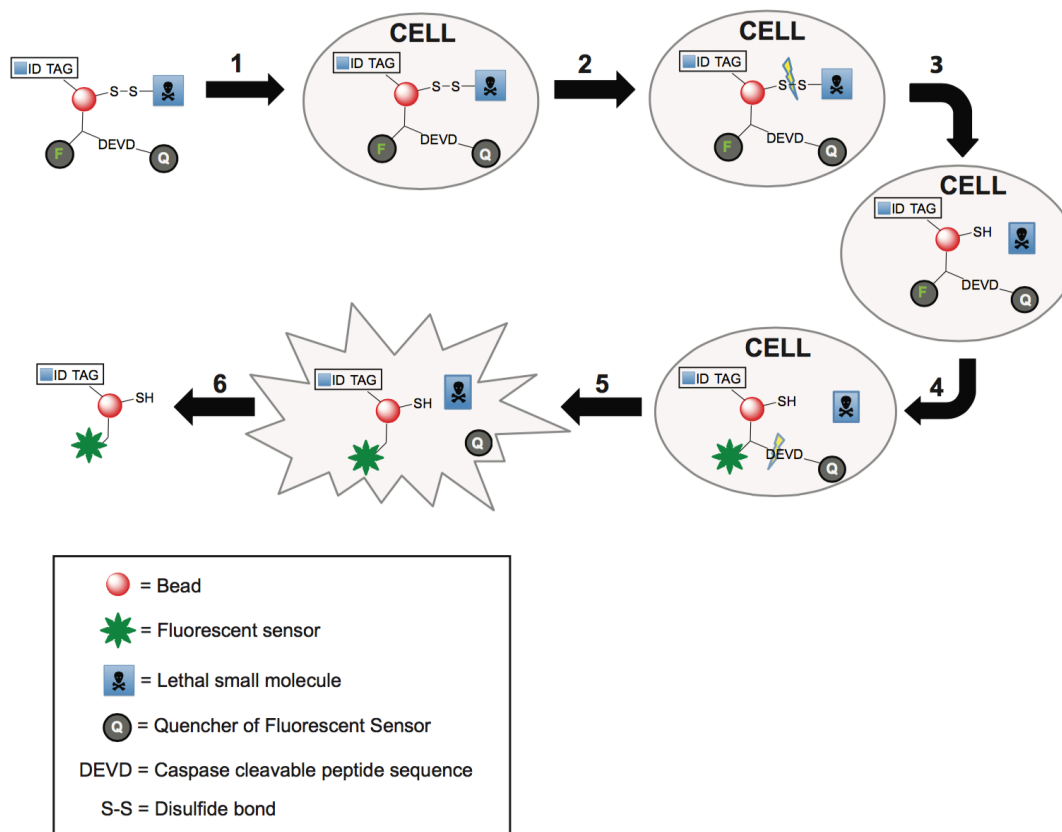
Figure 2.15 | Design of bead-based small molecule screening technology. (1) The technology, containing the covalently bound small molecule, identification tag, and activity reporter, is internalized by the cell. (2) Once inside the cell, the small molecule is released through the reduction of the disulfide bond linker. (3) The small molecule exists inside the cell without chemical modification. (4) If the small molecule causes apoptosis, activated caspases will cleave the DEVD peptide sequence linking the fluorophore to the quencher. (5) Loss of quencher results in loss of FRET (gain of fluorescent signal). (6) The activated system will be sorted based on this change in fluorescence, and the barcode will be sequenced to identify the small molecule that caused cell lethality. Red bead, silica microparticle; S-S, disulfide linker; blue square, lethal small molecule; green star, fluorescent dye.

2.2.4 *Design and analysis of FRET reporter*

To enable selection of small molecules that induce specific protease activity, the use of a FRET (Fluorescence Resonance Energy Transfer) sensor can be incorporated in our protease-reporter design (Edgington et al., 2011). The FRET phenomenon is a highly distance dependent effect, where the energy from an excited state fluorophore (the donor) is transferred to a nearby molecule (the acceptor), preventing the emission of a photon. The integrity of the FRET pair should be maintained in live cells and disrupted upon activation of a protease to yield a detectable change in fluorescence. We evaluated this concept initially with small molecules that cause cell death through apoptosis, continuing our study of caspase 3 activation as a biomarker.

Taking advantage of the distance-dependent FRET requirement, we placed the DEVD substrate between a FITC-Dabcyl FRET pair to create 'C3sensor' (**Figure 2.16**). Upon caspase 3 activation, the peptide should be cleaved, to increase the distance from the donor fluorophore (FITC) to the acceptor chromophore (Dabcyl). FRET pair separation should result in increased fluorescence signal of the FITC dye. Indeed, we found that the fluorescence intensity of FITC increased 15 fold when incubated with 0.5 units of purified active caspase 3 protein for 2 hours (**Figure 2.17**).

a Design of Fluorescent Reporter, Bead-C3Sensor
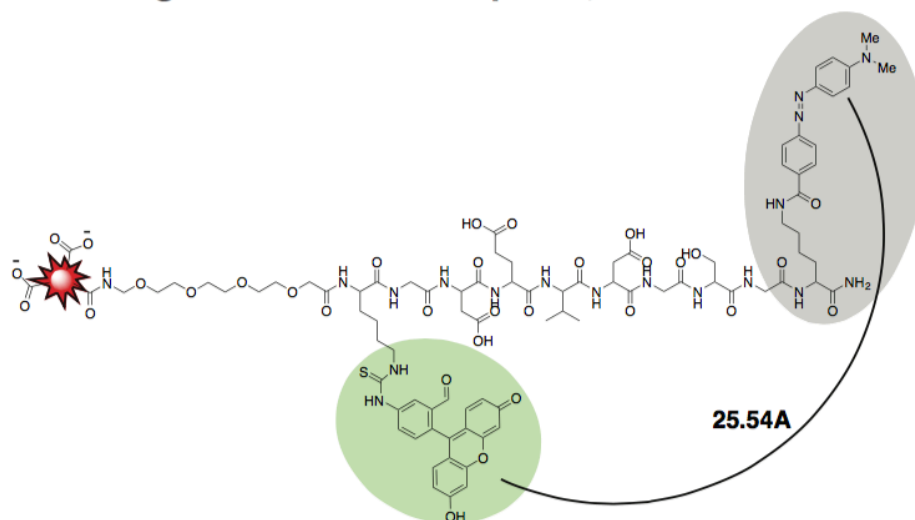
Figure 2.16 | Design of Bead-C3Sensor. The design of the fluorescent reporter includes the red fluorescent bead, covered in carboxylate groups. An amide linkage attaches the fluorescent reporter of biological activity, which includes a polyethylene glycol spacer to avoid steric obstruction of protease accessibility by the bead, a lysine amino acid with a FITC fluorescent moiety conjugated to the sidechain, a G*DEVD*GSG peptide sequence that incorporates the activate caspase 3 substrate, then finally a lysine residue differentiated with a dabcyl small molecule quencher attached to the sidechain. Molecular simulations reveal the fluorescent molecule is maximally separated from the dabcyl quencher by 25.54 angstroms, or roughly 2.5 nm—well within range to observe FRET quenching.
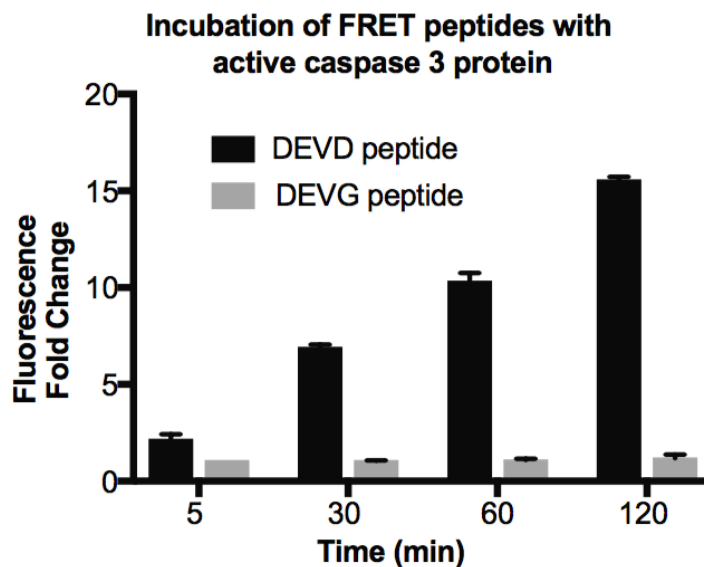
Figure 2.17 | Incubation of FRET peptides with active caspase 3 protein. The DEVG peptide sequence was synthesized to act as a control for caspase 3 cleavage; the exchange of an aspartic residue for a glycine residue eliminates the necessary amino acid after which the protease preferentially cleaves. The expected specificity was observed; a fluorescence fold change was increasingly observed for the DEVD FRET substrate, but absent in the control FRET pair.

The FRET-caspase sensor was conjugated to silica microparticles by an amide linkage via 1-ethyl-3-(3-dimethylaminopropyl)carbodiimide (EDC) coupling of the primary amino terminus to the carboxylate-bead coating. We designated this covalently linked reporter-bead complex as 'Bead-C3Sensor.' To ensure that the peptide was covalently bound to the bead, we analyzed the zeta potential of the microparticles. Zeta potential measurements assess the electrostatic potential of the surface of particles suspended in aqueous solution by tracking the movement of charged particles across an

53

applied electric field (Kirby, 2010). Similarly, charged particles in solution correlate to a large zeta potential, demonstrate stable colloidal dispersion, and low agglomeration of suspension. After conjugation, the zeta potential increased, demonstrating less repulsion between particles and thus supporting effective conjugation (**Figure 2.18**).

a

Zeta Potential of Bead-Based Technology

■ Bead Alone
■ Bead-C3Sensor
■ Bead-C3Sensor-Barcode
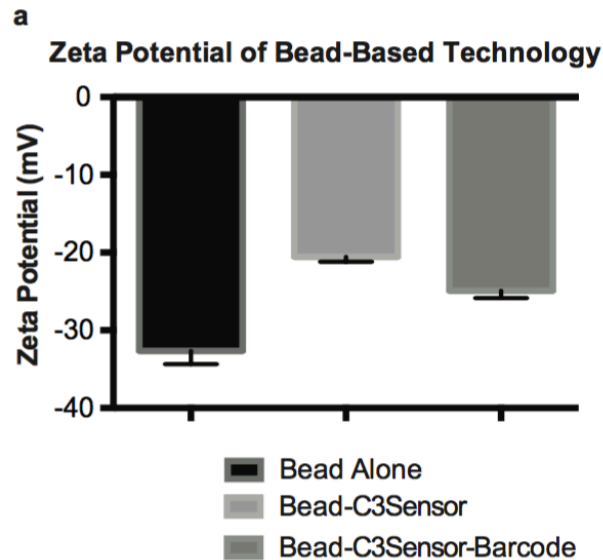
Figure 2.18 | Zeta potential measurement to assess covalent association of beads with sensor and barcode. Increase of zeta potential designates a loss of negative charge, observed upon sensor conjugation to the bead. An decrease in zeta potential relative to the Bead-C3Sensor occurs as a result of negatively charged oligonucleotides conjugated to the bead surface.

To examine cellular internalization of the microparticle-peptide system, a peptide labeled with fluorescent FITC without the dabcyl quencher was used as a control, which we had previously studied and characterized (outlined in the prior section) (**Figure 2.12**). The FITC-only containing peptide is equivalent to the cleaved product of the bead with the FRET pair exposed to caspase 3, and shows high fluorescent intensity at two emission

peaks corresponding to both the bead and the dye. This peptide fluorescence would be equivalent to 100% protease efficiency in cleaving each conjugated DEVD sequence. Fluorescence measurements demonstrated covalent attachment of the FITC-peptide to the bead, and confocal microscopy showed internalization of the peptide-bead system, Bead-FITC (investigated in the following chapter, **Figure 3.3**).

It is essential to distinguish the fluorescent reporter in the quenched FRET pair on beads from beads exposed to active caspase 3, so that flow cytometry can effectively separate each population. Ineffective separation would result in a high degree of false-positive hits. Flow cytometry analysis of the Bead-C3Sensor conjugated pair showed comparable FITC fluorescence intensity to the bead alone (**Figure 2.19**). Both of these populations were distinct from the Bead-FITC conjugated pair, which showed a distinct increase in fluorescence intensity on the reporter fluorescence detection channel (**Figure 2.19**).

After the Bead-C3Sensor was exposed to purified, active caspase 3 protein, there was a distinct shift to higher reporter emission fluorescence intensity when compared to the original, uncleaved FRET state (**Figure 2.20**b). When a gate that encompasses 93 +/- 2% of the native Bead-C3Sensor system (**Figure 2.20**a) was applied to the Bead-C3Sensor exposed to active caspase 3 protein, 70 +/- 7 % of the beads have increased reporter fluorescence sufficient to fall outside of the gate (**Figure 2.20**b). That population is the target for harvesting, and the barcode of those samples could be sequenced to identify apoptosis-inducing small molecules.
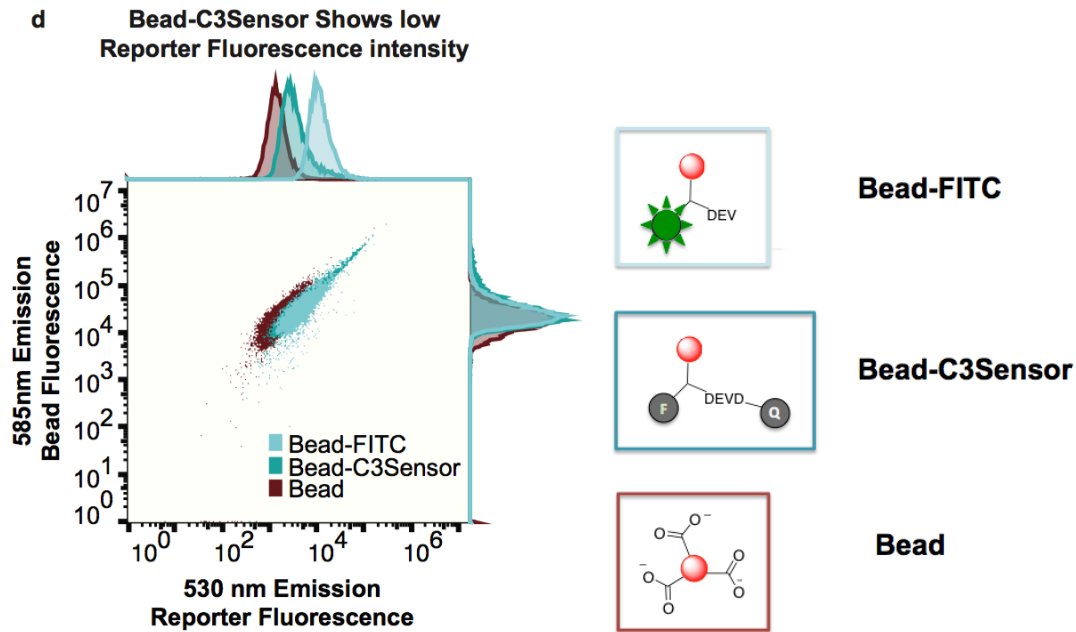
2.19 | Bead-C3Sensor demonstrates effective FRET. Flow cytometry data of the bead without peptide (red), the bead conjugated to FRET peptide: Bead-C3Sensor (dark blue) and the bead conjugated to the FITC peptide: Bead-FITC (light blue). 10,000 events were recorded for 7 different samples of each population. The bead emission detection signal (y-axis) stayed consistent between all populations, demonstrating the bead fluorescence was not altered. The reporter emission detection channel (x-axis) registers the FITC signal, and was quenched upon dabcyl addition. F test between FITC and FRET populations on the reporter emission detection channel = 0.26 (n = 7). Cartoons representing structures of the Bead, Bead-FITC, and Bead-C3Sensor are displayed.
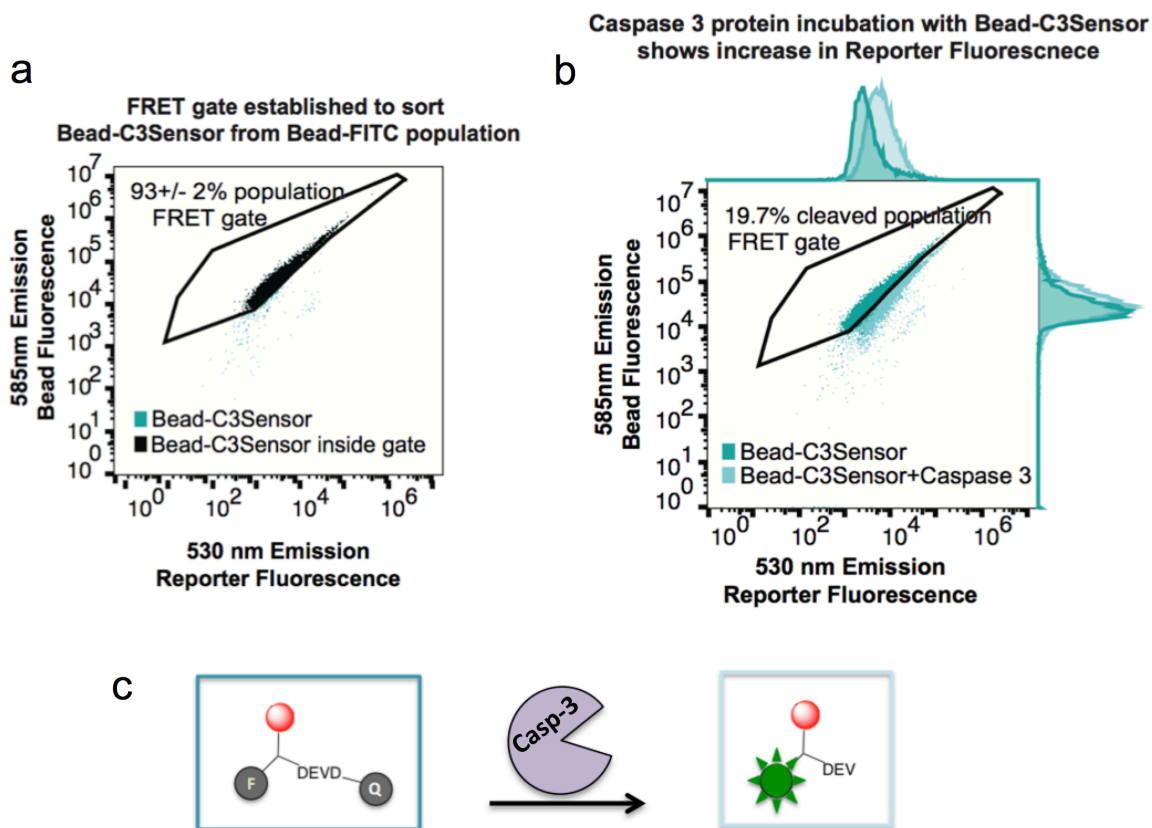
Figure 2.20 | Biochemical assay to assess FRET efficiency. (a) The FRET gate for FACS sorting. A gate (black) was included to encompass 93+/- 1.8% of the Bead-C3Sensor population (n = 8). (b) The FRET gate (black) is applied to the Bead-C3Sensor after 3 hour incubation with active caspase 3 protein. On average, the gate overlaps with 30 +/- 7.0% of the population (n = 10). The remainder of the sample (blue) will be harvested for barcode sequencing. On average, we can expect to sequence 70% of the lethal small molecule population. Overlay of the Bead-C3Sensor system with the Bead-C3Sensor + caspase 3 incubation shows a detectable difference in reporter fluorescence emission channel. (c) A cartoon representation of the biochemical assay. Bead-C3Sensor was subject to 1 unit of purified, active caspase 3 protein, which acts to cleave the DEVD sequence that bridges FRET pairs. An increase in reporter fluorescence is observed by a shift to higher fluorescence intensity on the 530 nm emission detector.

Cellular experiments were conducted, in which the Bead-FRET system was incubated with HT-1080 fibrosarcoma cells for 6 hours before addition of 1 μM staurosporine. Staurosporine is a broad kinase inhibitor well-established to induce apoptosis by caspase 3 activation (Johansson et al., 2003). After 24 hours, the entire flask was harvested, concentrated, and resuspended in lysis buffer to remove all beads from cells, as the final pooled screening procedure would require to accommodate barcode amplification. The entire sample was analyzed by flow cytometry. There was no observed change in the reporter fluorescence population of the beads **(Figure 2.21).** We hypothesize this is because the bead system does not have access to the cytosol, and therefore the reporter will not co-localize with caspases to report on their activation. This concept will be further investigated in the following chapter.
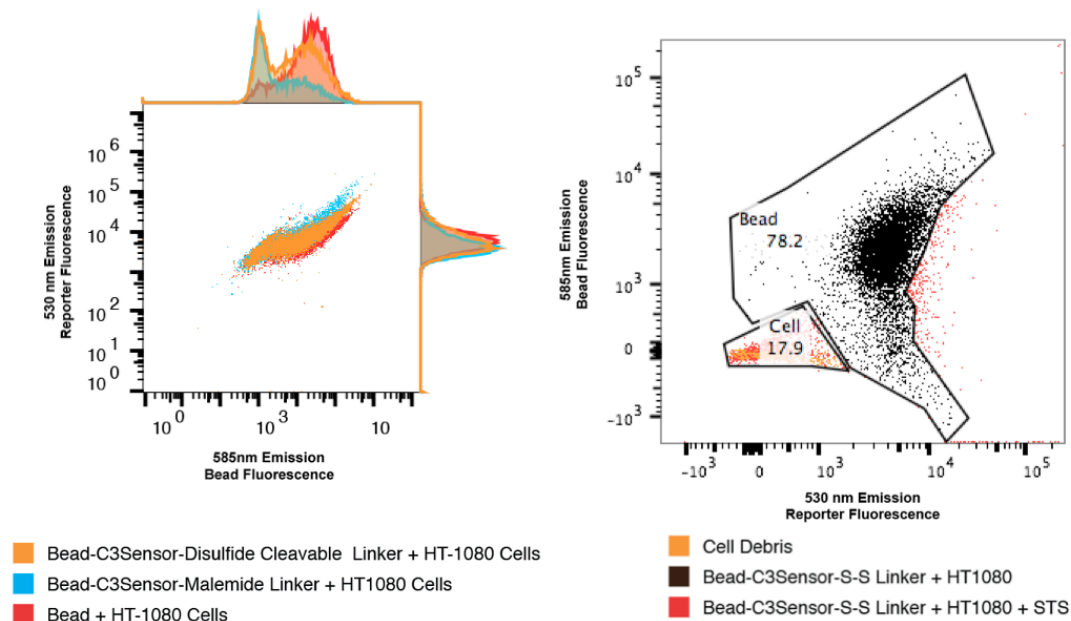
Figure 2.21 | Incubation of bead FRET system with cells and analysis after apoptosis. Beads conjugated to the C3sensor and two distinct small molecule linkers were incubated with HT-1080 cells, and displayed cellular uptake by flow cytometry. After 6 h incubation with beads, the HT-1080 medium was exchanged for medium containing 1 µM staurosporine. After 24 h incubation, the entire sample was collected, lysed, and subjected to analysis by flow cytometry. A gate encompassing Bead-C3Sensor- small molecule linker (black) based on 585 nm vs 530 nm fluorescence was applied to the scatterplot of the staurosporine incubated sample. A right shift (red) to higher 535 nm fluorescence intensity indicates the population where the C3Sensor was cleaved as a result of caspase 3 activation; there was no noticeable loss of FRET signal, denoting the C3Sensor did not report on the apoptosis that had occurred.

2.3 Discussion

The technology design herein outlines our approach to create a pooled small molecule screening technology. The identification of an appropriate delivery vehicle and determination of a FRET-based component to report on the biological activity of the small molecule under examination were discussed.

A 1 μm, red fluorescent silica bead coated with carboxylate groups demonstrated satisfactory fulfillment of each of our requirements initially outlined for an adequate delivery vehicle for the technology. The bead itself does not affect cell viability, yet the silica material and bead fluorescence can withstand a wide array of organic reaction conditions and cellular physiological changes that occur as a response to chemically induced lethality. A 1 μm diameter is small enough for cellular uptake, yet provides an acceptable surface area for chemical diversification. Bead fluorescence provides a convenient property for particle tracking throughout the duration of the assay and useful distinction from cellular debris for harvesting upon assay completion. The carboxylate moiety provides a robust handle, by which synthetic modification is convenient and amenable to oligonucleotides, peptides, and small molecules.

Next, we designed a fluorescent reporter of small molecule activity. We learned that detection of a gain-of-fluorescence event was a more successful metric than the initial loss of signal approach, emphasizing the potential of fluorescence sensitivity to detect biomarkers of cellular processes. When conjugated to the bead, the FRET-based reporter shows a distinct signal after exposure to enzymatic activity specific to apoptotic cell death. The reporter design provides initial insight into the 'hit' small molecule's mechanism of action, giving this pooled screen an additional, distinct advantage over

traditional phenotypic assays. Additional refinement is necessary for application to cell based assays, but the experiments outlined establish a foundation for further elaboration.

As summarized in this study, this technology can be applied to discover cytotoxic small molecules that specifically initiate cell death by apoptosis. We envision that the system can be tuned and applied to wide-ranging, diverse cell models and biochemical processes as a drug and probe discovery tool. The peptide linker of the reporter can be modified to report on other proteases, protein-protein interactions, transcription, or other biological events.

2.4   Methods

Polystyrene Bead incubation with cells.

FluoroSpheres Carboxylate-Modified Microspheres, Red fluorescent (580/605 nm) 2% solids, diameter ranging from 0.1 µm – 2 µm, were purchased from ThermoFisher (Waltham, MA, USA, Product Number F-8887). HT-1080 (fibrosarcoma) cells were obtained from American Type Culture Collection (Manassas, VA, ATCC CCL-121). HT-1080 cells were grown in DMEM High-glucose medium supplemented with 1% non-essential amino acids (Mediatech, Product Number 10-013-CM) 1% P/S, and 10% heat-inactivated fetal bovine serum (FBS). All the cell lines were grown at 37 °C under 5% CO_2 and harvested at 80% confluence for experiments. Uptake experiments were completed in 6 well plates (Corning costar (Corning, NY, 3516). 200,000 HT-1080 cells were plated per well and let adhere overnight at 37 °C under 5% CO_2. Before use, beads were washed with deionized water twice by adding 1000 µL water to 20 µL beads,

sonicating (15 seconds), vortexing, centrifuging for 5 minutes at 14800 rpm (16162 xg) and removing the supernatant. 10 µL of 1:1000 dilution of beads to media were added to each well of cells. After six hour incubation with beads at 37 °C, the cells were washed twice with PBS, harvested with 0.25% Trypsin-EDTA (1X) Phenol red (Invitrogen (Carlsbad, CA, 25200-114)), resuspended in growth medium, and strained by a 70 µm filter (Fisher Scientific, 352350) into Eppendorf tubes for flow analysis.

Flow Cytometry experiments.

Flow cytometric analysis was assessed on an Accuri C6 Flow Cytometer with a 488 nm Laser. The 530/30nm filter (FL1) was used for FITC discrimination and the 585/40nm filter (FL2) was used for bead identification. Using a live cell gate on DMSO treated cells, 10,000 events were recorded for each population.

Silica bead incubation with cells.

Red (540/625 nm) fluorescent, non-magnetic, monodisperse, carboxylate coated screenCORE microspheres were purchased from Chemicell (Berlin, Product Number 6101-1) HT-1080 (fibrosarcoma) cells were obtained from American Type Culture Collection (Manassas, VA, ATCC CCL-121). HT-1080 cells were grown in DMEM High-glucose medium supplemented with 1% non-essential amino acids (Mediatech, Product Number 10-013-CM) 1% P/S, and 10% heat-inactivated fetal bovine serum (FBS). All the cell lines were grown at 37 °C under 5% CO_2 and harvested at 80% confluence for experiments. Uptake experiments were completed in 6 well plates (Corning costar (Corning, NY, 3516). 200,000 HT-1080 cells were plated per well and let

adhere overnight at 37 °C under 5% CO_2. Before use, beads were washed with deionized water twice by adding 1000 µL water to 20 µL beads, sonicating (15 seconds), vortexing, centrifuging for 5 minutes at 14800 rpm (16,162 x g) and removing the supernatant. 10 µL of 1:1000 dilution of beads to media were added to each well of cells. After six hour incubation with beads at 37 °C, the cells were washed twice with PBS, harvested with 0.25% Trypsin-EDTA (1X) Phenol red (Invitrogen (Carlsbad, CA, 25200-114)), resuspended in growth medium, and strained by a 70 µm filter (Fisher Scientific, 352350) into Eppendorf tubes for flow analysis.

Bead incubation with different solvents

Beads were washed twice by adding 1000 µL deionized water to 20 µL beads, sonicating (15 seconds), vortexing, centrifuging at 14800 rpm (16162 xg) and removing the supernatant. Beads were resuspended in 20 µL deionized water by sonication, and 1 µL of the resulting suspension was added to 1000 µL solvent (DMSO, DMF, etc.). The mixture was vortexed, sonicated, and left to incubate at room temperature for 72 h before flow cytometry analysis and dynamic light scattering experiments.

Confocal fluorescence imaging

Coverslips with HT-1080 cells incubated with beads (procedure described above) were washed with PBS and fixed with 4% paraformaldehyde at room temperature for 10 minutes. After 3 washes with PBS, the cover slips were mounted on slides using ProLong Diamond Antifade Mountant with DAPI (Thermo Fisher (Rochester, NY, P36966)). Confocal images were taken with a Zeiss AxioOberever LSM700 at 63x and the Z Stacks

were compressed with Zen software. Analysis was done using ImageJ (National Institutes of Health, Bethesda MD). All pictures are a single confocal section imaged eight to twelve times to reduce noise.

Synthesis of Bead-FITC and Bead-FRET

All chemicals were obtained from Sigma Aldrich and used without further purification. This procedure was performed open to the atmosphere. 20 µL beads (Chemicell (Berlin, Product Number 6101-1)) were washed with 0.1 M MES buffer (pH 6.3) by centrifugation at 14800 rpm (16,162 x g) for 5 min, removing the supernatant, re-suspending in buffer, and centrifuging again. The bead pellet was re-suspended in 85 µL *N*-hydroxysulfosuccinimide sodium salt (sulfo-NHS) (10 µM in MES buffer), 0.68 µL peptide (5 mM, 0.001 equiv to carboxylate on bead surface), then 42.5 µL *N*-(3-dimethylaminopropyl)-*N*′-ethylcarbodiimide (EDC) (100 mM in MES buffer). The reaction was shaken at 37 °C overnight before washing five times with water, then four times with 0.5% Triton-X. Fluorescence of the supernatant of the final washing (494 nm excitation, 525 nm emission) was recorded to ensure no unconjugated fluorophore remained with the beads.

The absorbance of bead-FITC-coupling reaction supernatant was measured at 494 nm to assess peptide coupling efficiency. Concentration was calculated using the Beer-Lambert law(Swinehart, 1962). % Coupling efficiency = ([FITC Reaction] – [FITC Supernatant]) / [FITC Reaction] x 100.

Cell viability experiments

Assay plates were prepared by adding 1,000 HT-1080 cells per well in 35 µL of growth media to opaque white 384 well plates (PerkinElmer (Waltham, MA, 6007688). After adhering to the plate overnight, growth medium was removed from the cells and replaced with 35 µL lethal molecule or beads in a two-fold dilution series. After 24 hours in the incubator, CellTiter-Glo Luminescent Cell Viability Assay (Promega (Madison, WI, G7573) was completed. Percent viability was calculated using cell luminescence intensity values determined from a Victor 3 plate reader (PerkinElmer).

Biochemical assay for FRET detection: FRET peptide before conjugation to bead

1.5 units of purified, active caspase 3 protein (Abcam (Cambridge, MA, ab52101)) were added to 1 µL 10 mM DEVD- FRET peptide or DEVG-FRET peptide (uncleavable control) and 97.5 µL Apo-One buffer (Promega (Madison, WI, G7791)). The solution was split into 3 wells of a Corning 385-well black with clear bottom plate (Corning, NY, Product number 3764), each containing 30 µL of the mixture and kept at 37 °C between timepoints. Before each time point analysis, the plate was shaken for 15 seconds. Wells were analyzed for fluorescence (490 ex/535 em) on the Tecan Infinite M100 PRO multimode reader (Mannedorf, Switzerland) with a constant gain set to 100.

Biochemical assay for FRET detection: Bead-C3Sensor

0.5 units of purified, active caspase 3 protein (Abcam (Cambridge, MA, ab52101)) were incubated with 2 µL of beads in 100 µL Apo-One buffer (Promega (Madison, WI, G7791)) for two hours at 37 °C. The beads were washed twice with MilliQ water and resuspended in MilliQ water for flow cytometry analysis.

Chapter 3

Technology synthesis and cell-based analysis of system

3.1   Introduction

The third component of the pooled screening technology includes development of the small molecule identification tag. Barcoding by amplifying and sequencing oligonucleotides has demonstrated success in DNA encoded small molecule libraries (Clark, 2010) and pooled screens of genetic reagents (Wong et al., 2016). Based on this precedence, an oligonucleotide barcode could be applied and designed to fit the needs of the pooled small molecule screening technology.

The success in the application of this pooled screening technology to cellular systems largely relies on the capability of the bead to efficiently deliver the small molecule once inside a cell and then effectively report on the compound's activity. As the elaborated technology is applied to cellular systems, it is important to consider the mechanism by which the technology is internalized.

Macromolecules and other large particles enter the cell primarily through endocytosis. Endocytosis is an active process that involves an area of the plasma membrane engulfing the external material, then budding off to form a vesicle containing the ingested material. This uptake vesicle, or endosome, contains a mildly acidic pH that eventually matures to become a lysosome, which is an acidic compartment that houses hydrolytic enzymes to digest its components.

Thus, a limiting step in achieving an effective biological based screening technology is to facilitate escape from the endosome to ensure cytosolic delivery of the system before its lysosomal degradation. This challenge is recognized, and strategies taken to address this obstacle are discussed.

3.2   Results

3.2.1 Barcode design

For sufficient identification of one type of small molecule from a pool of diverse chemicals, each barcode must be unique to each small molecule structure, show no bias in PCR amplification, stay covalently bound to the bead throughout the assay, and be sequenced to reveal a statistical distribution of 'hits'. We developed oligonucleotide barcodes consisting of 45 unique base pair sequence flanked by forward and reverse primer regions (Appendix A, **Table A2**). Each distinct barcode sequence used the same set of primers, so multiple 'hit' small molecules out of the pool could be equally amplified and identified. The primer design includes an overhang region with a sequence compatible with existing DNA sequencing technology. Next generation sequencing

strategies provide a scalable means to directly apply this prototype to large libraries of oligonucleotides.

Prototype DNA barcodes were synthesized and attached to beads through an amide linkage after reaction with its terminal primary amine on the 5' end. Next, a nitrobenzyl, photocleavable linker was included in the barcode design **(Figure 3.1**a**),** which we found necessary to increase PCR efficiency. Upon irradiation with near-UV light (300 – 350 nm range to avoid DNA damage), cleavage of the DNA from the bead was observed after 10 minutes **(Figure 3.1**b**).** This cleavable linker was included to make PCR amplification of the oligonucleotide more efficient after isolation of the bead, as we found that PCR amplification was inefficient on beads: lack of amplification was observed when the oligonucleotide remained bound to the bead and can likely be explained by steric hindrance of the bead to the polymerase. The bulky bead may block the polymerase from binding to the oligonucleotide, preventing DNA extension. Two unique barcodes were initially used for a proof of principle to ensure effective primer binding to more than one sequence **(Figure 3.1**b**)**. Once the barcode was conjugated to the bead, the system was incubated for 24 h with the lysate of cells that were undergoing apoptosis. Despite protease activation and other environmental changes that occur during the programmed death pathway, the oligonucleotide was effectively PCR amplified after photo cleavage from the bead **(Figure 3.1**c**)**. This suggests the bead-barcode conjugated pair can persist throughout the entirety of the screen for small molecule identification, a key feature of a pooled small molecule screening system.

a **Design of barcode linker to bead**

$H_2N-(CH_2)_{12}-O$ ... O=P-OH ... Oligonucleotide Barcode 3'

NO$_2$
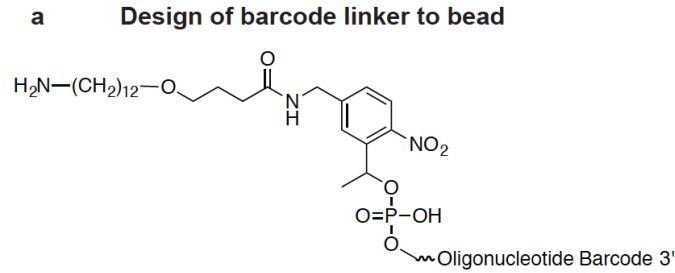
b **PCR of barcodes linked to bead**

FW Primer	+	+	+	+	+	+	+	+	+
RV Primer	+	+	+	+	+	+	+	+	+
Barcode 1	-	+	-	+	-	+	-	+	-
Barcode 2	-	-	+	-	+	-	+	-	+
Bead	-	-	-	-	-	+	+	-	-
Bead Wash Supernatant	-	-	-	+	+	-	-	-	-
365 nm light irradiation	-	-	-	-	-	-	-	+	+

c **PCR of Bead-Barcode after incubation with apoptotic cell lysate**

FW Primer	+	-	+	-	+	+	+
RV Primer	+	+	-	+	-	+	+
Barcode 2	-	-	-	+	+	+	+
365 nm light irradiation	-	-	-	-	-	+	+
Live cell lysate	-	-	-	-	-	+	-
Apoptotic cell lysiate	-	-	-	-	-	-	+

Figure 3.1 | Small molecule identification tag, design and amplification. (a) Design of barcode component. (b) Electrophoresis DNA gel after PCR amplification of the barcode. The photocleavable linker was necessary for adequate amplification. Using similar thermocycler conditions and identical primers, barcodes of different sequences were amplified with similar efficiency. There is no bias observed for one sequence over the other. (c) Electrophoresis DNA gel after PCR amplification of the barcodes incubated with cell lysate. A band at the appropriate molecular weight marker is observed, demonstrating that the oligonucleotide sequence is maintained throughout lysis conditions and exposure to enzymes and cellular components present during cell death by apoptosis.

3.2.2 *Bead-Barcode-Sensor system synthesis and characterization*

The first step of integrating all of the components of the system involves differentiating a portion of the surface of the bead with a functionality to react with the small molecule. We sought a high concentration of each small molecule to be bound to each bead, to maximize the ultimate cellular concentration achieved. When using 0.5 equivalents of mono-Boc protected diamine per one equivalent of carboxylate group on the bead surface, there is a large enough concentration of unreacted carboxylate handles on the bead for effective conjugation and detection of the barcode and fluorescent reporter, but the majority of chemical space on the bead surface will be unreactive to these moieties, having been coupled to the protected diamine. It is thus inert to the subsequent EDC couplings and reserved for small molecule attachment. Deprotection of the Boc moiety to reveal a primary amine was possible with concentrated trifluoroacetic acid because the silica bead withstands strong acid and the more sensitive groups (peptide, oligonucleotide) not yet attached. Facile coupling of 3-(2-pyridyldithio)propionic acid *N*-hydroxysuccinimide ester (SPDP) to the newly differentiated bead surface yields a pyridine- disulfide moiety that withstands the chemistry to attach the oligo and fluorophore, yet will react during a simple and robust thiol-sulfide exchange reaction to attach the lethal small molecule to the bead in the last step. The disulfide bond attachment designed for release in the cytosol is established for future study of technology in cell culture

Zeta potential measurements confirmed covalent coupling of both the sensor and the barcode to the bead during the one-pot EDC reaction. The addition of the oligonucleotide to the bead-peptide conjugate made the zeta potential slightly more

negative (previous chapter, **Figure 2.18**)). Additionally, dynamic light scattering showed

an increase in particle size upon barcode attachment (Jiang and Chen, 2013) (**Figure 3.2**).
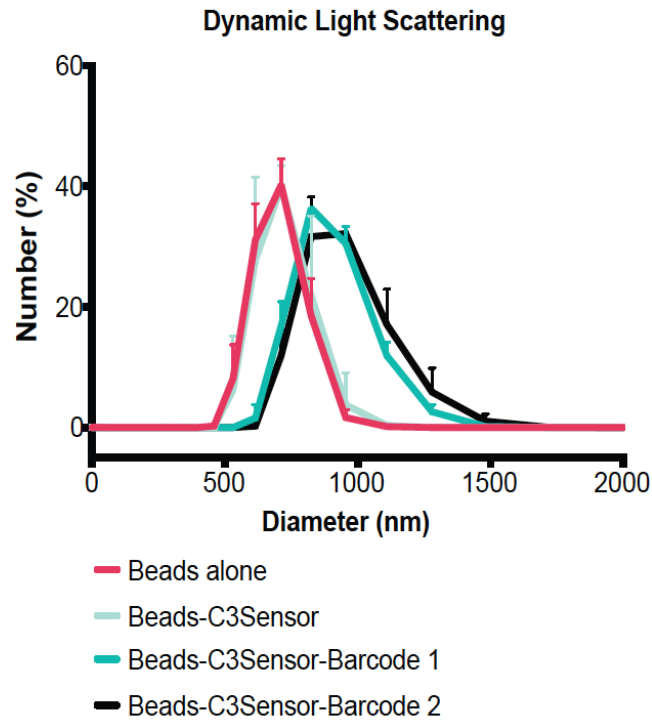
Figure 3.2 | Dynamic light scattering experiment shows size increase upon addition of the barcode to the bead.

Confocal microscopy showed internalization of this bead-dye-oligo reagent (**Figure 3.3**a and b), and that this system was not lethal to HT-1080 cells after 48 h incubation (**Figure 3.4**). Amplification of the barcode was possible after conjugation, demonstrating that simultaneous, one-pot coupling with the sensor, after first differentiating about half of the carboxylate groups on the bead to reserve enough space for eventual lethal molecule addition, did not affect ability for barcode sequencing. Additionally, caspase 3 protein incubation with the elaborated system showed detectable loss of FRET by flow cytometry.

a **Confocal image of Bead-FITC-Barcode incubated 6 h with HT-1080 cells**

b **Z-stack slices show Bead-FITC-Barcode is internalized**
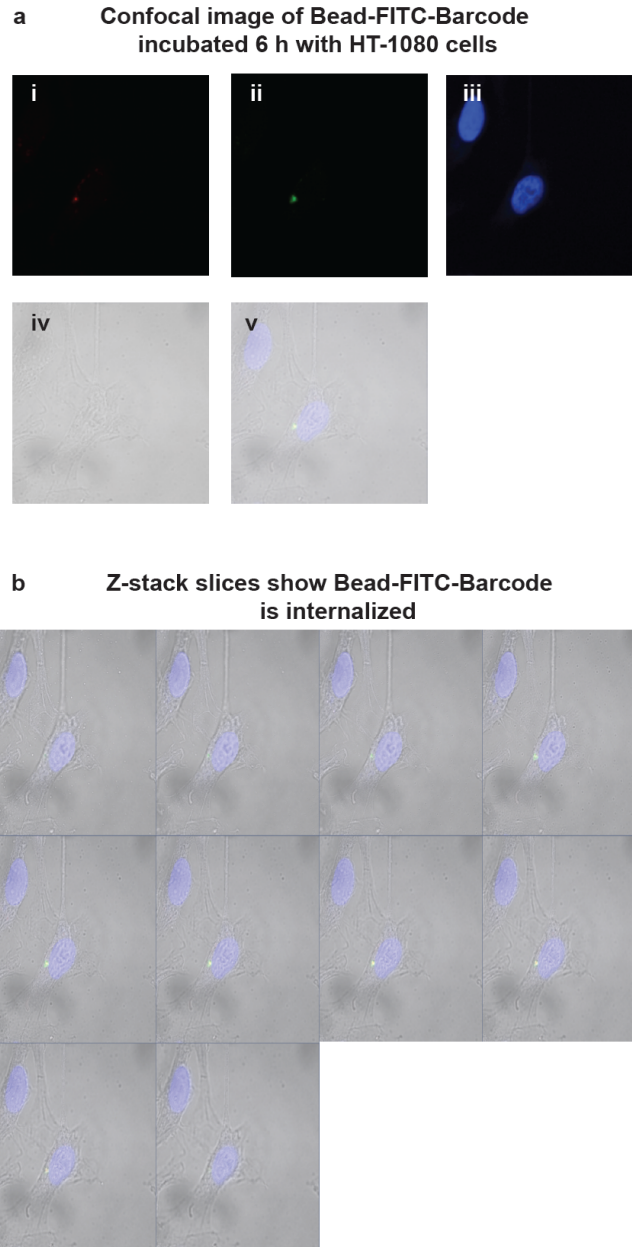
Figure 3.3 | Bead-FITC-Barcode internalization by HT-1080 cells. (a) Confocal microscopy internal slice of Z-stack image, after Bead-FITC-Barcode technology incubation with HT-1080 cells for 6 hours. (i) Bead fluorescence in red bandpass filter. (ii) FITC fluorescence of FITC-peptide conjugated to bead in green bandpass filter. (iii) Transmitted light. (iv) DAPI (v) Overlay. (vi) Full Z-stack overlay image. (b) Slices of Z-stack produced by confocal microscopy of Bead-FITC-Barcode technology with HT-1080 incubation. Yellow overlay shows co-localization of Bead-FITC signal. Outermost slices show no Bead presence, supporting the observation that the cell internalizes the bead.
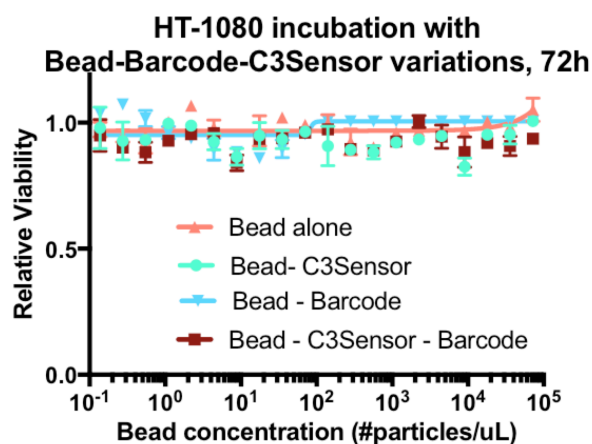
Figure 3.4 | Cell viability experiment with elaborated beads. HT-1080 cells incubated for 72 h with varying concentrations of bead conjugated to the barcode and fluorescent reporter show no decrease in cell viability.

3.2.3 Small molecule addition to complete system synthesis

The final component of the small molecule pooled screening technology required is covalent attachment of test small molecules. The small molecules should detach from the bead only once the system is internalized into cells. We first examined the utility of the potentially glutathione-reductase-rich environment of the cytosol to employ a disulfide-bond linker to connect the bead to the small molecule (**Figure 3.5**a). Although a covalent bond is maintained outside of the cellular environment, once internalized, the disulfide bond should be reduced to cleave the small molecule from the cell. Once inside the cell, the small molecule should not contain any additional chemical modifications that can alter its biological activity.

The lethal small molecule used for this proof of concept experiment was the microtubule inhibitor mertansine (DM1). DM1 was chosen because of its potency (4.6

74

nM in HT-1080 cells) to induce apoptosis. Additionally, DM1 possesses a terminal thiol moiety in its active state, thus simplifying the model by eliminating the need for a self-immolative linker. The chemistry used to covalently attach the known lethal molecule is outlined in **Scheme 3.1**.
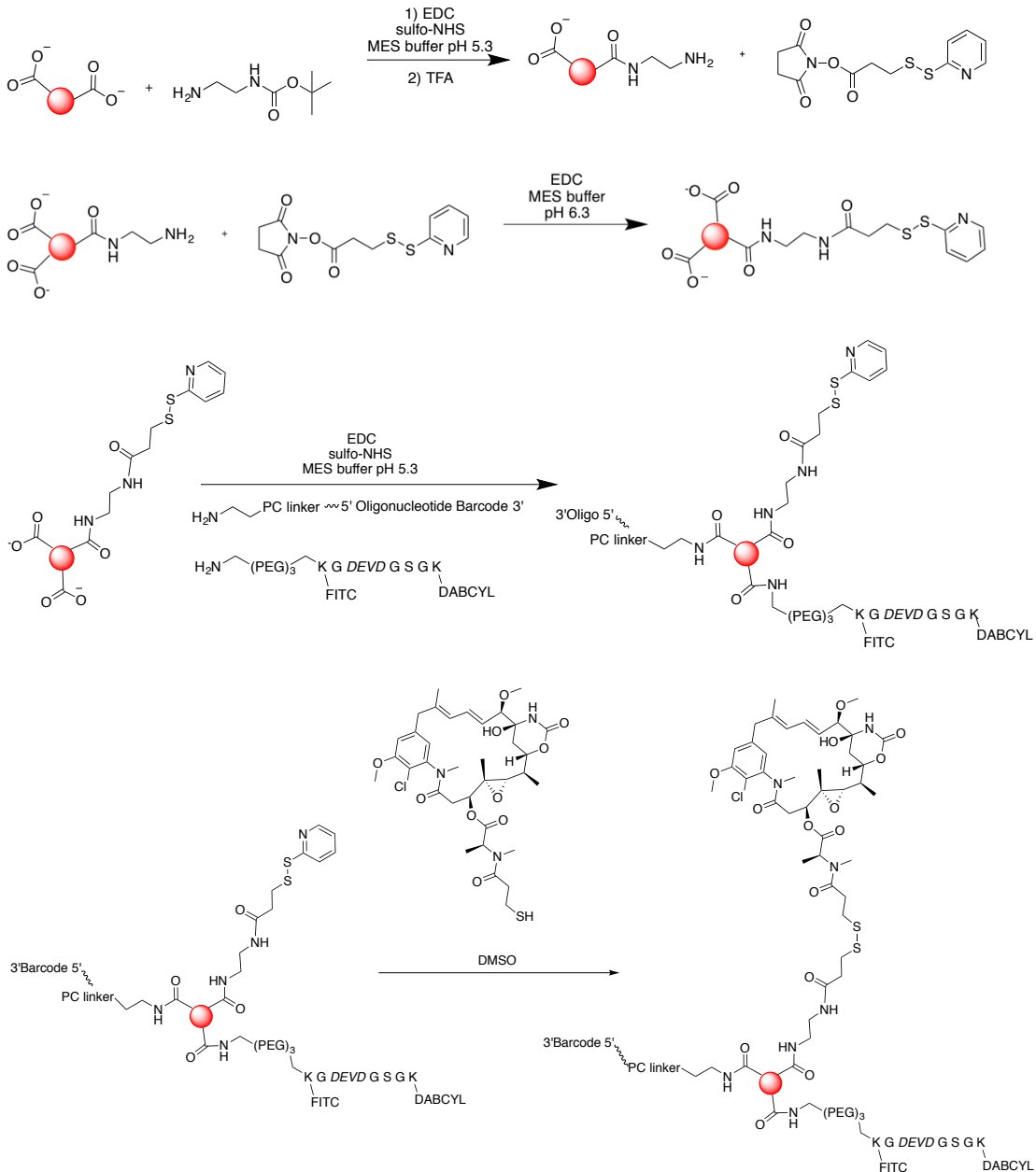
Scheme 3.1 | Technology synthesis. Instillation of the handle to connect the small molecule is added first, followed by one-pot EDC conjugation of the fluorescent sensor and barcode. The small molecule is conjugated as the final step.

To test the release of active small molecules in cells, we also synthesized a non-cleavable, thioether linker using maleimide bioconjugation chemistry to control for disulfide bond reduction and release of the small molecule after bead uptake **(Figure 3.5**b). However, we did not see cytotoxicity with either cleavable or non-cleavable small molecule-bead conjugated system **(Figure 3.5**d), suggesting cellular reductases could not release the compound from the disulfide linker.

This observation, combined with the lack of FRET dissipation upon incubation with cells undergoing apoptosis, supports the notion that the bead system does not have access to the cytosol upon internalization.

a Bead- Disulfide linker - DM1
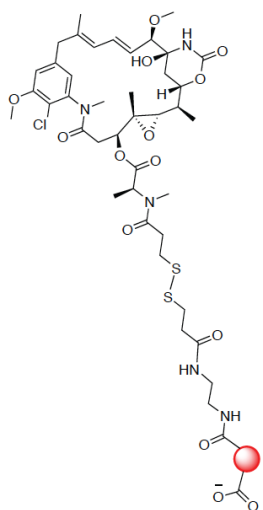
b Bead- Malemide linker - DM1
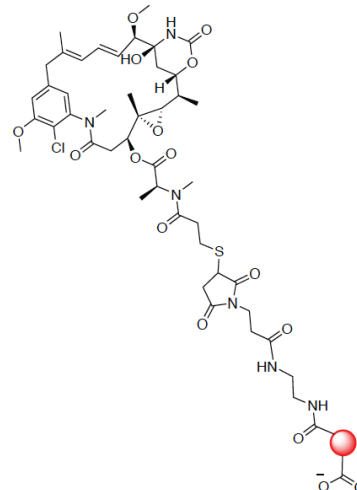
c

Bead + Lethal Molecule + HT1080 incubation, 36h
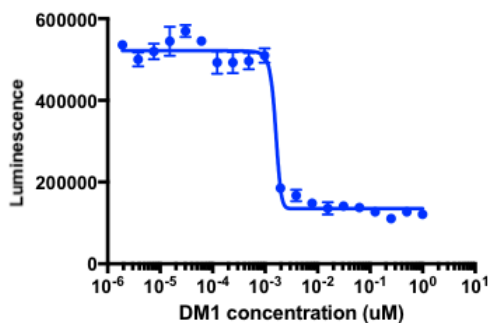
d

Bead + Lethal Molecule + HT1080 incubation, 36h

DM1
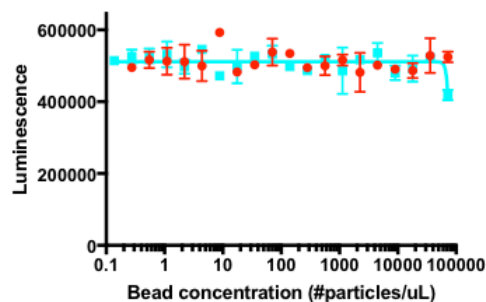
BPMS DM1 (CH2-CH2)
SPDP DM1 (S-S)

Figure 3.5 | Design of small molecule component. (a) Structure of Bead-Disulfide linker-DM1. (b) Structure of Bead-thioether linker-DM1. (c) Dose response curve of HT-1080 when incubated with constant excess 1 μm, carboxylate coated silica beads (Chemicell) and unconjugated DM1 in two-fold dilution concentration increments. An EC_{50} of 4.6 nm was observed. (d) Upon conjugation of DM1 to the bead with a disulfide bond sensitive to cytosolic reduction (SPDP DM1, blue), no cell lethality was observed after 36 h treatment with HT-1080 cells. The thioether linker (BPMS DM1, red) was synthesized through maleimide Michael addition chemistry to serve as a stable conjugate control for disulfide bond cleavage, preventing DM1 liberation from the bead.

Extracellular particles must cross the cell's plasma membrane in order to be internalized. This outer surface layer acts as a barrier separating interior cellular components from the environment. Large external particles are often trafficked across this barrier through a process called endocytosis. This active, actin-based process of ingestion begins by the movement of an area of the plasma membrane to surround the extracellular material. Eventually, the lipid bilayer completely engulfs the particle and buds off to create new intracellular vesicle containing the internalized matter. Pathways of endocytosis can be classified as (1) receptor-mediated endocytosis (which includes caveolae- and clathrin-mediated mechanisms) (2) pinocytosis, a non-specific pathway by which fluids and small particles are absorbed into small (~100 nm) vesicles, (3) macropinocytosis, the non-specific internalization of fluids and particles together and (4) phagocytosis, an energy dependent process specific to limited cell types (macrophages, etc.) and implemented to internalize foreign material larger than 0.5 μm (Doherty and McMahon, 2009). Physiochemical factors, including particle size, shape, and surface chemistry, as well as the cell type, determines the particle uptake, efficiency, and the mechanism of internalization (Oh and Park, 2014).

In biological environments, such as blood or culture cell medium, the surface charge of the microparticle dynamically changes; serum proteins in culture medium often coat the particle surface to influence the particle's interaction with the cellular plasma membrane. Changes in surface charge in different solutions can also cause particle aggregation or agglomeration in solution, affecting uptake capabilities. Additionally, the shape and material of the particle influences cellular uptake, which also differs based on cell type.

Internalized microparticles traffic through vesicles called endosomes, which eventually mature through a series of fission and fusion events to lysosomes. Once inside the lysosome, internalized cargo is subject to degradation through exposure to an acidic environment rich in lysosomal hydrolases (Bright et al., 2016). We hypothesize the endosomal trapping of the silica bead prevents the technology from accessing the reductive environment of the cytosol, therefore preventing release of DM1 from the bead by disulfide reduction. Moreover, caspases activated as a result of apoptosis induction would be excluded from endosomal or liposomal compartments of the cell. Even if the small molecule transported by the bead were to escape the endosome/lysosome, activated caspases would not be able to access the confined bead to report on compound activity.

We instead evaluated a cathepsin B and D cleavable linker to connect the lethal small molecule to the bead, which should release compounds from endosomal compartments when the bead system encounters cathepsin B or D. This lysosomal aspartic endopeptidase is localized in intracellular structures, such as endosomes, lysosomes, or phagosomes (Benes et al., 2008); as such, it should co-localize with the bead system if internalized by endocytosis.

We conjugated the lethal molecule monomethyl auristatin E (MMAE) to beads via a cathepsin D cleavable linker (**Figure 3.6**). This system is based on the design of antibody drug conjugate (ADC) brentuximab vedotin; the structure of this drug includes an anti-CD30 antibody bound to MMAE by a protease-cleavable linker. Upon interaction with the CD30 receptor, the ADC is internalized and trafficked into lysosomes, by which active proteases release MMAE. This microtubule inhibitor induces cell death through

cell cycle arrest and apoptosis (van de Donk and Dhimolea, 2012). To apply this effective ADC design to our technology, we replaced the CD30 antibody with a 1 μm silica bead.

After incubation of this bead system with HT-1080 cells, we observed cytotoxicity only when the cleavable compound was present **(Figure 3.7**b**)**, thereby demonstrating that cathepsin-cleavable linkers are more effective for small molecule release, compared to disulfide linkers (**Figure 3.7**a).

Design of small molecule conjugated to bead by a cathepsin D cleavable linker
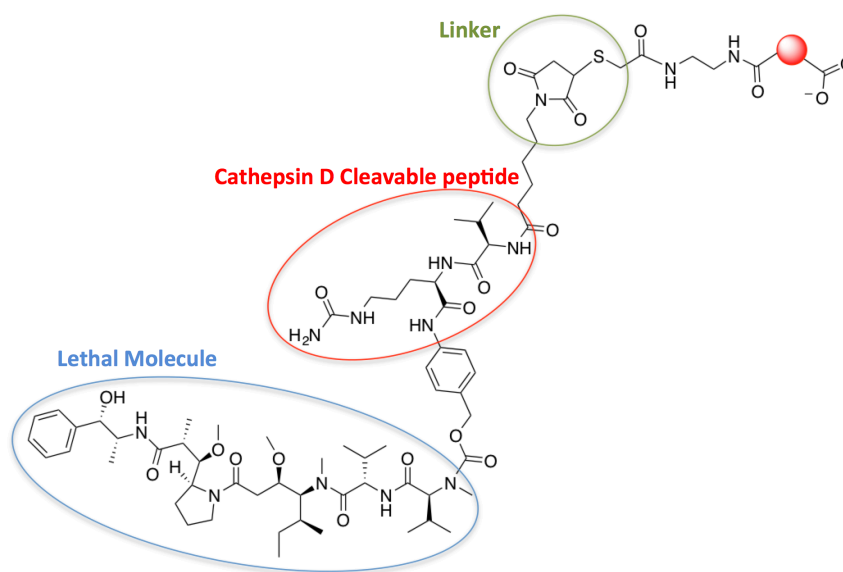
Figure 3.6 | Design of cathepsin D cleavable linker. Lethal molecule MMAE was linked to the silica bead by a cathepsin cleavable linker. The valine-citrulline dipeptide is the site of active protease cleavage; the *p*-aminobenzyloxycarbonyl is included as a self-immolative spacer for two reasons: (1) to facilitate access of the dipeptide to the enzyme active site and (2) to release the MMAE without modification, upon cathepsin cleavage. A maleimide terminus included on the dipeptide was reacted with thiol-differentiated moieties on the bead surface to generate the thiolether linker to the silica bead.
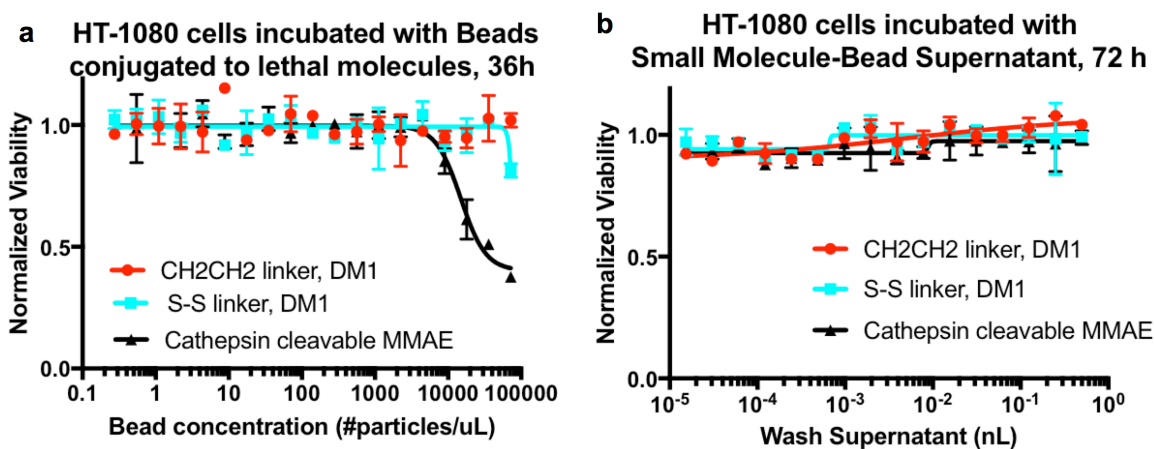
Figure 3.7 | Cathepsin D cleavable linker shows effective release of lethal molecule upon HT-1080 cell incubation. (a) HT-1080 cells showed a decrease in viability when incubated with MMAE conjugated to the bead by a cathepsin cleavable linker; the disulfide bond linked DM1 did not demonstrate lethality, supporting our hypothesis that the bead does not have access to the reductive environment of the cytosol to enable lethal molecule release. (b) DMSO supernatant from the lethal molecule conjugated beads were tested with HT-1080 cells to ensure cells were only exposed to lethal molecules covalently bound to beads (a). No ambient, unconjugated MMAE or DM1 remained in solution at concentrations large enough to influence cell viability.

This development established the final key element needed for a pooled small molecule screening system, including a suitable solid phase system that can be taken up by cells, a cleavable linker that gets released upon cellular uptake, a fluorescent reporter that can indicate compound activity, and an amplifiable barcode that can specify compound identity.

3.2.4 Investigation of endosomal escape mechanisms

In order for the particle to reach cytosolic space, strategies to reduce the entrapment of commonly endocytosed large particles like transfection agents, liposomal drug delivery systems, carbon nanotubes, or cell penetrating peptides have been investigated.

Endosome-disruption agents have been employed to increase bioavailability of peptide nucleic acids. Chloroquine is one such commonly used lysosomotropic agent. This small molecule has a weakly basic character that accumulates in endosomes and lysosomes after protonation, where it acts as an acidification agent. Through the accumulation of counter ions that accompany the influx of protons into the endosomal space, chloroquine encourages endosomal swelling and rupture to deliver entrapped cargo to the cytosolic space. Chloroquine has been efficacious in delivering endocytosed nucleic acid or protein cargos into the cytosolic environment during cellular assays (El-Sayed et al., 2009). Often, however, the high concentrations of chloroquine necessary to facilitate endosomal release of internalized components induce cellular lethality (Wadia et al., 2004). Moreover, chloroquine co-treatment has shown no efficacy for delivery of biological macromolecules *in vivo* animal models due to its toxicity (El-Sayed et al., 2009). These limitations deterred our investigation of lysosomotropic agents for applicability to our technology, as ambient addition of a small molecule known to exhibit pharmacological effects into the media of our assay would convolute our small molecule pooled screening results and significantly reduce technology efficiency.

Cationic polymers, such as polyethyleneimine (PEI), poly-L-lysine (PLL), or chitosan, are commonly used as gene delivery agents or as nanoparticle coatings. This

modification contributes to improved cellular uptake of normally neutral nanoparticles (either made of polymers such as PLGA or inorganic materials such as carbon nanotubes or silica). The increased cationic nature induces particle attraction to the negatively charged cell surface, facilitating uptake by endocytosis. Once internalized and exposed to the acidic environment of the endosome, the amine groups within these polymers become protonated and behave as a buffer. This 'proton sponge' effect prevents further acidification and maturation of the organelle, yet leads to an influx of protons and counter anions. The resulting osmotic swelling destabilizes the endosomal membrane, eventually disrupting the structure to release all components into the cytosol (Ma, 2014). Cationic polymers exhibit increased cellular toxicity, limiting their use in physiological contexts.

Particle modification with pH sensitive polymers provides an attractive solution to encourage endosomal escape with enhanced biocompatibility. The addition of imidazole groups to a particle surface decreases the degree of positive surface charge compared to cationic polymer coatings, yet exhibits a similar pH buffering capacity once the particle is internalized by endocytosis. This strategy has been widely employed for effective siRNA delivery (Mishra et al., 2006) (Gu et al., 2013) (Benns et al., 2000).
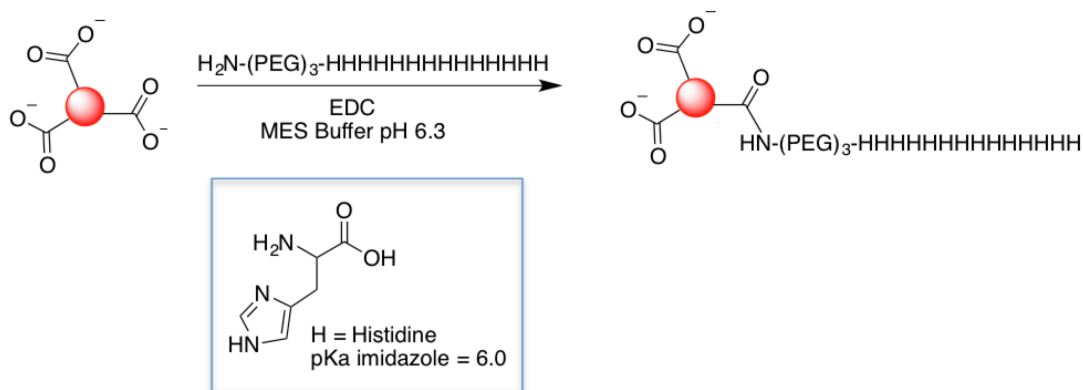
Figure 3.8 | Incorporation of histidine tag to encourage endosomal escape. Installation of histidine moieties to the silica bead could facilitate cytosolic access of endocytosed particles.

To enhance endosomal escape of our technology, we synthesized a histidine tag to add as a fourth component to our pooled screening system. Histidine amino acids are characterized by a sidechain containing an imidazole moiety, to which the conjugate acid form has a pK_a of approximately 6.0; below a pH of 6, the imidazole ring would be mostly protonated (**Figure 3.8**). We hypothesized this attribute should sufficiently disrupt the endosomal entrapment of our bead system. The design of the tag included fourteen histidine amino acids separated from a primary amino group with a $(PEG)_3$ spacer.

Using the Bead-SPDP-C3Sensor-barcode, three-component system, we conjugated increasing equivalents of the histidine tag using EDC bioconjugation chemistry, covalently linking the primary amino terminus of the tag with remaining carboxylate moieties coating the bead.

This system was incubated with HT-1080 cells for 16 hours before conducting uptake analysis by flow cytometry. There was sufficiently less cellular association of the

histidine-containing bead with analyzed cells than beads without the added peptide, signified by the low population with increased fluorescence intensity on the 585 nm emission, bead detection channel **(Figure 3.9)**.
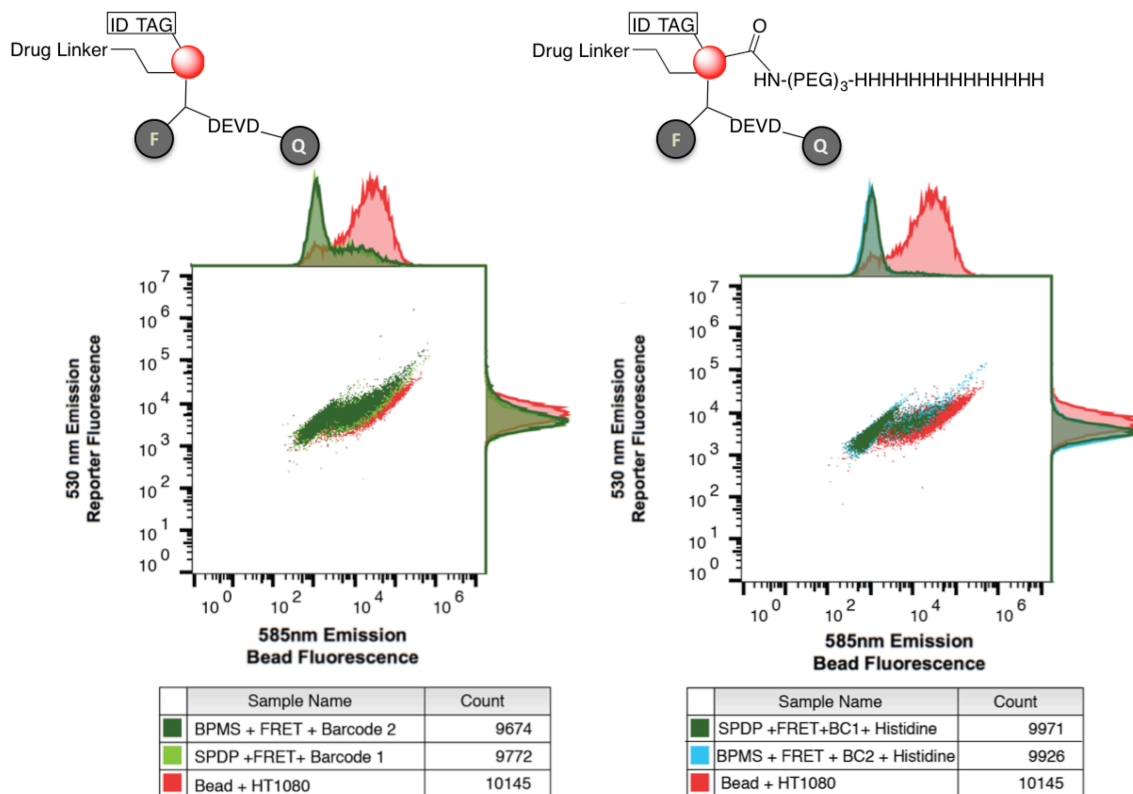
Figure 3.9 | Uptake analysis of total system with histidine peptide. (a) Complete system, with bead conjugated to C3Sensor, Barcode, and small molecule with two different linkers (designated in legend by BPMS or SPDP), were incubated with HT-1080 cells for 16 h. Bead association with cells was designated by the shift to higher bead fluorescence intensity (585 nm emission axis). Upon addition of the histidine tag, Bead-Barcode-C3Sensor association with cells decreased after 16 h incubation with HT-1080 cells, when compared to the level of uptake observed in the absence of the covalently bound histidine component.

To overcome the uptake barrier, further tuning of the equivalents of histidine should be investigated. The addition of separate, positively charged moieties to the bead surface may assist uptake (Salatin et al., 2015), but will also complicate the synthesis of

the system; this avenue was not immediately pursued. Alternative syntheses of histidine-rich peptides could include cell penetrating peptide (CPP, also known as protein transduction domain, PTD) sequences. These peptide sequences are known to overcome the lipophilic, cell membrane barrier and facilitate internalization of bulky cargos such as liposomes, pDNA, oligonucleotides, or proteins. A common CPP implemented for increased macroparticle uptake is the TAT peptide, derived from the trans-activator of transcription of the human immunodeficiency virus (Bechara and Sagan, 2013). The sequence of this peptide is GRKKRRQRRR (Brooks et al., 2005); in order to be productively applied to our system, the peptide should be conjugated after the EDC couplings of the reporter and barcode to avoid reaction of its two lysine sidechains.

Several studies have shown that the use of these peptides increase cellular uptake of macromolecules, but have had little influence on the endosomal escape when linked to bulky cargos (El-Sayed et al., 2009). An example of one peptide applicable to our system that may include both cell penetrating ability and a pH sensitive endosomal escape unit may look like NH_2-$(PEG)_3$-HHHH-GRKKRRQRRR; this has an appropriate amino terminus for EDC conjugation to our carboxylate coated bead, separated from the peptide sequence with a 9-carbon, polyethylene glycol, rigid spacer. This spacer is included to distance the primary amine terminus from the peptide, making the reactive moiety extremely accessible for prompt EDC coupling; presumably, the primary amine sidechains present in the lysine residues are more sterically hindered, making their reaction to form the amide kinetically unfavorable. The histidine unit is included as a lysosomotropic agent to facilitate cytosolic delivery of the bead, while the TAT component would assist its cellular uptake. Alternative approaches include replacing

TAT in our design with the CPP Arg-9 (peptide sequence: RRRRRRRRR) penetratin-Arg (peptide sequence: RQIRIWFQNRRMRWRR, where the lysines of penetratin are substituted with arginine residues), aiming to discover the CPP that offers an optimal balance between endosomal escape capability and bead coupling efficiency.

3.3 Discussion

The development of the barcode and the protease-cleavable small molecule linker established the final key elements needed for a pooled small molecule screening system. This technology includes a suitable solid phase system that can be taken up by cells, a cleavable linker that gets released upon cellular uptake, a fluorescent reporter that can indicate compound activity, and an amplifiable barcode that can specify compound identity.

The barcode is compatible with deep sequencing technology, so that a statistical distribution of small molecules can be determined from the pooled assay, thus reducing the 'false positive' hit molecules from the screen. The barcode does not affect the ability of the bead to be taken up by HT-1080 cells, stays with the bead throughout the duration of the assay, and can be amplified after incubation with cells undergoing death.

The conjugation of mertansine to the bead system requires thiol-sulfide exchange chemistry, but covalent attachment of the small molecule to the bead has been effective using maleimide chemistry or NHS-reactive linkers to expand the scope of reactive moieties on the small molecule. The ability to use simple, robust bioconjugation chemistry to conjugate diverse linkers to the bead system enhances the number of small molecules that can be screened in this type of system.

Future improvements of this technology are ongoing. To address applicability to a broader chemical library, we have plans to explore the usage of a self-immolative linker to attach the small molecule via the disulfide bond. After the disulfide bond is reduced, the terminal thiol can participate in a nucleophilic substitution reaction with the carbamate to form a five-membered ring; this releases the amine-containing small molecule, in its original state, without any chemical modification. Small molecules included in the library must include a reactive handle by which to conjugate the technology, which we acknowledge as a screening limitation. While this disulfide system was not effective at releasing compounds under the conditions we used, it might be possible to engineer cells overexpressing specific reductases that can cleave such a linker. We found that a cathepsin-cleavable linker was more readily used in HT-1080 cells, suggesting that this may be a simpler release mechanism.

Additional strategies to encourage endosomal escape can be pursued. Another approach of interest involves the photochemical disruption of the endosomal membrane. Photochemical internalization (PCI) methods involve the use of small molecule photosensitizers (disulfonated tetraphenyl porphine ($TPPS_4$), disulfonated tetraphenyl chlorin ($TPcS_{2a}$) (Berg et al., 2011), aluminum phthalocyanine disulfonate ($AlPcS_{2A}$), or dendrimer phthalocyanine (DPc)) that localize primarily in the membranes of endosomes and lysosomes. Upon exposure to light of an appropriate wavelength, these agents produce singlet reactive oxygen species that disrupt and destroy the endosomal/lysosomal membrane, thereby liberating entrapped contents into the cytosol. These reagents do show *in vivo* efficacy, as many have been successfully evaluated to enhance antibody drug conjugate activity in animal models of cancer (Bostad et al., 2015) (Selbo et al.,

90

2015). Co-treatment of these small molecules with our established technology may provide an attractive method by which to reduce endosomal entrapment of our 1 μm silica-bead-based technology. It is essential, however, that the wavelength necessary to activate the PCI does not interfere with the photocleavable linker that attaches the DNA barcode to the bead; for this reason, PCI reagents excited by a homogeneous red light source of 652 nm emission may show greater compatibility with our screening design than those excited with a blue, 410-435 nm light.

Ultimately, we suggest that further optimization and diversification of the components of the system may have numerous applications drug discovery and allow for diverse pooled small molecule screens.

3.4 Methods

Barcode detection

Beads were exposed to 365 nm light for 10 minutes for PC linker cleavage. The beads were centrifuged at 14800 rpm for 5 minutes, and 1 μL of the supernatant was removed for PCR amplification. Phusion Hi-Fidelity DNA polymerase (New England Biolabs) was used with primer pair CEY_TruSeq_RPI1: CEY_TruSeq_RP1 (Sequence provided in Supplementary Data).

Confocal fluorescence imaging

Coverslips with HT-1080 cells incubated with beads (procedure described above) were washed with PBS and fixed with 4% paraformaldehyde at room temperature for 10 minutes. After 3 washes with PBS, the cover slips were mounted on slides using ProLong Diamond Antifade Mountant with DAPI (Thermo Fisher (Rochester, NY, P36966)).

Confocal images were taken with a Zeiss AxioOberever LSM700 at 63x and the Z Stacks were compressed with Zen software. Analysis was done using ImageJ (National Institutes of Health, Bethesda MD). All pictures are single confocal section imaged eight to twelve times to reduce noise.

Cell viability experiments

Assay plates were prepared by adding 1,000 HT-1080 cells per well in 35 µL of growth media to opaque white 384 well plates (PerkinElmer (Waltham, MA, 6007688). After adhering to the plate overnight, growth medium was removed from the cells and replaced with 35 µL lethal molecule or beads in a two-fold dilution series. After 24 hours in the incubator, CellTiter-Glo Luminescent Cell Viability Assay (Promega (Madison, WI, G7573) was completed. Percent viability was calculated using cell luminescence intensity values determined from a Victor 3 plate reader (PerkinElmer).

Bead characterization

Microparticle size and zeta potential were measured on a Malvern Zetasizer Nano ZS (Malvern, United Kingdom). For all measurements, microparticles were diluted 1:1000 in MilliQ water at neutral pH. The reported diameters are the average of three measurements, where each measurement comprises at least 10 acquisitions. The zeta potential was calculated according to the Smoluchowski approximation (Sze et al., 2003).

Technology synthesis

All chemicals were obtained from Sigma Aldrich and used without further purification.

92

All peptides were synthesized by LifeTein (Somerset, NJ). Oligonucleotides were synthesized by Integrated DNA Technologies (Coralville, IO). Peptide and oligonucleotide sequences are detailed in Supplementary Tables 1 and 2. This procedure was performed open to the atmosphere. 20 µL beads (Chemicell (Berlin, Product Number 6101-1)) were washed with 0.1 M MES buffer (pH 6.3) by centrifugation at 14800 rpm (16162 xg) for 5 min, removing the supernatant, re-suspending in buffer, and centrifuging again. The bead pellet was re-suspended in 85 µL *N*-Hydroxysulfosuccinimide sodium salt (sulfo-NHS) (20 mM in MES buffer), 8.5 µL *N*-Boc- 2,2′-(ethylenedioxy)diethylamine (50 mM, 0.5 equiv to carboxylate on bead surface), then 42.5 µL *N*-(3-Dimethylaminopropyl)-*N*′-ethylcarbodiimide (EDC) (100 mM in MES buffer). The reaction was stirred overnight at 37 °C before Boc-deprotection with 1000 µL 1:1 water: trifluoroacetic acid. After 30 minutes, the reaction was washed six times by centrifugation and bead re-suspension as described above. To the differentiated beads, 3-(2-pyridyldithio)propionic acid *N*-hydroxysuccinimide ester (SPDP, 17 µL, 10 mM) was coupled by addition of 42.5 µL EDC (100 mM in MES buffer). The reaction was allowed to stir overnight at 37 °C before washing six times. The bead pellet was re-suspended in 85 µL *N*-hydroxysulfosuccinimide sodium salt (sulfo-NHS) (10 µM in MES buffer), 0.68 µL peptide (5 mM, 0.001 equiv to carboxylate on bead surface), 18 µL oligonucleotide (0.1 mM solution) then 42.5 µL *N*-(3-dimethylaminopropyl)-*N*′-ethylcarbodiimide (EDC) (100 mM in MES buffer). The reaction was shaken at 37 °C overnight before washing five times with water, then four times with 0.5% Triton-X. Fluorescence of the supernatant of the final washing (494 nm excitation, 525 nm emission) was recorded to ensure there no unconjugated fluorophore remained with the beads. PCR reactions

(procedure described below) of the final washing supernatant were completed to ensure no uncoupled barcode remained. Excess mertansine (DM1, Medchem Express, Monmouth Junction, New Jersey, Serial number G01432) (10 mM in DMSO, 17 µL) was added to the bead pellet for final coupling, shaken at 37 °C overnight before washing five times with DMSO. The final system was suspended in 20 µL DMSO (1 µL DMSO per 1 µL bead from stock solution).

Synthesis of Bead-Thioether-DM1 control

All chemicals were obtained from Sigma Aldrich and used without further purification. This procedure was performed open to the atmosphere. 20 µL beads (Chemicell (Berlin, Product Number 6101-1)) were washed with 0.1 M MES buffer (pH 6.3) by centrifugation at 14800 rpm (16162 xg) for 5 min, removing the supernatant, re-suspending in buffer, and centrifuging again. The bead pellet was re-suspended in 85 µL N-Hydroxysulfosuccinimide sodium salt (sulfo-NHS) (20 mM in MES buffer), 8.5 µL N-Boc- 2,2′-(ethylenedioxy)diethylamine (50 mM, 0.5 equiv to carboxylate on bead surface), then 42.5 µL N-(3-Dimethylaminopropyl)-N′-ethylcarbodiimide (EDC) (100 mM in MES buffer). The reaction was stirred overnight at 37 °C before Boc-deprotection with 1000 µL 1:1 water: trifluoroacetic acid. After 30 minutes, the reaction was washed six times by centrifugation and bead re-suspension as described above. To the differentiated beads, N-β-maleimidopropyl-oxysuccinimide ester (BPMS, Thermo Fisher Scientific, Grand Island, NY, Catalog number 22298, 17 µL, 10 mM) was coupled by addition of 42.5 µL EDC (100 mM in MES buffer). The reaction was allowed to stir overnight at 37 °C before washing six times. Excess mertansine (DM1, Medchem

Express, Monmouth Junction, New Jersey USA, Serial number G01432) (10 mM in DMSO, 17 µL) was added to the bead pellet for final coupling, shaken at 37 °C overnight before washing five times with DMSO. The final system was suspended in 20 µL DMSO (1 µL DMSO per 1 µL bead from stock solution).

Synthesis of Bead-Cathepsin D cleavable linker- monomethyl auristatin E

All chemicals were obtained from Sigma Aldrich and used without further purification. This procedure was performed open to the atmosphere. 20 µL beads (Chemicell (Berlin, Product Number 6101-1)) were washed with 0.1 M MES buffer (pH 6.3) by centrifugation at 14800 rpm (16162 x g) for 5 min, removing the supernatant, re-suspending in buffer, and centrifuging again. The bead pellet was re-suspended in 85 µL *N*-hydroxysulfosuccinimide sodium salt (sulfo-NHS) (20 mM in MES buffer), 8.5 µL Boc- 2,2′-(ethylenedioxy)diethylamine (50 mM, 0.5 equiv to carboxylate on bead surface), then 42.5 µL *N*-(3-Dimethylaminopropyl)-*N*′-ethylcarbodiimide (EDC) (100 mM in MES buffer). The reaction was stirred overnight at 37 °C before Boc-deprotection with 1000 µL 1:1 water: trifluoroacetic acid. After 30 minutes, the reaction was washed six times by centrifugation and bead re-suspension as described above. The differentiated beads and 42.5 µL EDC (100 mM in MES buffer) were added to a solution of 3-Mercaptopropionic Acid (17 µL, 10 mM) and 85 µL *N*-Hydroxysulfosuccinimide sodium salt (sulfo-NHS) (20 mM in MES buffer). The reaction was allowed to stir overnight at 37 °C before washing six times. The beads were resuspended in 50 µL DMSO and excess maleimidocaproyl-L-valine-L-citrulline-*p*-aminobenzyl alcohol *p*-nitrophenyl carbonate (MC-Val-Cit-BAP-PNP) (Accela Chemicals, San Diego, California, Compound ID

SY034490) was added to the reaction. The reaction was shaken at 37 °C overnight before washing five times with DMSO. To the beads was added excess monomethyl auristatin E (MMAE, Medchem Express, Monmouth Junction, New Jersey USA, Catalog number HY-15162) in DMSO. The reaction was shaken at 37 °C overnight before washing five times with DMSO. Supernatant from the final wash was kept for cell viability analysis.

Chapter 4

Targeted approach to discover apoptosis-inducing small molecules

4.1 Introduction

All protein members of the Bcl-2 family share one or more of the Bcl-2 homology (BH) domains, and are essential regulators of the intrinsic apoptotic pathway. Some protein members of the Bcl-2 family work to promote apoptosis, while other members function to inhibit this cell death pathway; the imbalance between pro- and anti-apoptotic Bcl-2 proteins to shift equilibrium towards cell survival is a key mechanism in tumorigenisis and chemotherapeutic resistance (for additional pathway biology, see sections **1.13** and **1.16**).

Small molecule inhibitors designed to mimic BH3-only protein binding to Bcl-2, Bcl-W and Bcl-X$_L$ (ABT-263, navitoclax) or solely Bcl-2 (ABT-199, venetoclax) have demonstrated clinical efficacy. Although these examples validate the 'BH3-mimetic' concept as an attractive targeted approach to induce apoptosis in cancers, these

compounds are subject to chemoresistance through overexpression of Mcl-1, a Bcl-2 pro-survival member unaffected by the aforementioned small molecule inhibitors (Walensky, 2012).

Thus, the longstanding challenge has been to develop a BH3-mimetic to target Mcl-1 that possesses 1) biological activity dependent on Bax/Bak, 2) low nanomolar affinity for the target protein, 3) cytotoxic activity correlated with cellular Bcl-2 protein family levels, and 4) *in vivo* treatment that triggers relevant biomarkers indicative of Bcl-2 family antagonists (Lessene et al., 2008). The discovery of such a small molecule that specifically targets Mcl-1 would have outstanding utility in the clinical setting as a cancer therapeutic, and the tactic upon which the molecule is discovered would lay the groundwork for drugging diverse protein-protein interactions. To reduce side effects observed by targeting multiple members of the anti-apoptotic Bcl-2 family (Bcl-X$_L$ inhibition is associated with thrombocytopenia), our goal stands to tailor a drug that exclusively inhibits Mcl-1. To date, there is one such inhibitor (S63845) that shows on-target efficacy to induce apoptosis in Mcl-1 dependent cancer cells *in vitro* and *in vivo,* but its clinical utility has yet to be investigated (Kotschy et al., 2016). This molecule, and other small molecules (Friberg et al., 2013) and stapled peptides (Cohen et al., 2012) that have shown Mcl-1 inhibition through protein-based assays, have been discovered using NMR-based fragment screening strategies. Subsequent SAR studies were guided by three-dimensional x-ray crystal structures of the bound fragments inside the Mcl-1 protein.

Inspired by the therapeutic relevance of Mcl-1, we set out to examine the applicability of alternate target-based screening strategies to more efficiently discover a

98

novel Mcl-1 inhibitor. We examined computer-aided drug design (CADD) screening of *in silico* libraries of compounds, aiming to generate BH3 mimetic small molecules that could be rationally elaborated upon to optimize binding affinity, target specificity, and ADME properties. High-throughput screening of *in silico* small molecule libraries would provide a time- and cost-effective alternative to physically screening thousands of chemical compounds for activity. Moreover, computational docking strategies illustrate the ideal pose assumed by the small molecule when interacting with the specified binding pocket, significantly aiding eventual lead compound optimization efforts.

4.2 Results

4.2.1. Protein structure selection

Three-dimensional structures of myeloid cell leukemia 1 (Mcl-1) have been experimentally elucidated by x-ray crystallography; these structural biology data drove our computational screen. Using the RCSB Protein Data Bank, we obtained a crystal structure of an inhibitor-bound Mcl-1 complex with 2.4 Å resolution (4HW3). We chose to use a crystal structure with a bound inhibitor for two main reasons: (1) the bound molecule has a known K_i of 0.32 μM (Friberg et al., 2013); removing and then re-docking the bound molecule in the designated target site to obtain a docking score would provide a scoring benchmark upon which to compare new small molecules, and (2) the ability to crystalize the protein-inhibitor complex gives an accurate picture of where the small molecule has a large probability of binding. The crystal structure chosen supports the ability of small molecules to interact directly with the BH3 domain to out-compete

BH3-only proteins and peptides for Mcl-1; small molecules that induce allosteric effects that render the protein inactive were not observed in the structural database, and therefore not considered during our screen. By examining the protein structure, it is clear that a deep hydrophobic pocket in the BH3 domain of Mcl-1 would accommodate small molecule binding (**Figure 4.1)**

60
$K_i = 0.32\ \mu M$
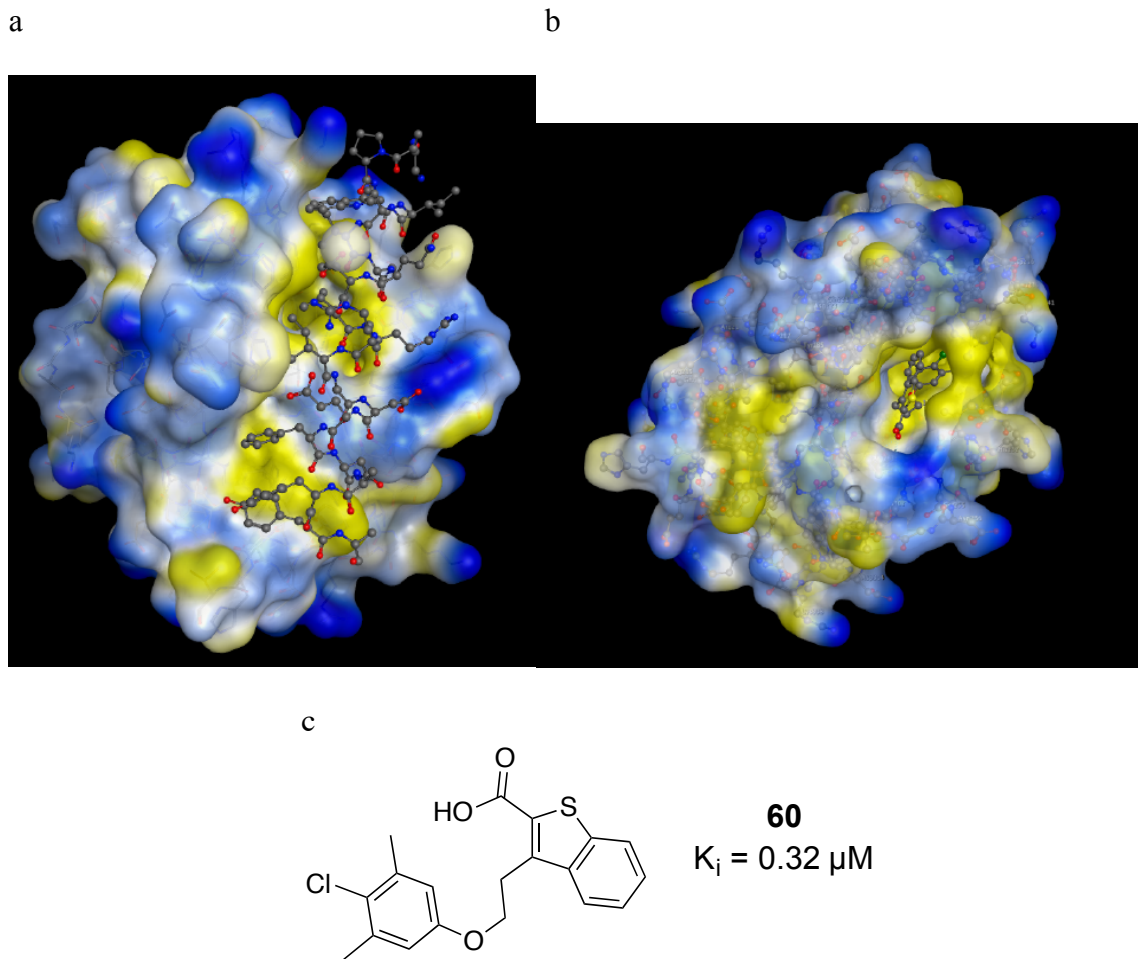
Figure 4.1 | Mcl-1 protein structures. The Mcl-1 protein structures are displayed with a surface demonstrating regions of hydrophobicity; blue regions depict hydrophilic residues, while yellow portions demonstrate lipophilic areas of the protein surface. (a) BH3-only peptide bound to the BH3 region of Mcl-1. (b) Re-docked structure of known inhibitor assumes similar binding pose as the crystalized protein-inhibitor structure. The site shown with the small molecule bound inside the BH3 region of Mcl-1 is the location of the center of our grid, in which all libraries of *in silico* small molecules were docked. (c) Structure of the small molecule from crystal structure, **60.**

4.2.2 *In silico ligand library screening*

Next, we compiled a computational library consisting of ~5 million commercially available small molecules found in the inventories of eight different vendors (Asinex, Enamine, Chembridge, ChemDiv, IBS, Life, Maybridge, and TimTec). The goal of this initial high-throughput computational screen was to examine a large amount of chemical space in order to identify promising molecular scaffolds. As such, before docking, the large library was filtered for 'fragment-like' properties: including LogP < 3, hydrogen bond acceptors ≤ 3, hydrogen bond donors ≤ 3, molecular weight < 300, aqueous solubility >0.5 mM were applied to whittle the library to 604,457 small molecules. After identification, rationally elaborating upon the structure of these core scaffolds would enhance target affinity.

After preparing both the ligand library and protein for virtual screening, all small molecules were docked using Maestro SP (Schrodinger) into the BH3 domain of Mcl-1 and each ligand's docking pose was scored. This empirical scoring function (GlideScore) is designed to approximate ligand binding free energy of the compound for the target; the more negative the score, the tighter the interactions. When re-docked into the crystal structure after extraction, molecule **60** assumed a similar pose to the crystalized model; this orientation demonstrated a Glide score of -8.3; we postulated that ligands with a score equal to or better than -8.5 may have similar or better binding affinity for Mcl-1. 1,054 compounds fit these criteria. These molecules were clustered based on a Tanimoto coefficient of 0.54 to represent a broad area of chemical diversity, and 96 of these commercially available compounds were ordered for biochemical testing.

4.2.3 *Fluorescence polarization assay*

A fluorescence polarization (FP) competition assay was used as the method to experimentally determine the affinity of these ligands for Mcl-1. When small fluorescent molecules in solution are excited with plane-polarized light, their Brownian motion (rotation and tumbling) causes scattering of emitted light. Scattering results in a lower degree of polarized signal compared to the polarization of the excitation. Larger molecules have a slower rotation rate in solution, light emitted is not as severely distorted from the plane of excitation; the polarization is preserved.

Bid is a BH3-only protein known to bind to the BH3 domain of Mcl-1 with high affinity. For our competition assay, the peptide binding domain of Bid was labeled with a fluorescein (FAM) fluorophore. If the small molecule of interest binds to this BH3 domain of Mcl-1 to displace the FAM-Bid fluorescent substrate, a higher concentration of fluorescent peptide would be present in solution. Because unbound FAM-Bid is much smaller than the peptide-protein complex, fluorescence emission is scattered as a result of the faster tumbling; a low polarization signal ensues (**Figure 4.2**). Controls used for this assay are included in **Figure 4.3**.
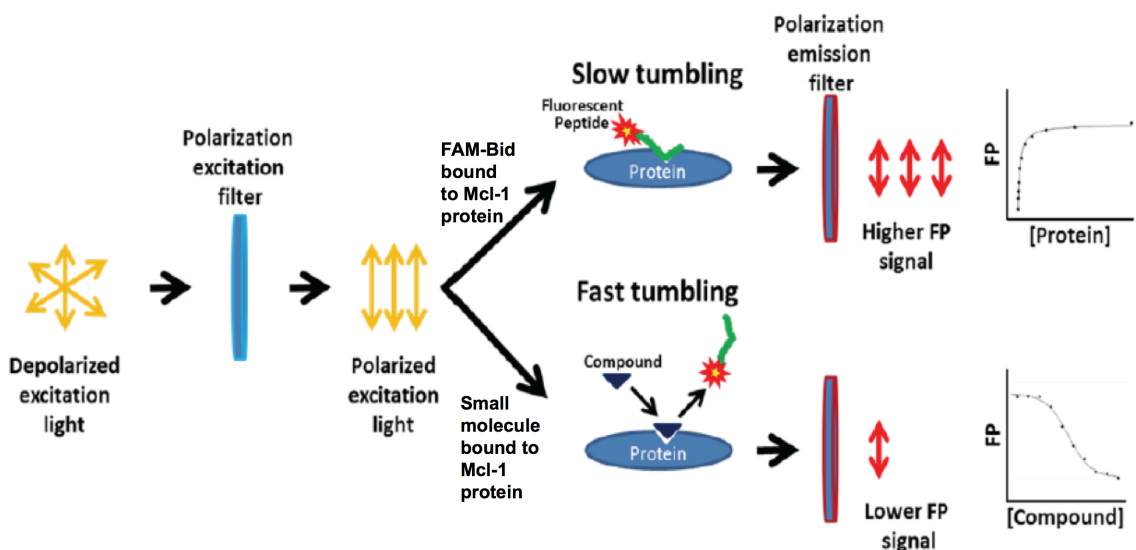
Figure 4.2 | Schematic of fluorescence polarization assay. Fluorescence anisotropy is based on the principle that a static fluorophore emits polarized light when excited by a polarized source; the movement of the fluorophore in solution 'scrambles' the emitted light relative to the angle of incident polarization. When a fluorescently labeled peptide that possesses the BH3-only domain of protein Bid (FAM-Bid) binds to Mcl-1, the size of the complex slows fluorophore tumbling. The emitted light from the complex remains on the same plane as the excitation light; the polarization signal is preserved. Small molecules tumble faster in solution, which more severely distorts the polarization plane of radiated light. If a compound binds to Mcl-1 as to displace or avert FAM-Bid binding, a higher concentration of FAM-Bid will persist in solution. The faster tumbling of the unbound fluorescent protein scrambles radiated light, resulting in a lower fluorescence polarization readout. Image adapted from TgK scientific: http://www.hi-techsci.com/techniques/anisotropy/

Fluorescence polarization assay controls

a EGCG competing out FAM-Bid for Mcl-1 binding

b Bid protein competing out FAM-Bid for Mcl-1 binding
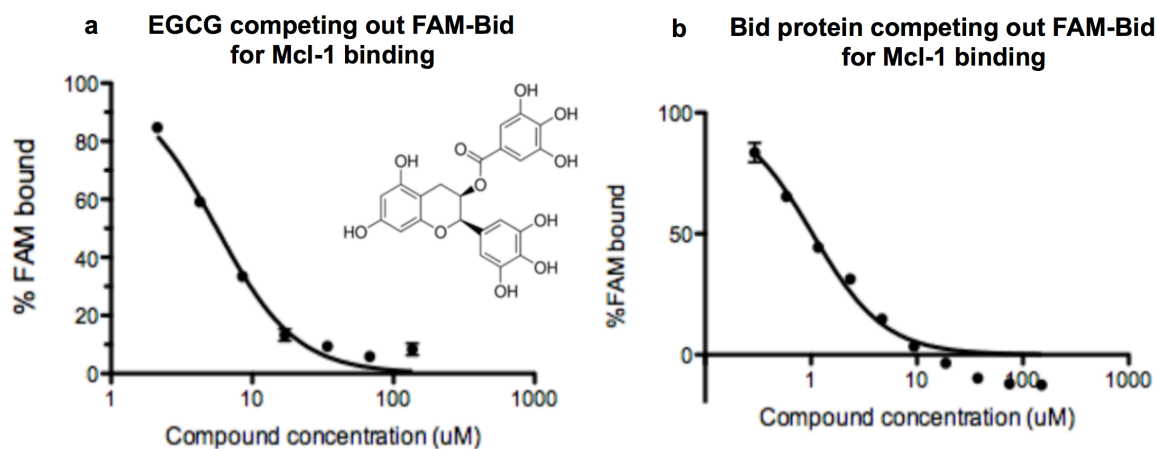
Figure 4.3 | Controls for fluorescence polarization assay. (a) (-)-Epigallocatechin gallate (EGCG), a compound commonly found in green and black tea, has been shown to have potent binding affinity to the BH3 domain of members of the Bcl-2 family. This small molecule was used as a control for our competition assay. (b) Titration of Bid protein showed to out compete constant concentrations of the fluorescent FAM-Bid substrate to provide an additional control to confirm fluorescence polarization assay conditions.

Seven small molecules out of the 96 screened demonstrated weak affinity in the protein-based assay; none of the molecules exhibited any effect near the potency recorded for **60** (0.32 µM) **(Figure 4.4)**. The purpose of the biochemical evaluation, however, was to narrow down the top scoring molecules from the virtual screen to determine a scaffold for upcoming rational elaboration.
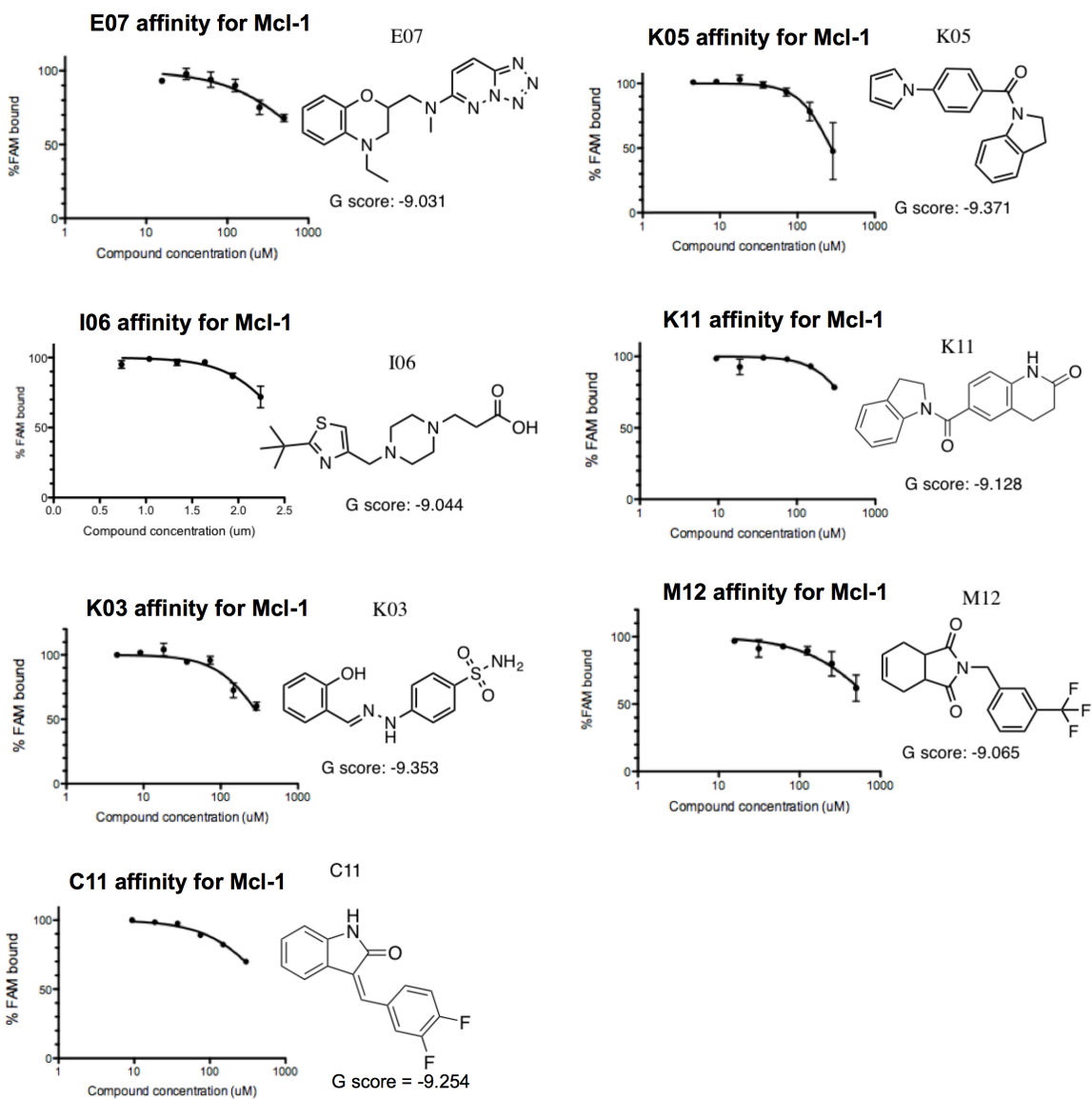
Figure 4.4 | Structures of 'hit' small molecules from initial FP assay. 96 compounds were

selected to represent 1,054 commercially available compounds that demonstrated a Glide score of

-8.5 or better for Mcl-1. The 96 compounds were tested in a fluorescence polarization assay to

experimentally assess affinity for the protein target. The structures of the compounds

biochemically tested accompany the results of the FP assay, and the Glide scores from

computational evaluation. The lower % FAM bound shows binding affinity for the molecule to

the target as a result of FAM-Bid BH3 protein displacement.

4.2.4. Selection of molecular scaffolds

To better select molecular scaffolds to use as a basis for further optimization, we returned to the ~600,000 small molecule *in silico* library, and filtered it for compounds that show >75% structural similarity to at least one of the experimentally validated 'hits.' 1,479 compounds resulted, which were each docked into the Mcl-1 crystal structure. Again, the top scoring compounds (-9.0 or greater) were ordered and experimentally analyzed by fluorescence polarization.

Again, compounds tested demonstrated very weak affinity for the purified Mcl-1 protein (>100 µM). Chemical structures and binding orientations were compared across the compounds that exhibited the greatest affinity for Mcl-1 in our fluorescence polarization assay, and trends were observed. The indolene scaffold was observed in K11, M12, and K05, and assumed similar occupation of the protein pocket upon docking.

We then built *in silico* libraries of commercially available indoles and indolenes to establish a scaffold amenable to synthetic modification. The structures of M12, K05, and similar compounds include substitution of the indole at the nitrogen; base-catalyzed alkylation and acylation at this position can be accomplished through deprotonation of the nitrogen atom to make the anion the most nucleophilic site on the ring. Guided by this hypothesized synthetic accessibility, we designed *in silico* libraries of commercially available alkyl and acyl halides, which we computationally reacted with the indole to create a new library that was docked into the crystal structure of Mcl-1. Elaboration at the indole nitrogen led to an increase in binding scores. We continued this iterative process of identifying locations on the molecule amenable to synthetic elaboration, designing libraries of commercially accessible reactants used to create more complex, yet

synthetically accessible compounds, and re-docking the newly established libraries into

the protein to assess affinity and determine sites amenable to further modification.
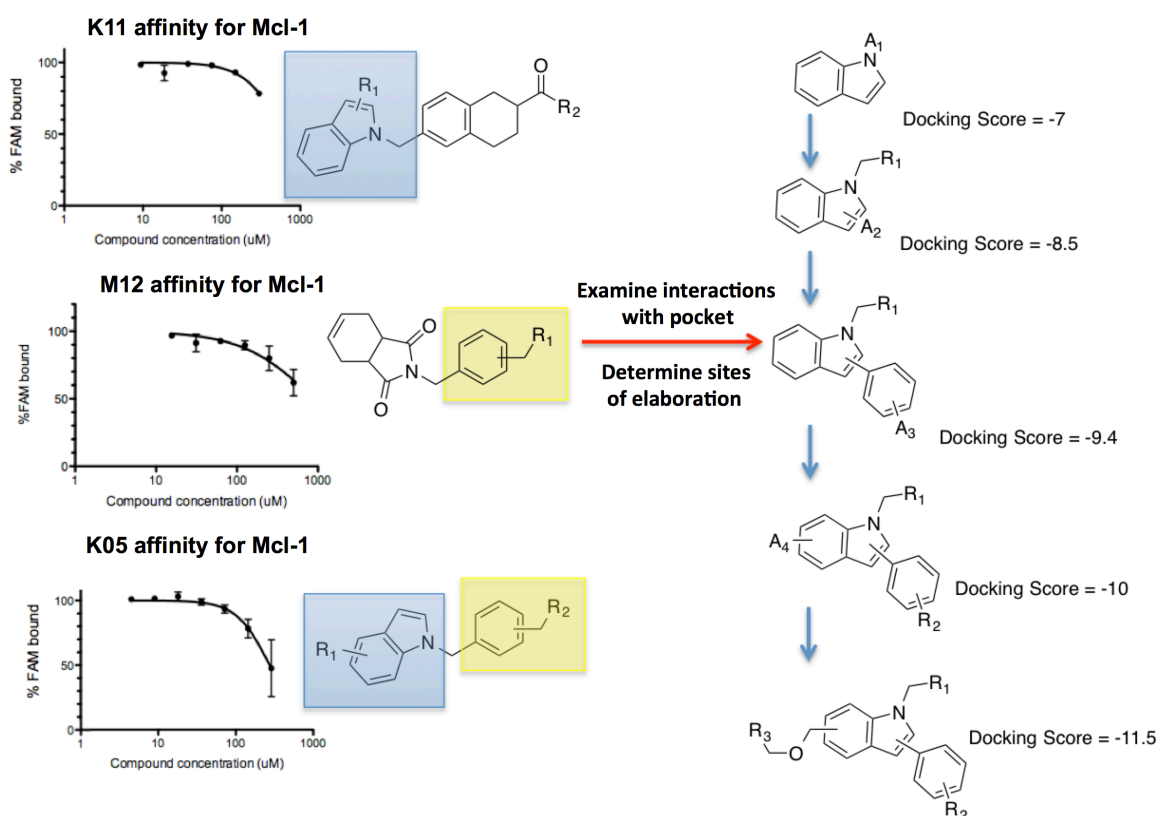
Figure 4.5 | Workflow to computationally design synthetically accessible small

molecules. The structures of molecules that demonstrated the best binding affinity in the

fluorescence polarization assay were analyzed for similarity. Guided by the docking pose

of the molecules in the receptor binding pocket, synthetically accessible reactive sites

were chosen. Using this strategy, we observed an increase in docking score, correlating

with our rational design of molecules to optimize interactions in the BH3 binding domain

of Mcl-1.
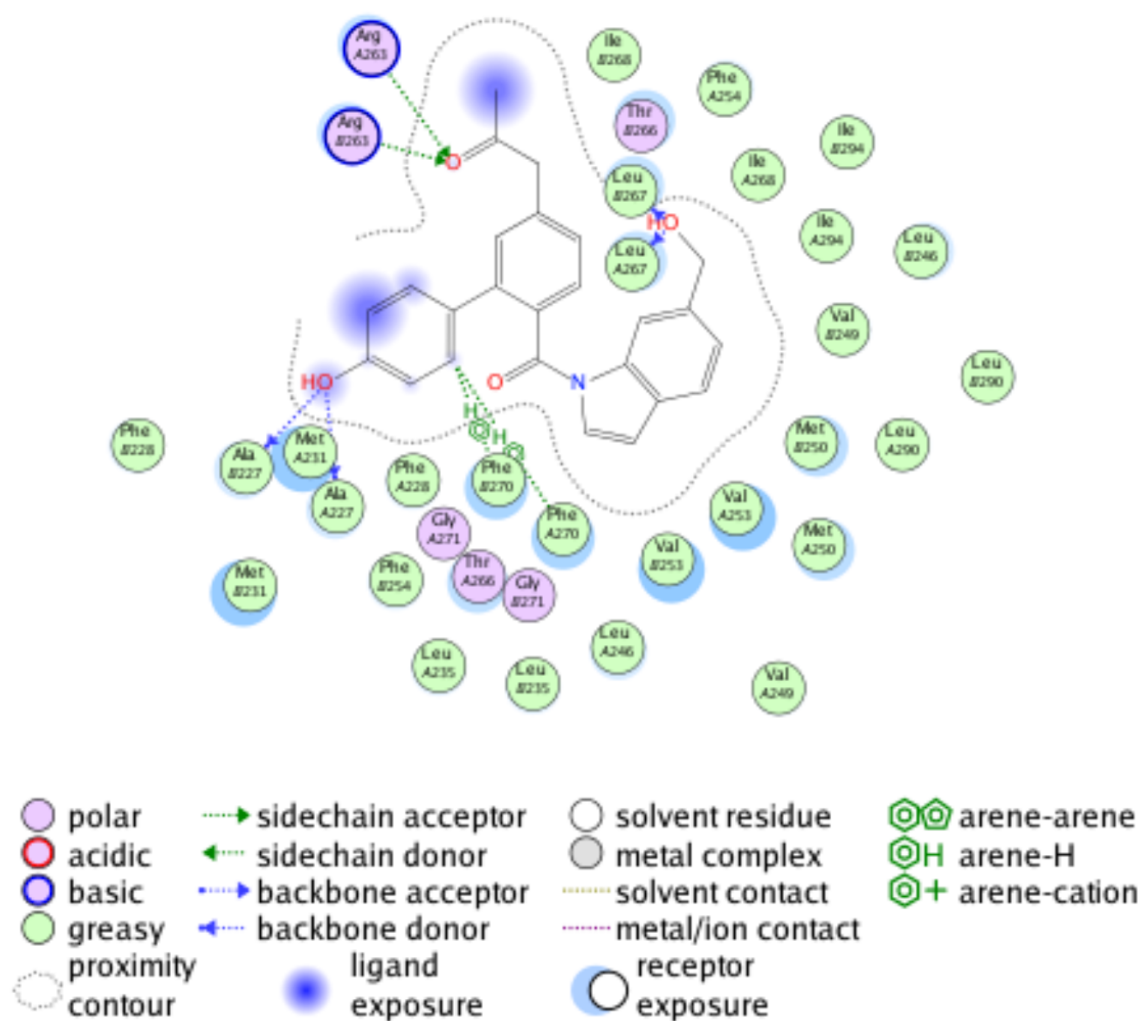
Figure 4.6 | Small molecule fit inside Mcl-1 binding pocket. The small molecule designed to fit inside the receptor was optimized to have strong interactions with the basic sidechain of the arginine amino acid residue in position 263. The molecule shown has a docking score of -12.25; interactions contributing to this increased affinity include the hydrogen donating capabilities of the hydroxyl-substituent on the phenyl ring with Ala 227, the pi-stacking interactions with that ring and Phe 270, and the Leu 267 interactions with the hydroxyl substituent on the 6-position of the indole.
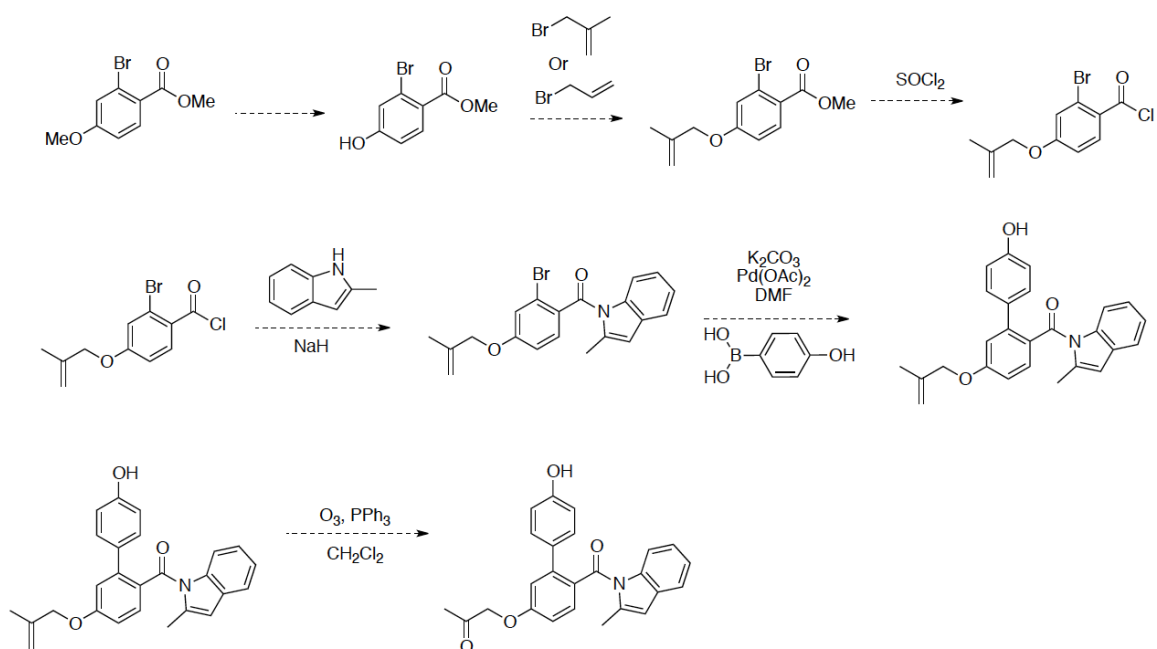
Scheme 4.1 | Proposed synthesis of designed small molecules. Starting with the commercially available tri-substituted aromatic compound, the methoxy substituent could be selectively deprotected with BBr$_3$ in the presence of the ester. The resulting hydroxyl group could undergo subsequent alkylation with methylallyl bromide. Next, saponification of the ether moiety to an acid, followed by thionyl chloride addition could reveal a reactive acyl chloride, to which an indole could be conjugated at the N-position under basic conditions. Subsequent Suzuki coupling using the aromatic boronic acid to react with the aromatic bromide, followed by oxidative cleavage of the terminal olefin results in synthesis of the final small molecule for biochemical analysis.
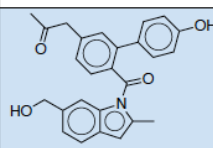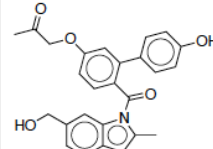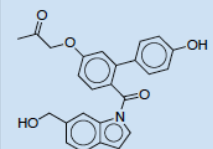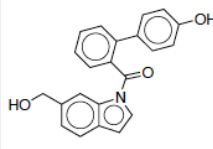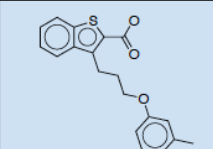
4.2.5 Computational assessment of small molecule specificity for Mcl-1

Part of our criteria was to design a small molecule that demonstrated specificity for Mcl-1 over other members of the Bcl-2 family of proteins. We hypothesize this binding selectivity would reduce off-target effects. The 'hit' compounds (Glide scores

ranging from -11 to -13 for Mcl-1) were docked into one crystal structure of Bcl-2 and two crystal structures of Bcl-X$_L$. Our molecules did not demonstrate comparable affinity to either Bcl-2 or Bcl-X$_L$ as for Mcl-1; Bcl-2 Glide scores (PDB structure 4AQ3) ranged from -4.21 to -5.88, and Bcl-X$_L$ docking scores (PDB structures 2O1Y and 3ZK6) range from -4.6 to -7.7. Although the docking scores predict our molecules have greater affinity for Mcl-1 over Bcl-2 and Bcl-X$_L$, these scores do not correlate to a specific K$_D$ value. Consequently, when comparing the docking scores for one small molecule across all protein targets, we cannot assume differential affinity observed is sufficient to confer physical selectivity. Although there is no substitute to experimentation, small molecules known to bind to Bcl-2 and Bcl-X$_L$ (*e.g.,* ABT-263 and ABT-199) could be docked in Bcl-2 family protein structures to generate scores for comparison. Computationally studying small molecules with experimentally determined affinities can better guide our computational assessment of new compound selectivity for Mcl-1 over other Bcl-2 family proteins.

To computationally predict ADME properties (absorption, distribution, metabolism, excretion) of the set, QikProp calculations were run. Including ADME prediction and optimization early in the drug development process can significantly lower late-stage therapeutic attrition rate, as almost 40% of lead candidates fail in clinical trials because of poor pharmacokinetic/pharmacodynamic properties (Li, 2001). QikProp calculations (Schrodinger) can quickly predict over twenty pharmaceutically relevant, physical descriptors, including aqueous solubility, octanol/water or water/gas partition coefficients, predicted blood/brain barrier coefficient, Caco-2 cell permeability, or predicted IC$_{50}$ for blockage of HERG K$^+$ channels. When applied to our top-scoring,

synthetically accessible molecules, good drug-like characteristics were predicted for all designs, as each fell within the ranges determined for 95% of all known drugs **(Figure 4.7)**.

	Glide Score	Rule of Five	QPPCaco	QPlogPo/w	%Human Oral Absorption
Docking Score: -12.25	-12.2	0	367.688	3.629	94.113
Docking Score: -11.47	-11.47	0	205.019	3.09	86.45
Docking Score: -11.21	-11.21	0	205.019	3.09	86.45
Docking Score: -10.6	-10.797	0	154.899	2.89	38.07
Docking Score: -8.34	-8.3	1	607	5.8	100

Figure 4.7 | Calculated ADME properties of designed Mcl-1 inhibitors. Shown here are a few parameters of those calculated, including predicted octanol/water partition coefficient (QPlogPo/w, range of recommended values: -2.0 - 6.5), predicted apparent Caco-2 cell permeability to model the gut-blood barrier (QPPCaco, range of recommended values: < 25 = poor, > 500 = great), rule of five (number of violations of Lipinski's rule of five: molecular weight < 500, hydrogen bond donor </= 5, hydrogen bond acceptor </= 10, and Log value of the octanol/water partition coefficient < 5), and percent human oral absorption (< 25% is poor, > 80% is high).

4.3 Discussion

We set to examine computer-aided drug design methods as an alternative to NMR-based screening of fragment libraries for Mcl-1 target specificity. Informing *in silico* drug development methods with biochemical assays provides an attractive approach to synchronize the efficiency of computational methods with the experimental molecule activity. We observed challenges in small molecule solubility when working with ligands in the fluorescence polarization assay, which were valuable physical phenomena that can greatly influence further rational lead compound design. Virtual docking strategies are much less laborious than the physical screening, yet we did not elucidate any fragments with potent binding *in vitro*. This is not surprising, as the Mcl-1-BH3-only protein-protein interaction area is very large, and is extremely difficult to abrogate solely through low MW (< 300 KDa) small molecule binding.

The generation of additional, distinct docking grids, centered over diverse sites on the BH3 domain of Mcl-1, could allow us to cover a larger surface area with the fragments. Fragments that demonstrate good docking scores for different regions of the BH3 binding groove can then be synthetically tethered together to create a large molecule with increased affinity.

We were able to design synthetically accessible small molecules that demonstrated a favorable docking pose inside the BH3 domain of Mcl-1, which may act as efficacious BH3-mimetics. The scoring functions were extremely promising (< -12). Although empirical scoring functions do not correlate to any measure of small molecule activity (*e.g.,* a dissociation constant, K_D), it does give a good illustration of the conformation the ligand assumes inside the binding pocket, and informs us that there are

very favorable physical parameters for binding to occur. The eventual synthesis of the designed small molecules, followed by testing for Mcl-1 specific activity (*e.g.,* activity in Mcl-1 dependent cell lines, activity dependent on Bax/Bak oligmerization, specificity for Mcl-1 over Bcl-2/Bcl-X_L) would shed light on the actual efficacy of our CADD methodology towards Mcl-1 inhibition.

4.4. Methods

Docking Software

Molecular docking was performed using GLIDE (version 2012, Schrodinger, Inc). Modeling of proteins and ligands were performed using Molecular Operating Environment [MOE] (Chemical Computing Group). All chemical structures were drawn using ChemDraw Ultra version 10.0. (Perkin Elmer). All statistical analyses, EC_{50} determinations, and viability curves were produced using Prism 5.0c (GraphPad Software).

***In silico* libraries**

Libraries of commercially available compounds were compiled from the inventories of Asinex, Enamine, Chembridge, ChemDiv, IBS, Life, Maybridge and TimTec. A subset of ~600,000 compounds was obtained from the unfiltered library using the following filter criteria: LogP <3, hydrogen bond acceptors $\leq$ 3, hydrogen bond donors $\leq$ 3, molecular weight <300, aqueous solubility > 0.5 mM. Chemical descriptors were

calculated using MOE (Chemical Computing Group). Designed libraries of synthetically accessible compounds were compiled using selected commercially available reagents from the inventory of Sigma-Aldrich and Chem-Impex using the Combigen application in MOE (Chemical Computing Group).

His-tagged Mcl-1 ΔC ΔN protein purification

Transformed *Escherichia coli* BL21 (DE3) were cultured in kanamycin-containing Luria Broth, and protein expression was induced by the addition of 0.5 mM isopropyl β-D-1-thiogalactopyranoside (IPTG) once the optical density reached 0.8. The bacterial pellets were resuspended in buffer (50 mM Tris, 50 mM NaCl, 1 mM DTT, pH 8.0, complete protease inhibitor tablet) for sonication. After centrifugation at 45,000 xg (15,000 rpm) for 45 minutes, the supernatant was applied to a column of Ni Sepharose Fast Flow beads (GE Healthcare, Catalog 17-5318-01) for affinity purification. A 20 mM imidazole wash (x 3) was completed before applying 250 mM imidazole solution to the column for protein elution. Gel electrophoresis confirmed His-tagged Mcl-1 presence; additional purification by FPLC was accomplished if necessary to enhance purity.

Fluorescence polarization binding assay

Direct binding curves were obtained through the incubation of FAM-labeled BID protein (30 nM) with serial dilutions of purified His-tagged Mcl-1 protein in FPA buffer (50 mM NaCl, 50 mM Tris, pH 7.4, 1mM DTT), and fluorescence polarization measured at 30 min on the Victor 3 plate reader (PerkinElmer). For competition assays, a serial dilution of small molecule or acetylated peptide was added to 1 μM MCL-1. Fluorescence

polarization was measured at equilibrium by nonlinear regression analysis of competitive

binding curves using Prism software (Graphpad).

Chapter 5

Conclusions and future directions

5.1 Summary and conclusions

Experimental approaches to the discovery of small molecule probes and drug candidates often use biochemical or cell-based screening of large libraries ($>10^5$) of small molecules. Small molecules of interest are tested one at a time in individual wells of a microtiter plate, at a significant cost in time and resources. Furthermore, evaluation of large numbers of compounds in such assays requires robust cellular or biochemical screening formats that may not be relevant to the contexts found in human patients.

The purpose of this dissertation is to examine these challenges encountered in currently implemented methods of small molecule drug discovery, and to propose a microparticle-based screening system that can allow for screening of small molecules in such a pooled fashion, analogous to the pooled, cell-based screens of genetic reagents that have been powerfully deployed in recent years.

First, we define an appropriate solid phase vehicle upon which to develop this small molecule delivery system for pooled screening. Fluorescent, carboxylate-coated silica microparticles provided enough sites for chemical diversification while sufficiently

being internalized by human cell lines. The beads maintained their structure and fluorescence throughout organic chemical reaction conditions. Their fluorescent property allows for convenient particle tracking throughout the assay and for clear distinction from cellular debris produced upon assay completion.

Next, we developed a cleavable linker that can link small molecules of interest to silica microparticle beads. Chemical diversification was possible through common bioconjugation reactions (EDC couplings, maleimide chemistry). Because the bead enters the cell through endocytosis, it is exposed to an environment rich in proteases instead of cytosolic thio-reductases; a cathepsin D cleavable linker provided more efficient release of the small molecule from the bead, as evidenced by observed cellular lethality, than a disulfide linker.

We introduced a bead-based fluorescent sensor that can report on the activity of small molecules in cells. A FRET-based, gain-of-function sensor of apoptotic activity effectively distinguished the beads exposed to active caspase 3 from an uncleaved, population. This reporter was designed to provide initial insight into the 'hit small molecule's mechanism of action, allowing this pooled screening method a clear improvement over traditional phenotypic screens.

The final component to this screening system is a DNA tag encoding the identity of the small molecule, attached to each silica bead through a photocleavable linker to enable its amplification. This barcode is unique to each small molecule subject to the assay, yet is designed to possess identical priming regions, conserved throughout each barcode to allow for equal amplification probability. The system is amenable to

sequencing using NGS techniques, so that a statistical distribution of barcodes results from the screen.

We suggest that a pooled small molecule screening system could ultimately have a significant impact on drug discovery, by allowing rapid and inexpensive screening of small molecules in more complex assays potentially of greater relevance to human diseases.

Finally, we investigated *in silico* strategies to design a small molecule inhibitor of the anti-apoptotic protein, MCL-1. This target-based, computational approach can be used to efficiently build molecular complexity in a directed fashion, keeping the structure of the binding site in mind while elaborating on the molecule's structure to optimize affinity for the designated pocket. Molecular scaffolds were established through iterative docking and biophysical assessment of fragments. The computational course by which to elaborate on the small molecule's structure was motivated by the experimental results; more complex, yet synthetically accessible compounds were proposed. Each demonstrates strong computational binding scores for Mcl-1 inhibition.

5.2 Future directions

Targeting specific organelles to guide a therapeutic to its specific intracellular active site has become an objective in drug discovery, with the goal to reduce side effects such as systemic toxicity, and to lower the effective dosage required for activity. Endosomal/ lysosomal targeting is one application of this technology, as there are numerous diseases associated with the disruption of lysosomal function. Lysosomal

storage disorders include Tay-Sachs disease, Gaucher's disease, Fabry disease, Hurler syndrome, Pompe disease, etc.; however, lysosomes have also been implicated in Alzheimer's disease and autoimmune diseases. Often, low enzymatic activity in the endosome or lysosome contributes to these disorders. The reduced digestion of internalized components acts to diminish cellular function through downstream protein deactivation.

As the system stands, this technology enables the cell-based screening for small molecules that mechanistically enhance enzymatic activity in endosomes or lysosomes. The design of this technology would include the small molecule linked to the bead through a cathepsin-cleavable or pH sensitive linker, so that the small molecule is released only when exposed to the acidic environment of the organelle to be targeted. We have demonstrated the efficacy of the cathepsin cleavable linker to join lethal molecule MMAE to the bead. Similarly, a reporter of lysosomal enzymatic activity would include a FRET pair with a specific substrate sensitive to cleavage by enzymes known to have diminished or eradicated activity as result of the diseased state, replacing our current caspase-sensitive peptide sequence.

A reporter sensitive to cleavage by lysosomal glycoside hydrolase glucocerebrosidase (GCase) activity could be designed, to screen for small molecules that specifically increase its enzymatic activity. Mutations in the *GBA1* gene, which encodes for GCase, are a key pathological feature of the lysosomal storage disorder Gaucher's disease, and have been identified as a genetic risk factor for Parkinson's disease. Depletion of GCase results in abnormal accumulation of glucosyl ceramide inside lysosomes; current therapeutic strategies rely on enzyme replacement therapy to increase

GCase presence inside the lysosome. Fluorogenic substrates of GCase activity in live cells have been described for imaging in fibroblasts (Yadav et al., 2015) and can be adapted to develop a reporter specific to GCase for application to our technology.

This principle can also be applied to Tay-Sachs disease. This disease is characterized by mutations of the gene *HEXA*, which encodes for the lysosomal enzyme β-hexosaminidase A. Significantly decreased amounts of β-hexosaminidase A prevents degradation of the GM2 ganglioside lipid in neurons, leading to its accumulation which results in neurodegeneration (Myerowitz, 1997). Provided a specific peptide substrate for β-hexosaminidase A is included between FRET pairs of our reporter, libraries of small molecule candidates can be screened in a pooled-method to cherry-pick molecules that enhance the enzymatic activity of β-hexosaminidase A.

Endosomal escape of the internalized bead would expand the scope of this technology. Methods to increase the internalization of histidine-labeled microparticles by including cell-penetrating peptides may enable both efficient cell uptake and cytosolic access to the established technology. Endosomal escape of the three- component Bead-Barcode-Reporter-Small molecule system may also be encouraged by the co-treatment of the system with photosensitizers that specifically embed in the lysosomal membrane. Upon exposure to light, the ROS production from these organic molecules destructs the organelle's membrane to allow access of the system to the cytosol.

Once the bead has access to the cytosolic environment, screening for apoptosis-inducing small molecules is possible through the disulfide-cleavable, small molecule linker in conjunction with the cleaved caspase 3-sensitive, FRET-based activity reporter. The reporter acts to provide a first-pass insight into the hit small molecule's mechanism

of action, greatly aid in narrowing down the possibilities of the molecule's direct protein target to enhance the probability of discovering a successful therapy. Moreover, the reporter can shed light on unexpected mechanisms of action of small molecules, contributing to a more complete picture of how the molecule perturbs a biological system.

In addition to caspase detection, the reporter can be tuned to provide mechanistic information on the activation of diverse enzymes in response to small molecule intervention. Autophagy, for example, is a catabolic, protective cellular process associated with the lysosomal degradation of unnecessary or harmful biological products. The dysregulation of autophagy can contribute to neurodegeneration, cancer, or infectious diseases; as such, up-regulating autophagy, and thereby encouraging the removal of toxic and aggregate proteins or harmful microbes, has become an attractive therapeutic strategy (Rubinsztein et al., 2015). By designing the linker that bridges the FRET pair to include peptide substrates specific for Atg4 cysteine proteases, the pooled screen can be used to discover small molecules that promote autophagy. Atg4 is present in the cytosol; the cleavage of Atg8 by Atg4 is essential for autophagosome biogenesis and eventual autophagy (Shu et al., 2010). Simply tweaking the reporter component to respond to protease activity indicative of a distinct physiological process enables efficient identification of small molecules as therapeutic candidates or biological probes through a pooled, cell-based screen.

Eventual synthesis of the small molecules designed to bind to the BH3 groove on Mcl-1 would be completed and tested for Bax/Bak dependent apoptosis to examine MOA.

This work establishes a strategy upon which to create libraries of compounds for pooled small molecule screening, which is a powerful means to combine targeted drug discovery with phenotypic screening and efficient, first-pass mechanism of action confirmation.

REFERENCES

Adams, J.M., and Cory, S. (2007). The Bcl-2 apoptotic switch in cancer development and therapy. Oncogene *26*, 1324-1337.

Agaisse, H., Burrack, L.S., Philips, J.A., Rubin, E.J., Perrimon, N., and Higgins, D.E. (2005). Genome-wide RNAi screen for host factors required for intracellular bacterial infection. Science *309*, 1248-1251.

Anderson, A.C. (2003). The process of structure-based drug design. Chem Biol *10*, 787-797.

Ashlock, M.A., and Olson, E.R. (2011). Therapeutics development for cystic fibrosis: a successful model for a multisystem genetic disease. Annu Rev Med *62*, 107-125.

Baig, M.H., Ahmad, K., Roy, S., Ashraf, J.M., Adil, M., Siddiqui, M.H., Khan, S., Kamal, M.A., Provaznik, I., and Choi, I. (2016). Computer Aided Drug Design: Success and Limitations. Curr Pharm Des *22*, 572-581.

Bechara, C., and Sagan, S. (2013). Cell-penetrating peptides: 20 years later, where do we stand? FEBS Lett *587*, 1693-1702.

Becker, J., Czamara, D., Scerri, T.S., Ramus, F., Csepe, V., Talcott, J.B., Stein, J., Morris, A., Ludwig, K.U., Hoffmann, P.*, et al.* (2014). Genetic analysis of dyslexia

candidate genes in the European cross-linguistic NeuroDys cohort. European journal of human genetics : EJHG *22*, 675-680.

Becker, O.M., Dhanoa, D.S., Marantz, Y., Chen, D., Shacham, S., Cheruku, S., Heifetz, A., Mohanty, P., Fichman, M., Sharadendu, A.*, et al.* (2006). An integrated in silico 3D model-driven discovery of a novel, potent, and selective amidosulfonamide 5-HT1A agonist (PRX-00023) for the treatment of anxiety and depression. J Med Chem *49*, 3116-3135.

Benes, P., Vetvicka, V., and Fusek, M. (2008). Cathepsin D--many functions of one aspartic protease. Crit Rev Oncol Hematol *68*, 12-28.

Benns, J.M., Choi, J.S., Mahato, R.I., Park, J.S., and Kim, S.W. (2000). pH-sensitive cationic polymer gene delivery vehicle: N-Ac-poly(L-histidine)-graft-poly(L-lysine) comb shaped polymer. Bioconjug Chem *11*, 637-645.

Berg, K., Nordstrand, S., Selbo, P.K., Tran, D.T., Angell-Petersen, E., and Hogset, A. (2011). Disulfonated tetraphenyl chlorin (TPCS2a), a novel photosensitizer developed for clinical utilization of photochemical internalization. Photochem Photobiol Sci *10*, 1637-1651.

Bernardo, P.H., Sivaraman, T., Wan, K.F., Xu, J., Krishnamoorthy, J., Song, C.M., Tian, L., Chin, J.S., Lim, D.S., Mok, H.Y.*, et al.* (2010). Structural insights into the design of small molecule inhibitors that selectively antagonize Mcl-1. Journal of medicinal chemistry *53*, 2314-2318.

Beroukhim, R., Mermel, C.H., Porter, D., Wei, G., Raychaudhuri, S., Donovan, J., Barretina, J., Boehm, J.S., Dobson, J., Urashima, M.*, et al.* (2010). The landscape of somatic copy-number alteration across human cancers. Nature *463*, 899-905.

Blakely, K., Ketela, T., and Moffat, J. (2011). Pooled lentiviral shRNA screening for functional genomics in mammalian cells. Methods Mol Biol *781*, 161-182.

Boehm, H.J., Boehringer, M., Bur, D., Gmuender, H., Huber, W., Klaus, W., Kostrewa, D., Kuehne, H., Luebbers, T., Meunier-Keller, N.*, et al.* (2000). Novel inhibitors of DNA gyrase: 3D structure based biased needle screening, hit validation by biophysical methods, and 3D guided optimization. A promising alternative to random screening. J Med Chem *43*, 2664-2674.

Boisvert-Adamo, K., Longmate, W., Abel, E.V., and Aplin, A.E. (2009). Mcl-1 is required for melanoma cell resistance to anoikis. Molecular cancer research : MCR *7*, 549-556.

Bostad, M., Olsen, C.E., Peng, Q., Berg, K., Hogset, A., and Selbo, P.K. (2015). Light-controlled endosomal escape of the novel CD133-targeting immunotoxin AC133-saporin by photochemical internalization - A minimally invasive cancer stem cell-targeting strategy. J Control Release *206*, 37-48.

Boutros, M., and Ahringer, J. (2008). The art and design of genetic screens: RNA interference. Nat Rev Genet *9*, 554-566.

Brenner, S., and Lerner, R.A. (1992). Encoded combinatorial chemistry. Proc Natl Acad Sci U S A *89*, 5381-5383.

Bright, N.A., Davis, L.J., and Luzio, J.P. (2016). Endolysosomes Are the Principal Intracellular Sites of Acid Hydrolase Activity. Curr Biol *26*, 2233-2245.

Brooks, H., Lebleu, B., and Vives, E. (2005). Tat peptide-mediated cellular delivery: back to basics. Adv Drug Deliv Rev *57*, 559-577.

Brotin, E., Meryet-Figuiere, M., Simonin, K., Duval, R.E., Villedieu, M., Leroy-Dudal, J., Saison-Behmoaras, E., Gauduchon, P., Denoyelle, C., and Poulain, L. (2010). Bcl-XL and MCL-1 constitute pertinent targets in ovarian carcinoma and their concomitant inhibition is sufficient to induce apoptosis. International journal of cancer Journal international du cancer *126*, 885-895.

Brown, D. (2007). Unfinished business: target-based drug discovery. Drug Discov Today *12*, 1007-1012.

Buller, F., Zhang, Y., Scheuermann, J., Schafer, J., Buhlmann, P., and Neri, D. (2009). Discovery of TNF inhibitors from a DNA-encoded chemical library based on diels-alder cycloaddition. Chem Biol *16*, 1075-1086.

Chapman, P.B., Hauschild, A., Robert, C., Haanen, J.B., Ascierto, P., Larkin, J., Dummer, R., Garbe, C., Testori, A., Maio, M.*, et al.* (2011). Improved survival with vemurafenib in melanoma with BRAF V600E mutation. N Engl J Med *364*, 2507-2516.

Chen, J.K., Lane, W.S., Brauer, A.W., Tanaka, A., and Schreiber, S.L. (1993). Biased Combinatorial Libraries - Novel Ligands for the Sh3 Domain of Phosphatidylinositol 3-Kinase. J Am Chem Soc *115*, 12591-12592.

Chen, L., Willis, S.N., Wei, A., Smith, B.J., Fletcher, J.I., Hinds, M.G., Colman, P.M., Day, C.L., Adams, J.M., and Huang, D.C. (2005). Differential targeting of prosurvival Bcl-2 proteins by their BH3-only ligands allows complementary apoptotic function. Molecular cell *17*, 393-403.

Clark, M.A. (2010). Selecting chemicals: the emerging utility of DNA-encoded libraries. Curr Opin Chem Biol *14*, 396-403.

Clark, M.A., Acharya, R.A., Arico-Muendel, C.C., Belyanskaya, S.L., Benjamin, D.R., Carlson, N.R., Centrella, P.A., Chiu, C.H., Creaser, S.P., Cuozzo, J.W.*, et al.* (2009). Design, synthesis and selection of DNA-encoded small-molecule libraries. Nat Chem Biol *5*, 647-654.

Cohen, N.A., Stewart, M.L., Gavathiotis, E., Tepper, J.L., Bruekner, S.R., Koss, B., Opferman, J.T., and Walensky, L.D. (2012). A competitive stapled peptide screen identifies a selective small molecule that overcomes MCL-1-dependent leukemia cell survival. Chem Biol *19*, 1175-1186.

Decurtins, W., Wichert, M., Franzini, R.M., Buller, F., Stravs, M.A., Zhang, Y., Neri, D., and Scheuermann, J. (2016). Automated screening for small organic ligands using DNA-encoded chemical libraries. Nat Protoc *11*, 764-780.

Derenne, S., Monia, B., Dean, N.M., Taylor, J.K., Rapp, M.J., Harousseau, J.L., Bataille, R., and Amiot, M. (2002). Antisense strategy shows that Mcl-1 rather than Bcl-2 or Bcl-x(L) is an essential survival protein of human myeloma cells. Blood *100*, 194-199.

Dessi, N., Pascariello, E., and Pes, B. (2013). A comparative analysis of biomarker selection techniques. Biomed Res Int *2013*, 387673.

Diehl, P., Tedesco, D., and Chenchik, A. (2014). Use of RNAi screens to uncover resistance mechanisms in cancer cells and identify synthetic lethal interactions. Drug Discov Today Technol *11*, 11-18.

Dienstmann, R., Rodon, J., and Tabernero, J. (2013). Biomarker-driven patient selection for early clinical trials. Curr Opin Oncol *25*, 305-312.

Ding, Q., He, X., Xia, W., Hsu, J.M., Chen, C.T., Li, L.Y., Lee, D.F., Yang, J.Y., Xie, X., Liu, J.C.*, et al.* (2007). Myeloid cell leukemia-1 inversely correlates with glycogen synthase kinase-3beta activity and associates with poor prognosis in human breast cancer. Cancer Res *67*, 4564-4571.

Ding, Y., Li, J., Enterina, J.R., Shen, Y., Zhang, I., Tewson, P.H., Mo, G.C., Zhang, J., Quinn, A.M., Hughes, T.E.*, et al.* (2015). Ratiometric biosensors based on dimerization-dependent fluorescent protein exchange. Nat Methods *12*, 195-198.

Doak, B.C., Norton, R.S., and Scanlon, M.J. (2016). The ways and means of fragment-based drug design. Pharmacol Ther *167*, 28-37.

Doherty, G.J., and McMahon, H.T. (2009). Mechanisms of endocytosis. Annu Rev Biochem *78*, 857-902.

Doman, T.N., McGovern, S.L., Witherbee, B.J., Kasten, T.P., Kurumbail, R., Stallings, W.C., Connolly, D.T., and Shoichet, B.K. (2002). Molecular docking and high-throughput screening for novel inhibitors of protein tyrosine phosphatase-1B. J Med Chem *45*, 2213-2221.

Dowell, J., Minna, J.D., and Kirkpatrick, P. (2005). Erlotinib hydrochloride. Nat Rev Drug Discov *4*, 13-14.

Edgington, L.E., Verdoes, M., and Bogyo, M. (2011). Functional imaging of proteases: recent advances in the design and application of substrate-based and activity-based probes. Curr Opin Chem Biol *15*, 798-805.

El-Sayed, A., Futaki, S., and Harashima, H. (2009). Delivery of macromolecules using arginine-rich cell-penetrating peptides: ways to overcome endosomal entrapment. AAPS J *11*, 13-22.

Elmore, S. (2007). Apoptosis: a review of programmed cell death. Toxicol Pathol *35*, 495-516.

Ferreira, L.G., Dos Santos, R.N., Oliva, G., and Andricopulo, A.D. (2015). Molecular docking and structure-based drug design strategies. Molecules *20*, 13384-13421.

Fong, P.C., Boss, D.S., Yap, T.A., Tutt, A., Wu, P., Mergui-Roelvink, M., Mortimer, P., Swaisland, H., Lau, A., O'Connor, M.J., *et al.* (2009). Inhibition of poly(ADP-ribose) polymerase in tumors from BRCA mutation carriers. N Engl J Med *361*, 123-134.

Franzini, R.M., Ekblad, T., Zhong, N., Wichert, M., Decurtins, W., Nauer, A., Zimmermann, M., Samain, F., Scheuermann, J., Brown, P.J., *et al.* (2015). Identification of structure-activity relationships from screening a structurally compact DNA-encoded chemical library. Angew Chem Int Ed Engl *54*, 3927-3931.

Franzini, R.M., Neri, D., and Scheuermann, J. (2014). DNA-encoded chemical libraries: advancing beyond conventional small-molecule libraries. Acc Chem Res *47*, 1247-1255.

Friberg, A., Vigil, D., Zhao, B., Daniels, R.N., Burke, J.P., Garcia-Barrantes, P.M., Camper, D., Chauder, B.A., Lee, T., Olejniczak, E.T., *et al.* (2013). Discovery of potent myeloid cell leukemia 1 (Mcl-1) inhibitors using fragment-based methods and structure-based design. J Med Chem *56*, 15-30.

Furka, A., Sebestyen, F., Asgedom, M., and Dibo, G. (1991). General method for rapid synthesis of multicomponent peptide mixtures. Int J Pept Protein Res *37*, 487-493.

Gane, P.J., and Dean, P.M. (2000). Recent advances in structure-based rational drug design. Curr Opin Struct Biol *10*, 401-404.

Ganesan, A. (2016). Romidepsin and the Zinc-Binding Thiol Family of Natural Product HDAC Inhibitors. In Successful Drug Discovery, J.a.C. Fischer, W.E., ed. (Weinheim, Germany: Wiley-VCH Verlag GmbH & Co. KGaA).

Garcia, V.M., Cassier, P.A., and de Bono, J. (2011). Parallel anticancer drug development and molecular stratification to qualify predictive biomarkers: dealing with obstacles hindering progress. Cancer Discov *1*, 207-212.

Gargiulo, G., Serresi, M., Cesaroni, M., Hulsman, D., and van Lohuizen, M. (2014). In vivo shRNA screens in solid tumors. Nat Protoc *9*, 2880-2902.

Gartner, Z.J., Tse, B.N., Grubina, R., Doyon, J.B., Snyder, T.M., and Liu, D.R. (2004). DNA-templated organic synthesis and selection of a library of macrocycles. Science *305*, 1601-1605.

Goodnow, R.A., Jr., Dumelin, C.E., and Keefe, A.D. (2017). DNA-encoded chemistry: enabling the deeper sampling of chemical space. Nat Rev Drug Discov *16*, 131-147.

Grant, S., Easley, C., and Kirkpatrick, P. (2007). Vorinostat. Nat Rev Drug Discov *6*, 21-22.

Gu, W., Jia, Z., Truong, N.P., Prasadam, I., Xiao, Y., and Monteiro, M.J. (2013). Polymer nanocarrier system for endosome escape and timed release of siRNA with complete gene silencing and cell death in cancer cells. Biomacromolecules *14*, 3386-3389.

Hajduk, P.J., and Greer, J. (2007). A decade of fragment-based drug design: strategic advances and lessons learned. Nat Rev Drug Discov *6*, 211-219.

Hall, R.J., Mortenson, P.N., and Murray, C.W. (2014). Efficient exploration of chemical space by fragment-based screening. Prog Biophys Mol Biol *116*, 82-91.

Hanahan, D., and Weinberg, R.A. (2000). The hallmarks of cancer. Cell *100*, 57-70.

Haney, C.M., Wissner, R.F., and Petersson, E.J. (2015). Multiply labeling proteins for studies of folding and stability. Curr Opin Chem Biol *28*, 123-130.

Hengartner, M.O. (2000). The biochemistry of apoptosis. Nature *407*, 770-776.

Huang, S.Y., Grinter, S.Z., and Zou, X. (2010). Scoring functions and their evaluation methods for protein-ligand docking: recent advances and future directions. Phys Chem Chem Phys *12*, 12899-12908.

Hughes, J.P., Rees, S., Kalindjian, S.B., and Philpott, K.L. (2011). Principles of early drug discovery. Br J Pharmacol *162*, 1239-1249.

Ichim, G., and Tait, S.W. (2016). A fate worse than death: apoptosis as an oncogenic process. Nat Rev Cancer *16*, 539-548.

Iqbal, N., and Iqbal, N. (2014). Imatinib: a breakthrough of targeted therapy in cancer. Chemother Res Pract *2014*, 357027.

Jiang, Y., and Chen, J.Z. (2013). Self-consistent field theory and numerical scheme for calculating the phase diagram of wormlike diblock copolymers. Phys Rev E Stat Nonlin Soft Matter Phys *88*, 042603.

Johansson, A.C., Steen, H., Ollinger, K., and Roberg, K. (2003). Cathepsin D mediates cytochrome c release and caspase activation in human fibroblast apoptosis induced by staurosporine. Cell Death Differ *10*, 1253-1259.

Kainkaryam, R.M., and Woolf, P.J. (2009). Pooling in high-throughput drug screening. Curr Opin Drug Discov Devel *12*, 339-350.

Kapetanovic, I.M. (2008). Computer-aided drug discovery and development (CADDD): in silico-chemico-biological approach. Chem Biol Interact *171*, 165-176.

Kirby, B.J. (2010). Micro- and nanoscale fluid mechanics transport in microfluidic devices (New York: Cambridge University Press,).

Kitchen, D.B., Decornez, H., Furr, J.R., and Bajorath, J. (2004). Docking and scoring in virtual screening for drug discovery: methods and applications. Nat Rev Drug Discov *3*, 935-949.

Kotschy, A., Szlavik, Z., Murray, J., Davidson, J., Maragno, A.L., Le Toumelin-Braizat, G., Chanrion, M., Kelly, G.L., Gong, J.N., Moujalled, D.M.*, et al.* (2016). The MCL1 inhibitor S63845 is tolerable and effective in diverse cancer models. Nature *538*, 477-482.

Krajewska, M., Krajewski, S., Epstein, J.I., Shabaik, A., Sauvageot, J., Song, K., Kitada, S., and Reed, J.C. (1996). Immunohistochemical analysis of bcl-2, bax, bcl-X, and mcl-1 expression in prostate cancers. The American journal of pathology *148*, 1567-1576.

Lam, K.S., Salmon, S.E., Hersh, E.M., Hruby, V.J., Kazmierski, W.M., and Knapp, R.J. (1991). A new type of synthetic peptide library for identifying ligand-binding activity. Nature *354*, 82-84.

Lee, C.H., Huang, H.C., and Juan, H.F. (2011). Reviewing ligand-based rational drug design: the search for an ATP synthase inhibitor. Int J Mol Sci *12*, 5304-5318.

Lee, J.A., Uhlik, M.T., Moxham, C.M., Tomandl, D., and Sall, D.J. (2012). Modern phenotypic drug discovery is a viable, neoclassic pharma strategy. J Med Chem *55*, 4527-4538.

Lessene, G., Czabotar, P.E., and Colman, P.M. (2008). BCL-2 family antagonists for cancer therapy. Nature reviews Drug discovery *7*, 989-1000.

Li, A.P. (2001). Screening for human ADME/Tox drug properties in drug discovery. Drug Discovery Today *6*, 357-366.

Li, J., Nowak, P., and Otto, S. (2013). Dynamic combinatorial libraries: from exploring molecular recognition to systems chemistry. J Am Chem Soc *135*, 9222-9239.

Li, K., Wu, D., Chen, X., Zhang, T., Zhang, L., Yi, Y., Miao, Z., Jin, N., Bi, X., Wang, H*., et al.* (2014). Current and emerging biomarkers of cell death in human disease. Biomed Res Int *2014*, 690103.

Liao, C., and Nicklaus, M.C. (2010). Computer tools in the discovery of HIV-1 integrase inhibitors. Future Med Chem *2*, 1123-1140.

Liao, C., Sitzmann, M., Pugliese, A., and Nicklaus, M.C. (2011). Software and resources for computational medicinal chemistry. Future Med Chem *3*, 1057-1085.

Lionta, E., Spyrou, G., Vassilatis, D.K., and Cournia, Z. (2014). Structure-based virtual screening for drug discovery: principles, applications and recent advances. Curr Top Med Chem *14*, 1923-1938.

Lokey, R.S. (2003). Forward chemical genetics: progress and obstacles on the path to a new pharmacopoeia. Curr Opin Chem Biol *7*, 91-96.

Lu, G., Middleton, R.E., Sun, H., Naniong, M., Ott, C.J., Mitsiades, C.S., Wong, K.K., Bradner, J.E., and Kaelin, W.G., Jr. (2014). The myeloma drug lenalidomide promotes the cereblon-dependent destruction of Ikaros proteins. Science *343*, 305-309.

Ma, D. (2014). Enhancing endosomal escape for nanoparticle mediated siRNA delivery. Nanoscale *6*, 6415-6425.

Maianti, J.P., McFedries, A., Foda, Z.H., Kleiner, R.E., Du, X.Q., Leissring, M.A., Tang, W.J., Charron, M.J., Seeliger, M.A., Saghatelian, A.*, et al.* (2014). Anti-diabetic activity of insulin-degrading enzyme inhibitors mediated by multiple hormones. Nature *511*, 94-98.

McStay, G.P., Salvesen, G.S., and Green, D.R. (2008). Overlapping cleavage motif selectivity of caspases: implications for analysis of apoptotic pathways. Cell Death Differ *15*, 322-331.

Merrifield, R.B. (1963). Solid Phase Peptide Synthesis .1. Synthesis of a Tetrapeptide. J Am Chem Soc *85*, 2149-&.

Mishra, S., Heidel, J.D., Webster, P., and Davis, M.E. (2006). Imidazole groups on a linear, cyclodextrin-containing polycation produce enhanced gene delivery via multiple processes. J Control Release *116*, 179-191.

Miyamoto, Y., Hosotani, R., Wada, M., Lee, J.U., Koshiba, T., Fujimoto, K., Tsuji, S., Nakajima, S., Doi, R., Kato, M.*, et al.* (1999). Immunohistochemical analysis of Bcl-2, Bax, Bcl-X, and Mcl-1 expression in pancreatic cancers. Oncology *56*, 73-82.

Moffat, J., and Sabatini, D.M. (2006). Building mammalian signalling pathways with RNAi screens. Nat Rev Mol Cell Biol *7*, 177-187.

Moffat, J.G., Rudolph, J., and Bailey, D. (2014). Phenotypic screening in cancer drug discovery - past, present and future. Nat Rev Drug Discov *13*, 588-602.

Mortenson, P.N., Berdini, V., and O'Reilly, M. (2014). Fragment-based approaches to the discovery of kinase inhibitors. Methods Enzymol *548*, 69-92.

Mullard, A. (2015). The phenotypic screening pendulum swings. Nat Rev Drug Discov *14*, 807-809.

Mullard, A. (2016). DNA tags help the hunt for drugs. Nature *530*, 367-369.

Myerowitz, R. (1997). Tay-Sachs disease-causing mutations and neutral polymorphisms in the Hex A gene. Hum Mutat *9*, 195-208.

Nagy, P., Vereb, G., Damjanovich, S., Matyus, L., and Szollosi, J. (2006). Measuring FRET in flow cytometry and microscopy. Curr Protoc Cytom *Chapter 12*, Unit12 18.

Nair, P., Lu, M., Petersen, S., and Ashkenazi, A. (2014). Apoptosis initiation through the cell-extrinsic pathway. Methods Enzymol *544*, 99-128.

Oh, N., and Park, J.H. (2014). Endocytosis and exocytosis of nanoparticles in mammalian cells. Int J Nanomedicine *9 Suppl 1*, 51-63.

Ola, M.S., Nawaz, M., and Ahsan, H. (2011). Role of Bcl-2 family proteins and caspases in the regulation of apoptosis. Mol Cell Biochem *351*, 41-58.

Oltersdorf, T., Elmore, S.W., Shoemaker, A.R., Armstrong, R.C., Augeri, D.J., Belli, B.A., Bruncko, M., Deckwerth, T.L., Dinges, J., Hajduk, P.J.*, et al.* (2005). An inhibitor of Bcl-2 family proteins induces regression of solid tumours. Nature *435*, 677-681.

Ouyang, L., Shi, Z., Zhao, S., Wang, F.T., Zhou, T.T., Liu, B., and Bao, J.K. (2012). Programmed cell death pathways in cancer: a review of apoptosis, autophagy and programmed necrosis. Cell Prolif *45*, 487-498.

Pelish, H.E., Westwood, N.J., Feng, Y., Kirchhausen, T., and Shair, M.D. (2001). Use of biomimetic diversity-oriented synthesis to discover galanthamine-like molecules with biological properties beyond those of the natural product. J Am Chem Soc *123*, 6740-6741.

Petros, A.M., Swann, S.L., Song, D., Swinger, K., Park, C., Zhang, H., Wendt, M.D., Kunzer, A.R., Souers, A.J., and Sun, C. (2014). Fragment-based discovery of potent inhibitors of the anti-apoptotic MCL-1 protein. Bioorganic & medicinal chemistry letters *24*, 1484-1488.

Poreba, M., Strozyk, A., Salvesen, G.S., and Drag, M. (2013). Caspase substrates and inhibitors. Cold Spring Harb Perspect Biol *5*, a008680.

Rees, D.C., Congreve, M., Murray, C.W., and Carr, R. (2004). Fragment-based lead discovery. Nat Rev Drug Discov *3*, 660-672.

Richard, D.J., Lena, R., Bannister, T., Blake, N., Pierceall, W.E., Carlson, N.E., Keller, C.E., Koenig, M., He, Y., Minond, D.*, et al.* (2013). Hydroxyquinoline-derived

compounds and analoguing of selective Mcl-1 inhibitors using a functional biomarker. Bioorganic & medicinal chemistry *21*, 6642-6649.

Riedl, S.J., and Shi, Y. (2004). Molecular mechanisms of caspase regulation during apoptosis. Nat Rev Mol Cell Biol *5*, 897-907.

Rowland, C.E., Brown, C.W., Medintz, I.L., and Delehanty, J.B. (2015). Intracellular FRET-based probes: a review. Methods Appl Fluores *3*.

Rubinsztein, D.C., Bento, C.F., and Deretic, V. (2015). Therapeutic targeting of autophagy in neurodegenerative and infectious diseases. J Exp Med *212*, 979-990.

Salatin, S., Maleki Dizaj, S., and Yari Khosroushahi, A. (2015). Effect of the surface modification, size, and shape on cellular uptake of nanoparticles. Cell Biol Int *39*, 881-890.

Sams-Dodd, F. (2005). Target-based drug discovery: is something wrong? Drug Discov Today *10*, 139-147.

Santos, L.H., Ferreira, R.S., and Caffarena, E.R. (2015). Computational drug design strategies applied to the modelling of human immunodeficiency virus-1 reverse transcriptase inhibitors. Mem Inst Oswaldo Cruz *110*, 847-864.

Schenone, M., Dancik, V., Wagner, B.K., and Clemons, P.A. (2013). Target identification and mechanism of action in chemical biology and drug discovery. Nat Chem Biol *9*, 232-240.

Sekar, R.B., and Periasamy, A. (2003). Fluorescence resonance energy transfer (FRET) microscopy imaging of live cell protein localizations. J Cell Biol *160*, 629-633.

Selbo, P.K., Bostad, M., Olsen, C.E., Edwards, V.T., Hogset, A., Weyergang, A., and Berg, K. (2015). Photochemical internalisation, a minimally invasive strategy for light-controlled endosomal escape of cancer stem cell-targeting therapeutics. Photochem Photobiol Sci *14*, 1433-1450.

Shu, C.W., Drag, M., Bekes, M., Zhai, D., Salvesen, G.S., and Reed, J.C. (2010). Synthetic substrates for measuring activity of autophagy proteases: autophagins (Atg4). Autophagy *6*, 936-947.

Sliwoski, G., Kothiwale, S., Meiler, J., and Lowe, E.W., Jr. (2014). Computational methods in drug discovery. Pharmacol Rev *66*, 334-395.

Smith, C. (2003). Drug target validation: Hitting the target. Nature *422*, 341, 343, 345 passim.

Song, L., Coppola, D., Livingston, S., Cress, D., and Haura, E.B. (2005). Mcl-1 regulates survival and sensitivity to diverse apoptotic stimuli in human non-small cell lung cancer cells. Cancer biology & therapy *4*, 267-276.

Song, T., Li, X., Chang, X., Liang, X., Zhao, Y., Wu, G., Xie, S., Su, P., Wu, Z., Feng, Y.*, et al.* (2013). 3-Thiomorpholin-8-oxo-8H-acenaphtho [1,2-b] pyrrole-9-carbonitrile (S1) derivatives as pan-Bcl-2-inhibitors of Bcl-2, Bcl-xL and Mcl-1. Bioorganic & medicinal chemistry *21*, 11-20.

Strimbu, K., and Tavel, J.A. (2010). What are biomarkers? Curr Opin HIV AIDS *5*, 463-466.

Swaney, S.M., Aoki, H., Ganoza, M.C., and Shinabarger, D.L. (1998). The oxazolidinone linezolid inhibits initiation of protein synthesis in bacteria. Antimicrob Agents Chemother *42*, 3251-3255.

Swinehart, D.F. (1962). The Beer-Lambert Law. Journal of Chemical Education *39*.

Swinney, D.C. (2013). Phenotypic vs. target-based drug discovery for first-in-class medicines. Clin Pharmacol Ther *93*, 299-301.

Sze, A., Erickson, D., Ren, L., and Li, D. (2003). Zeta-potential measurement using the Smoluchowski equation and the slope of the current-time relationship in electroosmotic flow. J Colloid Interface Sci *261*, 402-410.

Szymanski, P., Markowicz, M., and Mikiciuk-Olasik, E. (2012). Adaptation of high-throughput screening in drug discovery-toxicological screening tests. Int J Mol Sci *13*, 427-452.

Tan, D.S., Foley, M.A., Shair, M.D., and Schreiber, S.L. (1998). Stereoselective synthesis of over two million compounds having structural features both reminiscent of natural products and compatible with miniaturized cell-based assays. J Am Chem Soc *120*, 8565-8566.

Tan, D.S., Thomas, G.V., Garrett, M.D., Banerji, U., de Bono, J.S., Kaye, S.B., and Workman, P. (2009). Biomarker-driven early clinical trials in oncology: a paradigm shift in drug development. Cancer J *15*, 406-420.

Tanaka, Y., Aikawa, K., Nishida, G., Homma, M., Sogabe, S., Igaki, S., Hayano, Y., Sameshima, T., Miyahisa, I., Kawamoto, T.*, et al.* (2013). Discovery of potent Mcl-1/Bcl-xL dual inhibitors by using a hybridization strategy based on structural analysis of target proteins. Journal of medicinal chemistry *56*, 9635-9645.

Taylor, R.C., Cullen, S.P., and Martin, S.J. (2008). Apoptosis: controlled demolition at the cellular level. Nat Rev Mol Cell Biol *9*, 231-241.

Thornberry, N.A., and Lazebnik, Y. (1998). Caspases: enemies within. Science *281*, 1312-1316.

Timmer, J.C., and Salvesen, G.S. (2007). Caspase substrates. Cell Death Differ *14*, 66-72.

Tse, C., Shoemaker, A.R., Adickes, J., Anderson, M.G., Chen, J., Jin, S., Johnson, E.F., Marsh, K.C., Mitten, M.J., Nimmer, P.*, et al.* (2008). ABT-263: a potent and orally bioavailable Bcl-2 family inhibitor. Cancer Res *68*, 3421-3428.

van de Donk, N.W., and Dhimolea, E. (2012). Brentuximab vedotin. MAbs *4*, 458-465.

van Delft, M.F., Wei, A.H., Mason, K.D., Vandenberg, C.J., Chen, L., Czabotar, P.E., Willis, S.N., Scott, C.L., Day, C.L., Cory, S.*, et al.* (2006). The BH3 mimetic ABT-737 targets selective Bcl-2 proteins and efficiently induces apoptosis via Bak/Bax if Mcl-1 is neutralized. Cancer cell *10*, 389-399.

VanEngelenburg, S.B., and Palmer, A.E. (2008). Fluorescent biosensors of protein function. Curr Opin Chem Biol *12*, 60-65.

Varadarajan, S., Vogler, M., Butterworth, M., Dinsdale, D., Walensky, L.D., and Cohen, G.M. (2013). Evaluation and critical assessment of putative MCL-1 inhibitors. Cell death and differentiation *20*, 1475-1484.

Vincent, F., Loria, P., Pregel, M., Stanton, R., Kitching, L., Nocka, K., Doyonnas, R., Steppan, C., Gilbert, A., Schroeter, T.*, et al.* (2015). Developing predictive assays: the phenotypic screening "rule of 3". Sci Transl Med *7*, 293ps215.

Wadia, J.S., Stan, R.V., and Dowdy, S.F. (2004). Transducible TAT-HA fusogenic peptide enhances escape of TAT-fusion proteins after lipid raft macropinocytosis. Nat Med *10*, 310-315.

Walensky, L.D. (2012). From mitochondrial biology to magic bullet: navitoclax disarms BCL-2 in chronic lymphocytic leukemia. J Clin Oncol *30*, 554-557.

Wan, K.H., Yu, C., George, R.A., Carlson, J.W., Hoskins, R.A., Svirskas, R., Stapleton, M., and Celniker, S.E. (2006). High-throughput plasmid cDNA library screening. Nat Protoc *1*, 624-632.

Ward, T.H., Cummings, J., Dean, E., Greystoke, A., Hou, J.M., Backen, A., Ranson, M., and Dive, C. (2008). Biomarkers of apoptosis. Br J Cancer *99*, 841-846.

Wei, S.H., Dong, K., Lin, F., Wang, X., Li, B., Shen, J.J., Zhang, Q., Wang, R., and Zhang, H.Z. (2008). Inducing apoptosis and enhancing chemosensitivity to gemcitabine via RNA interference targeting Mcl-1 gene in pancreatic carcinoma cell. Cancer chemotherapy and pharmacology *62*, 1055-1064.

Welch, D.R. (2016). Tumor Heterogeneity--A 'Contemporary Concept' Founded on Historical Insights and Predictions. Cancer Res *76*, 4-6.

Wertz, I.E., Kusam, S., Lam, C., Okamoto, T., Sandoval, W., Anderson, D.J., Helgason, E., Ernst, J.A., Eby, M., Liu, J*., et al.* (2011). Sensitivity to antitubulin chemotherapeutics is regulated by MCL1 and FBW7. Nature *471*, 110-114.

Westphal, D., Kluck, R.M., and Dewson, G. (2014). Building blocks of the apoptotic pore: how Bax and Bak are activated and oligomerize during apoptosis. Cell death and differentiation *21*, 196-205.

Wilhelm, S., Carter, C., Lynch, M., Lowinger, T., Dumas, J., Smith, R.A., Schwartz, B., Simantov, R., and Kelley, S. (2006). Discovery and development of sorafenib: a multikinase inhibitor for treating cancer. Nat Rev Drug Discov *5*, 835-844.

Wilson, D.N., Schluenzen, F., Harms, J.M., Starosta, A.L., Connell, S.R., and Fucini, P. (2008). The oxazolidinone antibiotics perturb the ribosomal peptidyl-transferase center and effect tRNA positioning. Proc Natl Acad Sci U S A *105*, 13339-13344.

Wong, A.S., Choi, G.C., Cui, C.H., Pregernig, G., Milani, P., Adam, M., Perli, S.D., Kazer, S.W., Gaillard, A., Hermann, M.*, et al.* (2016). Multiplexed barcoded CRISPR-Cas9 screening enabled by CombiGEM. Proc Natl Acad Sci U S A *113*, 2544-2549.

Yadav, A.K., Shen, D.L., Shan, X., He, X., Kermode, A.R., and Vocadlo, D.J. (2015). Fluorescence-quenched substrates for live cell imaging of human glucocerebrosidase activity. J Am Chem Soc *137*, 1181-1189.

Yang, S.Y. (2010). Pharmacophore modeling and applications in drug discovery: challenges and recent advances. Drug Discov Today *15*, 444-450.

Yap, T.A., and Workman, P. (2012). Exploiting the cancer genome: strategies for the discovery and clinical development of targeted molecular therapeutics. Annu Rev Pharmacol Toxicol *52*, 549-573.

You, A.J., Jackman, R.J., Whitesides, G.M., and Schreiber, S.L. (1997). A miniaturized arrayed assay format for detecting small molecule-protein interactions in cells. Chem Biol *4*, 969-975.

Zheng, W., Thorne, N., and McKew, J.C. (2013). Phenotypic screens as a renewed approach for drug discovery. Drug Discov Today *18*, 1067-1073.

Zhou, Y., Zhu, S., Cai, C., Yuan, P., Li, C., Huang, Y., and Wei, W. (2014). High-throughput screening of a CRISPR/Cas9 library for functional genomics in human cells. Nature *509*, 487-491.

Appendix A

Table A1: Peptide sequences used for reporter component

	Peptide Name	Sequence
Bead-FRET	CEY-FAM/DABCYL	$NH_2(PEG_3)(FITC)KGDEVDGSGK(Dansyl)$
	CEY NH$_2$DansylFITC	$NH_2(PEG_3)(FITC)KGDEVDGSGK(Dabcyl)$
	CEY_NH$_2$_HIS	$NH_2(PEG_3)$-HHHHHHHHHHHHHHH
Bead-FITC	CEY NH$_2$FITC	$NH_2(PEG_3)(FITC)KGDEVD$
	CEY-DEVD2	NH_2-(miniPEG$_3$)-Gly-Asp-Glu-Val-Asp-Gly-Gly-Lys-(FITC)
	CEY-DEVD	NH_2(mini-PEG$_3$)-DEVD-FITC

Table A2: Barcode sequences and primers

	Sequence Name	Sequence
Bead-oligo	CEY_PCNH_rc_TruSeqBC1	/5AmMC12//iSpPC/CCT TGG CAC CCG AGA ATT CCA ACG GCA TAC GAG ATC GTG ATG TGA CTG GAG TTC AGA CGT GTG CGA TCG TCG GAC TGT AGA ACT CTG AAC

Bead-oligo	CEY_PCNH_TruSeqBC2	/5AmMC12//iSpPC/GTT CAG AGT TCT ACA GTC CGA CTG AAC TCC AGT CAC CGA TGT ATC TCG TAT GCC GTC TTC TGC ACA TTG TGG AAT TCT CGG GTG CCA AGG
control	CEY_TruSeq_BC2_PAGE	GTT CAG AGT TCT ACA GTC CGA CTG AAC TCC AGT CAC CGA TGT ATC TCG TAT GCC GTC TTC TGC ACA TTG TGG AAT TCT CGG GTG CCA AGG
control	CEY_TruSeqBC1	GTT CAG AGT TCT ACA GTC CGA CGA TCG CAC ACG TCT GAA CTC CAG TCA CAT CAC GAT CTC GTA TGC CGT TGG AAT TCT CGG GTG CCA AGG
control	CEY_TruSeqBC1_revcomp	CCT TGG CAC CCG AGA ATT CCA ACG GCA TAC GAG ATC GTG ATG TGA CTG GAG TTC AGA CGT GTG CGA TCG TCG GAC TGT

		AGA ACT CTG AAC
control	CEY_NH_TruSeqBC1	/5AmMC12/GTT CAG AGT TCT ACA GTC CGA CGA TCG CAC ACG TCT GAA CTC CAG TCA CAT CAC GAT CTC GTA TGC CGT TGG AAT TCT CGG GTG CCA AGG
Primer 1	CEY_TruSeq_RPI1	CAA GCA GAA GAC GGC ATA CGA GAT CGT GAT GTG ACT GGA GTT CCT TGG CAC CCG AGA ATT CCA
Primer 2	CEY_TruSeq_RP1	AAT GAT ACG GCG ACC ACC GAG ATC TAC ACG TTC AGA GTT CTA CAG TCC GA